MODELING NONLINEAR ULTRASOUND PROPAGATION IN TISSUE

by

Roger James Zemp

A thesis submitted in conformity with the requirements for the degree of
Masters of Applied Science
Graduate Department of Electrical and Computer Engineering
and Institute of Biomaterials and Biomedical Engineering
University of Toronto

0-612-53448-0

Canada

MODELING NONLINEAR ULTRASOUND PROPAGATION IN TISSUE

A Thesis Submitted in conformity with the requirements for the degree of
Masters of Applied Science
Graduate Department of Electrical and Computer Engineering and
Institute of Biomaterials and Biomedical Engineering
University of Toronto

ABSTRACT

A new, computationally efficient approach for modelling finite amplitude ultrasound propagation is described. The model is able to simulate nonlinear distortion of CW and pulsed excitations from non-axisymmetric sources in tissue. We have developed a second order operator splitting approach, enabling the effects of diffraction, nonlinearity, and absorption to be calculated separately over relatively large incremental distances using a fractional step marching scheme. A computationally efficient angular spectrum algorithm has also been developed to calculate the diffractive propagation from non-axisymmetric, non-separable sources. Results of our model have shown close agreement with published data. Moreover, our approach may offer computational savings compared with existing models. Indeed, with our algorithm it should be possible to simulate the nonlinear propagation of sound beams from realistic medical ultrasound scanners, and perhaps to investigate ways to improve the design of tissue harmonic imaging systems.

Acknowledgements

I would like to express my sincere appreciation to Prof. Richard S.C. Cobbold, and to Dr. Jahangir Tavakkoli for their mentorship, friendship, and patience. Prof. Cobbold has always been cheerfully available, and open to discuss matters academic or casual. Dr. Tavakkoli has likewise been a guiding hand and an encouraging force.

Thanks go to Ted Christopher for helpful conversations and email regarding the angular spectrum method, David Hope Simpson for discussions regarding pulse inversion, Thanassis Misaridis for email correspondence regarding coded excitation, and Chuck Bradley for insights into tissue harmonic imaging.

I would especially like to acknowledge my wonderful wife Denyse for her support, encouragement and love. My son Justin has been with us for the last eight months of my thesis, and it is my family that has given me much inspiration and happiness.

Table of Contents

Chapter 1: Introduction and Motivation

1.1 Medical Ultrasound Imaging

Ultrasound imaging has an important, and growing role in modern clinical medicine. Benefits of ultrasound imaging include real-time imaging capabilities, relatively low cost, and safety due to use of non-ionizing radiation. Some limitations of ultrasound compared to other modalities include inferior resolution and poor penetration depth. Because ultrasound attenuation is more severe for higher frequencies, there is typically an implicit tradeoff between resolution, and penetration depth. Moreover, artefacts due to clutter, beam defocusing due to tissue path inhomogeneities, and multiple reflections can distort the image and cause erroneous interpretation.

Reduction of artefacts due to clutter, have been investigated by a number of researchers. Beam-forming techniques such as phased array focusing and apodization have been used to reduce sidelobe levels, and thus decrease clutter (e.g. Macovski, 1983; t'Hoen 1982; Kino, 1987, Cincotti et. al. 2000). Other promising techniques include the use of limited diffraction beams (Lu and Greenleaf, 1994), and 1.5 and 2D arrays (e.g. Smith et. al. 1995, for example).

The problem of improving spatial resolution without compromising penetration depth (or conversely trying to improve penetration depth without loss of resolution) is a challenging one, nevertheless, efforts in using coded excitation show great promise (e.g. O'Donnell, 1992; Welch and Fox, 1998). Ultrasound contrast agents have, moreover, increased echo signal strength, and enabled visualization of new kinds of clinically relevant information (Burns, 1996; Simpson et al. 1999).

Efforts to overcome loss of contrast resolution due to inhomogeneity-induced phase aberration (Nock and Trahey, 1989; Liu and Waag, 1994 a & b; Hinckleman et. al. 1994; Mallart and Fink, 1994; Zhu and Steinberg, 1993 a & b; Karaman et. al. 1993) have had limited clinical success.

1.2 Tissue Harmonic Imaging and Nonlinear Propagation

The last few years has seen the emergence a new ultrasound technology called Tissue Harmonic Imaging (THI), or Finite Amplitude Distortion-Based Harmonic Imaging, which overcomes some of the problems of phase aberration, clutter artefacts, reverberation artefacts, and offers improved spatial resolution. The premise of THI is to use harmonic information from nonlinear ultrasound propagation to form an image. Nonlinear propagation arises from a convective phenomenon, and from a nonlinear relationship between pressure and density. The compression phase of a wave will travel faster than the rarefaction phase, and thus, as the wave propagates, it will undergo distortion, which will be more severe for higher pressure amplitudes. In the frequency domain, nonlinearity means that harmonics and sum and difference frequencies will be generated.

The concept of nonlinear propagation, goes back to the work of Euler in 1755. In the medical field, although the vast majority of research and development in medical ultrasonics has assumed linear propagation, it has been well understood that nonlinear effects play a non-negligible role – especially for ultrasonic devices which use high amplitude sources. Therapeutic applications such as lithotripsy for minimally invasive kidney stone fragmentation, generate very high source amplitudes. In these cases, nonlinear propagation can be quite significant.

Harmonic Imaging, based on nonlinear ultrasound propagation can be traced back to the work of Muir (1980), who presented ideas on nonlinear effects in acoustical imaging. Interestingly, however, commercial development of THI has in large part stemmed from research in ultrasound contrast agents. Microbubble contrast agents have been used to increase the backscatter from the vasculature and microvasculature. Because bubbles behave in a nonlinear way, they generate harmonics of incident insonifying frequencies, as well as sum and difference frequencies. Contrast Harmonic Imaging is based on using harmonic echoes from contrast microbubbles to form an image. When investigating the potential use of ultrasound contrast agents, researchers found that relatively clear B-mode ultrasound images could be formed by receiving at twice the frequency of the transmitted

beam, even when no contrast agents were present. The second harmonic image in the absence of contrast agents, is formed from backscatter of harmonics generated in nonlinear propagation through tissue.

A key paper by Ward et. al. (1997) demonstrated the feasability of applying nonlinear propagation to B-mode imaging. Averkiou et. al. (1997) further demonstrated that adequate harmonic signal level could be obtained from tissue propagation to enable its use for imaging. Christopher (1997, 1998) has demonstrated with modeling and experimental work that sufficient harmonic signal can be obtained within current standards, and that harmonic imaging can reduce the degrading effects of phase aberration. Li et. al. (2000) have recently published a computer model for simulating realistic tissue harmonic images using an axisymetric source, and have studied the improvement in resolution and image contrast derived from THI compared with conventional B-mode imaging. Clinically, THI has been used in a number of fields, including cardiology, and has shown promising results. Clinical images show a marked improvement in haze and other artefacts compared with fundamental imaging, not to mention higher resolution (Tranquart et. al. 1999). Tissue Harmonic Imaging is already in widespread clinical use, and medical ultrasound manufacturers such as ATL, Acuson, General Electric, Hewlet Packard, Siemens, etc. all have machines with THI capabilities.

Many investigators will agree, however, that THI is still in its infancy, and has much room for optimization. Humphrey, in a recent review article (Humphrey, 2000) comments on the need for "more efficient algorithms and simpler models to be able to predict the effects of nonlinearity in a given field." He notes some recent developments, and hypothesizes that there is "room for considerable development".

1.3 Modeling Nonlinear Propagation

An important aspect of modern engineering design, is the use of computer models to simulate a technology before manufacturing. Often modeling not only saves money by allowing virtual research and development, but it also helps foster an understanding of

principles needed for an optimal design. Our work centers on modeling nonlinear propagation in tissue from a realistic medical ultrasound scanner.

The model we have developed contributes a new perspective in modeling methodology. Currently, there are a number of approaches to modeling nonlinear propagation. Many are based on the 'KZK' equation, which is valid for nonlinear propagation in thermoviscous fluids, for fairly directional sources, and for sources which are not too focused. Results are not valid in the extreme nearfield, or far off axis as it makes the parabolic approximation. Numerical solutions have been investigated in the time domain (Lee and Hamilton, 1994), and the frequency domain (Aanonsen et. al., 1984). Much of the work has been done for propagation in water, and for axisymetric (piston or focused disk) transducers. Cahill and Baker (1998) have simulated nonlinear propagation in water from a (non-axisymmetric) phased array transducer.

Christopher and Parker (1991) have developed another method, not based on the KZK equation, wherein they model nonlinear propagation by breaking up diffraction and nonlinearity over small steps, and solve for diffraction using a fast transform – based angular spectrum method, and solve for nonlinearity using a frequency domain approach. Their results are valid for propagation in arbitrary media (not just thermoviscous fluids), and their work can be applied to non-axisymmetric sources.

Tavakkoli et. al. (1998) developed a time domain model based on a second order operator splitting. They used the Rayleigh integral to compute the effects of diffraction, a time domain algorithm to compute nonlinearity, and a minimal phased FIR filter to calculate attenuation. Their model has been verified for axisymmetric lithotripter sources.

One of the difficulties in using computational modeling of nonlinear propagation is the heavy computational burden. Axisymmetric codes dominate the literature, and even with this symmetry, computational complexities of current models are fairly intense, requiring hours or days on supercomputers. Simulating non-axisymmetric sources requires an additional order of magnitude in computational complexity, and boosts time and memory

requirements. The step from continuous wave sources to pulsed sources requires yet an additional degree of computational complexity.

So far, published literature is devoid of papers exploring the modeling of nonlinear propagation in tissue from a linear phased array. The computational burden needed to accomplish such a task may be one explanation for this. Simulating finite amplitude propagation in tissue from a phased array will be addressed in this work.

1.4 Thesis Objective

The objective of this thesis is to develop a computationally efficient model of nonlinear ultrasound propagation, which may be used as a simulation tool for use in design of a harmonic imaging system. The model should enable simulation of nonlinear propagation in arbitrary media, and specifically, should accurately model propagation in tissue. Simulation of various types of transducers (including linear phased arrays) and arbitrary waveforms should be possible. Computational efficiency is a primary concern, and we hope that our modeling methodology may prove to yield some degree of computational savings compared to existing models. Simulation of nonlinear pulse propagation in tissue from non-axisymmetric sources should be realizable on a personal computer with a run time of a few hours. Verification of our model should be possible, by comparison with published experimental and theoretical results.

Ultimately it is hoped that our model can be used to investigate optimal design schemes and parameters for a tissue harmonic imaging system. With this motivation, peripheral investigations stemming from this thesis will include using coded excitation and pulse inversion to improve the signal to noise ratio in harmonic imaging.

1.5 Thesis Outline

Following this introductory chapter, chapter 2 will establish some fundamental theory relevant to nonlinear propagation. Model equations will be presented, and their relevance to propagation in tissue will be discussed. Chapter 3 will discuss numerical methods used so far in modeling nonlinear propagation. The principles of the numerical model we

choose to implement will be discussed in the Chapter 4. In Chapter 5 we will discuss the numerical implementation of the Angular Spectrum method for linear propagation. Chapter 6 will discuss the application of the second order operator splitting and 2D-FFT to propagation of continuous wave sources in nonlinear media. Chapter 7 will discuss nonlinear pulsed propagation. The concluding chapter will summarize this work and its main contributions, give recommendations for future work, and outline conclusions.

Chapter 2: Theoretical Background

2.1 Linear Propagation and the Small Signal Approximation

Ultrasound waves can be thought of as pressure variations in a media, which propagate periodically in space and time. To a first order approximation, ultrasound propagation is well described as a linear process, governed by a linear, second order homogeneous differential equation. The assumption of linear propagation, however, is valid only for relatively small disturbances.

In considering wave propagation in fluids, one can obtain the linear wave equation from the Navier-Stokes Equation by making a small signal approximation for the density and pressure, given by

(1)
$$\rho = \rho_o + \rho_1$$
$$p = p_0 + p_1$$

where the subscript 'o' denotes the equilibrium quantity, and the subscript '1' indicates the changes in the quantities, which are small. This small signal approximation leads to the well known equation

(2)
$$\kappa \rho_o \frac{\partial^2 p_1}{\partial t^2} = \nabla^2 p_1 + \kappa \left(\mu_B + \frac{4}{3}\mu \right) \frac{\partial}{\partial t} \left(\nabla^2 p_1 \right),$$

where μ_B is the bulk viscosity, μ is the shear viscosity, and κ is the adiabatic compressibility. This is a linear equation, and can also be expressed in terms of the normal particle velocity u, or the velocity potential ϕ.

In the frequency domain this becomes the homogeneous Helmholtz equation:

(3)
$$\nabla^2 \Phi + \underline{k}^2 \Phi = 0$$

where

(4)
$$\underline{k}^2 = \frac{k^2}{1 + j\omega\kappa \left(\mu_B + \frac{4}{3}\mu \right)}$$

and k is the wavenumber ω/c_o.

In the absence of viscous loss, the time domain equation becomes the familiar homogeneous wave equation:

(5) $\nabla^2\phi - \dfrac{1}{c_o^2}\dfrac{\partial^2\phi}{\partial t^2} = 0$

and the frequency domain equation looks the same except that $\underline{k} = k$.

It is useful to consider the 1-D version of this equation for particle velocity - and express it in the form:

(6) $\left\{\dfrac{\partial^2}{\partial t^2} - c_o^2\dfrac{\partial^2}{\partial z^2}\right\}u = 0$

which can be factored to obtain two uncoupled wave equations called reduced equations or evolution equations, one of which is:

(7) $\dfrac{\partial u(t,z)}{\partial z} = \dfrac{1}{c_o}\dfrac{\partial u(t,z)}{\partial t}$

which describes plane waves propagating in the positive z-direction. Going to retarded time, $\tau = t - z / c_o$ we have:

(8) $\dfrac{\partial u(\tau,z)}{\partial z} = 0$.

2.2 Attenuation

The assumption of viscous loss in the equation of state gives rise to a quadratic frequency dependence for the attenuation of the wave propagation. This assumption is only valid for thermo-viscous fluids, however, and is not true for tissue. Tissues generally have a more complicated loss model, and the attenuation coefficient is governed by a f^n dependence where n is typically in the range 1.1 to 1.5.

2.3 Propagation of Finite Amplitude Waves in Fluids

Many diagnostic and therapeutic ultrasound systems employ excitations for which the small signal approximation is not valid. Although linear analysis of propagation is a good first order approximation, nonlinear effects are often non-negligible. Disturbances which are large enough to invalidate the small signal approximation are often referred to as

finite amplitude waves. Finite amplitude wave propagation is a nonlinear process, and is a good deal more complicated than linear wave motion. A sound beam travelling through a medium will involve the effects of diffraction, absorption, and nonlinearity, and the sound beam can be thought of as interacting with itself as it propagates. In the following sections, sources of nonlinear distortion will be investigated, and the nonlinear equations of motion will be developed.

2.3.1 Nonlinear Distortion of Plane Waves

As an initial step to development of the full 3-D nonlinear wave equations, consider the simple case of a finite amplitude plane wave of normal particle velocity u in a dissipationless medium. One peculiarity of nonlinear acoustics is that the propagation speed of a wave depends on the amplitude of excitation. While it is true that the beginning and end of a pulse propagate with the small signal speed c_o, within the pulse, the propagation speed varies. The variation of propagation speed with initial amplitude is actually due to two separate effects: convection, and nonlinearity of the medium.

Convection effects can be thought of as being like an oscillating wind travelling with the wave. Overall, the oscillation propagates with small signal speed c_o, however, the peak of the oscillation will also have a local particle velocity u above and beyond the wave velocity c_o.

Effects due to the nonlinearity of the medium can be understood as a dependence of the speed of sound with temperature and pressure. The compression phase of a wave will cause a local increase in pressure and temperature compared with the rarefaction phase. Locally, an increase in pressure and temperature causes an increase in the speed of sound. Thus the compression phase of a wave travels faster than the rarefaction phase. Note that because the speed of sound is dependent on density, the plane wave impedance relation, is no longer a linear relation. The slope of a graph of pressure versus density, is thus not a straight line, but is rather a curve, where the local slope is proportional to the square of the speed of sound.

The general propagation speed of sound can thus be written as (Beyer, 1974)

$$(9) \qquad \frac{dx}{dt} = c_o + \beta u,$$

where we will call β the parameter of nonlinearity. We will show in section 2.3.2 that

$$(10) \qquad \beta = 1 + \frac{B}{2A}.$$

where first term (unity) is due to convection, and the second term ($B/2A$) is a parameter related to the nonlinear relationship between pressure and density. In the case where u is very low, the speed of sound reduces to c_o, the small signal speed. Convective and nonlinear effects can collectively be referred to as nonlinear effects, as both these effects will contribute a nonlinear term in the differential equations describing nonlinear propagation.

These nonlinear effects can contribute to distortion of a given initial waveform. The compression phase of a sinusoid, for example, will have a propagation speed greater than that of the rarefaction phase. In an ideal dissipationless medium, a sinusoid will thus distort into something which may approach a sawtooth wave, as illustrated in Fig. 1.

(a)

(b)
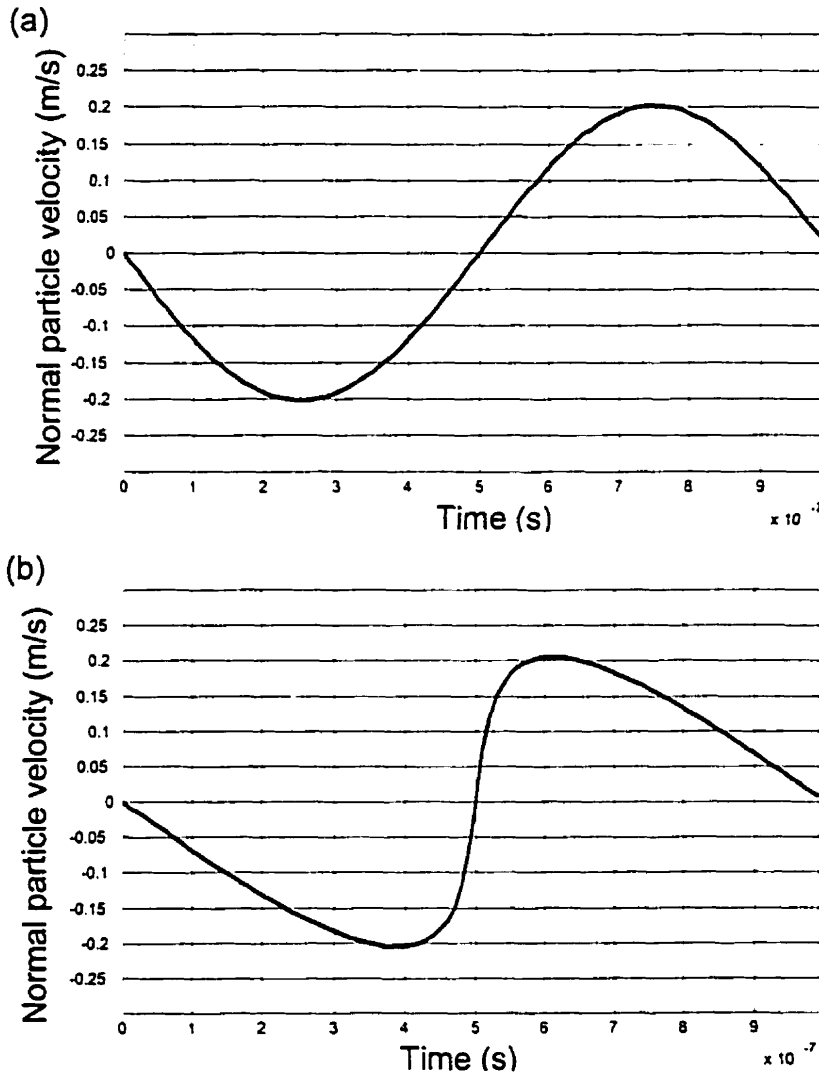
Figure 1 Effects of nonlinear distortion of a plane sinusoidal wave. (a) Initial waveform of a 1 MHz wave. (b) Showing the distortion after propagating 0.8 of the shock distance in a lossless medium where the coefficient of nonlinearity is given by $\beta=3.5$.

Nonlinear distortion of a waveform in the frequency domain represents generation of harmonics. A sinusoid distorting in the process of nonlinear propagation transforms a monofrequency source at f_o, into an entire spectrum of harmonics, at f_o, $2f_o$, $3f_o$, $4f_o$, ..., as shown in Fig. 2.

In addition to harmonics, sum and difference frequencies may be generated in the
nonlinear propagation process.
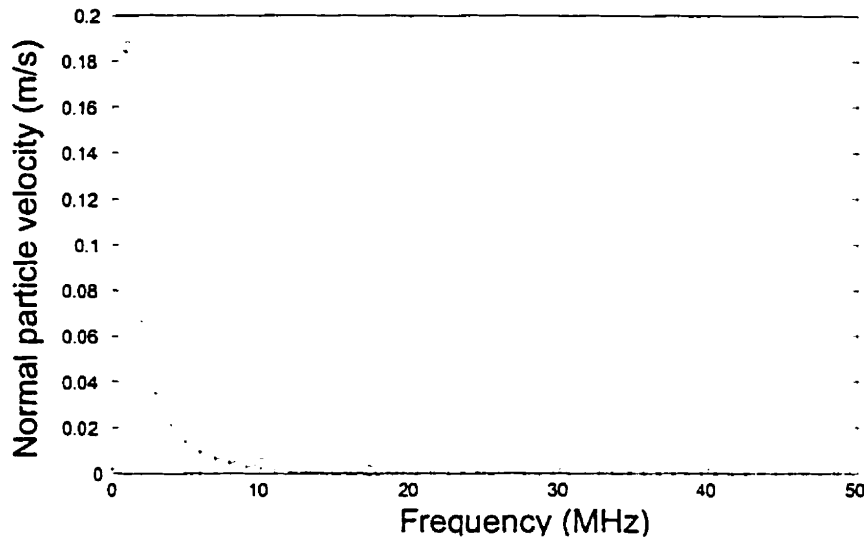
Figure 2: Frequency spectrum of the waveform in Fig. 1b. Harmonics above 10 MHz are
present in the spectrum.

2.3.2 The Parameter B/A

The thermodynamic relationship between pressure and density, is in general not a linear
one. The pressure-density relation can be written as $p=p(\rho,s)$, where $p=p_o+p_I$ and
$\rho=\rho_0+\rho_I$, and the subscripts denote the equilibrium and perturbation values respectively.
A Taylor series expansion can be done:

$$(11) \quad p_1 = \frac{\partial p}{\partial \rho}\bigg|_0 \rho_1 + \frac{1}{2!}\frac{\partial^2 p}{\partial \rho^2}\bigg|_0 \rho_1^2 + ... = A\frac{\rho_1}{\rho_o} + \frac{B}{2!}\left(\frac{\rho_1}{\rho_o}\right)^2 + \frac{C}{3!}\left(\frac{\rho_1}{\rho_o}\right)^3 + ...$$

where

$$(12) \quad A = \rho_o\frac{\partial p}{\partial \rho}\bigg|_o = \rho_o c_o^2, \quad B = \rho_o^2\frac{\partial^2 p}{\partial \rho^2}\bigg|_o, \quad C = \rho_o^3\frac{\partial^3 p}{\partial \rho^3}\bigg|_o$$

The first order measure of nonlinearity, B/A, is the parameter of nonlinearity (Beyer,
1974). The coefficient of nonlinearity is defined as

$$(13) \quad \beta = 1 + \frac{B}{2A}.$$

The Eulerian speed of sound under adiabatic conditions can be written as (e.g. Hamilton and Blackstock, 1998)

$$(14) \quad c = c_o + u + \frac{B}{2A}u = c_o + \beta u$$

It should be noted that for a linear medium, $\beta=0$ and $B/A=-2$ (rather than 0).

2.3.3 Reduced Nonlinear Wave Equations

The reduced evolution equation for finite amplitude waves in a non-dissipative medium can be written as

$$(15) \quad \frac{\partial u}{\partial t} + (c_o + \beta u)\frac{\partial u}{\partial z} = 0$$

By rearranging, doing a binomial expansion, assuming that $\beta u / c_o \ll 1$, and transforming to retarded time, we get the approximate form of the evolution equation of a plane wave, valid to second order (e.g. Hamilton and Blackstock, 1998):

$$(16) \quad \frac{\partial u}{\partial z} = \frac{\beta u}{c_o^2}\frac{\partial u}{\partial \tau}$$

This is often called the equation of nonlinearity, and has been solved in both time and frequency domain.

2.3.4 The Poisson Solution

Given the initial value problem $u(x,0)=G(x)$, or the boundary value problem $u(0:t)=F(t)$, a solution to the reduced wave equation can be written intrinsically as:

$$(17) \quad \begin{aligned} u &= G\{x - (\beta u + c_o)t\} \\ u &= F\{t - x/(\beta u + c_o)\} \end{aligned}$$

Essentially the solution represents distortion of the initial waveform, governed by the nonlinear compression of the argument.

2.3.5 The Fubini Solutin and Harmonic Generation

Assuming a sinusoidal plane source propagating in an inviscid medium, the Fubini solution (Fubini, 1935; Beyer, 1984) represents an Fourier series solution to the nonlinear equation. Given a source amplitude vo, the distorted wave can be represented as:

(18) $u = 2u_o \sum\limits_{n=1}^{\infty} \dfrac{J_n(nx/\bar{x})\sin n(\omega t - kx)}{nx/\bar{x}}$,

for $x/\bar{x} \leq 1$ and $\beta u_o / c_o \ll 1$, where

(19) $\bar{x} = \dfrac{c_o^2}{\beta \omega u_o}$

is the shock distance, which will be discussed later.

The Fubini Solution represents a frequency domain solution, and gives the amplitude of the nth harmonic as

(20) $u_n = \dfrac{2u_o J_n(nx/\bar{x})}{nx/\bar{x}}$

A plot of the harmonic amplitudes of a plane wave up to the shock distance is shown in Fig. 3.
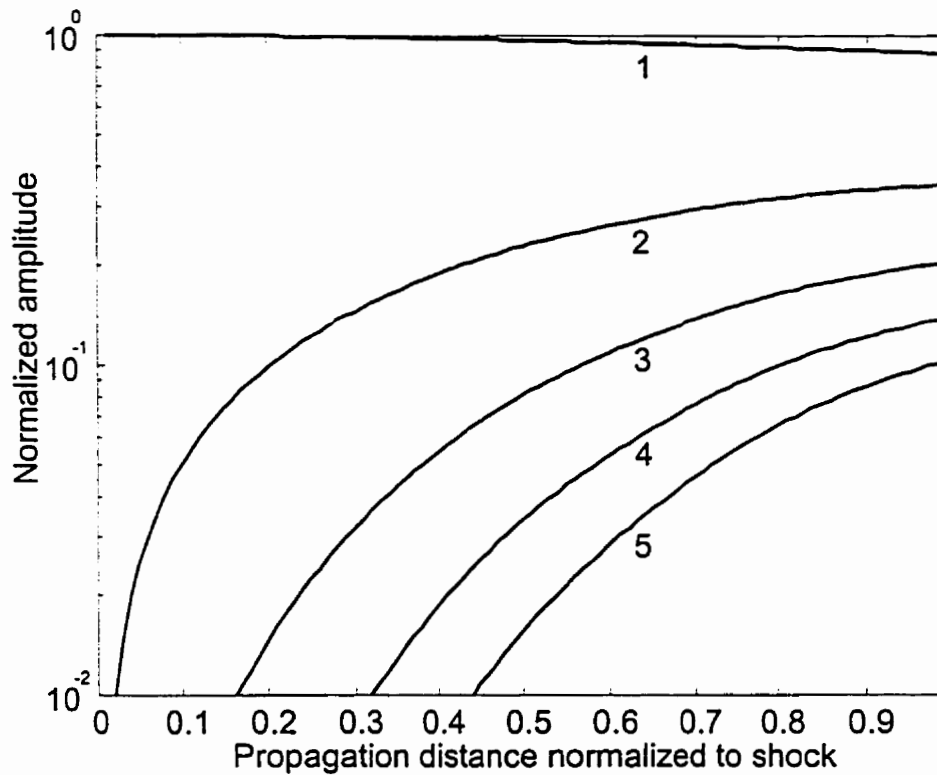
Figure 3 First five harmonic amplitudes generated from nonlinear plane wave propagation in a lossless medium.

2.3.6 Shock Waves

A shock wave is a very abrupt change in the pressure and particle velocity. For a plane wave travelling in a non-attenuating medium, a shock wave forms when the maximal slope of the wave becomes infinite. This happens at the shock formation distance $\bar{x}$. Although we do not expect shock waves in a tissue medium when diagnostic pressure levels are used, $\bar{x}$ will be used as a scaling parameter in the nonlinear algorithm.

2.3.7 The Effect of Attenuation and Burgers Equation

Attenuation will tend to dampen higher harmonics generated by nonlinear propagation. One way of accounting for attenuation for a plane wave in a viscous fluid is to add a viscous loss term to the nonlinear equation, resulting in

$$(21) \quad \frac{\partial u(z,\tau)}{\partial z} = \frac{\beta u}{c_o^2} \frac{\partial u}{\partial \tau} + \frac{1}{2c_o^3 \rho_o} \frac{\partial^2 u}{\partial \tau^2} \left(\mu_B + \frac{4}{3}\mu \right),$$

which is known as Burgers Equation (Beyer, 1974). We may note that in an attenuating medium, a plane wave will never really shock in the true sense, but rather, the 'shock-front' will have a finite thickness, rather than an abrupt discontinuity.

2.4 Modeling Finite Amplitude Sound Beams in 3-Dimensions

Approximations can be made to enable us to derive a second order differential equation describes acoustic propagation of finite amplitude waves without invoking the small signal approximation. The derivation makes use of the equations of state, motion, and continuity of a thermoviscous fluid..

2.4.1 The KZK Equation

The most widely used equation for modeling finite amplitude sound beam propagation, and which accounts for the effects of diffraction, nonlinearity, and absorption, is that due to Khokhlov, Zabolotskaya and Kuznetsov, which is commonly referred to as the KZK equation. It can be written as (Kuznetsov, 1971)

$$(22) \quad \frac{\partial^2 p}{\partial \tau \partial z} - \frac{c_o}{2} \nabla_\perp^2 p = \frac{1}{2c_o^3 \rho_o} \frac{\partial}{\partial \tau} \left[(\mu_B + \frac{4}{3}\mu) \frac{\partial^2 p}{\partial \tau^2} + \beta \frac{\partial p^2}{\partial \tau} \right]$$

where

$$\nabla_\perp^2 = \frac{\partial^2}{\partial x^2} + \frac{\partial^2}{\partial y^2}$$

is the transverse Laplacian operator. Moreover, it can be cast in the form of an evolution equation by taking the temporal (retarded time) integral of the above equation. We could also express the KZK equation in terms of the z-component of the particle velocity by using a linear plane-wave impedance relation, $u_z \approx p/(\rho_o c_o)$, which is valid to the order of the approximations made in the derivation of the KZK equation.

2.4.2 Approximations in the KZK Model

An excellent summary of the approximations used to synthesize the second order KZK equation can be found in Hamilton and Blackstock (1998; Ch. 3).

The right hand side of equation (22) describes absorption and nonlinearity, and the left hand side describes spatial evolution and diffraction. The KZK equation describes quasi-plane wave propagation, and is based on the so called parabolic approximation, which is that the angular spectrum is assumed to be sufficiently narrow so that the wave will be close to planar, and evolving slowly in the z-direction. This approximation is not valid for strongly focused beams or for beams with strong irregularities in the transverse structure, such as occurs in the nearfield zone. Thus, the model is limited to cases where diffraction effects are minimal and focusing gains are small. The parabolic approximation is valid for focused sources provided that

$$d/a \gg 1, \text{ and } z > \frac{1}{k}\left(\frac{d}{a}\right)^{4/3},$$

where d is the focal length.

The KZK equation provides a reasonable approximation to the ultrasonic field for sources whose aperatures are large compared to the wavelength ($ka \gg 1$), for observation points that are beyond a few source radii, and for points whose off axis locations are not too great.

One significant drawback of the KZK equation is that its scope of validity is restricted to thermoviscous fluids. The viscous absorption term in the KZK equation implies an attenuation coefficient proportional to ω^2 as opposed to a near linear dependence as is the case in soft tissue.

In the next chapter, a discussion of numerical methods for solving the KZK equation, will also include a brief description of how arbitrary attenuation may be accounted for in a computational scheme to solve the KZK.

Chapter 3: Background on Numerical Methods

The subject of numerical modeling of nonlinear propagation has received modest attention, and a number of authors have contributed to the subject. The book edited by Hamilton and Blackstock (1998) is an excellent resource on the subject, and contains a thorough literature review. In this chapter we shall discuss some of the contributions to 1-D (plane wave) and 3-D nonlinear propagation, including the effects of diffraction, attenuation and nonlinearity, that are relevant to the contributions of this thesis.

3.1 Computational Models for Nonlinear Plane Wave Distortion

3.1.1 Frequency Domain Algorithm

A frequency domain solution to Burgers equation may be obtained by considering a trial solution of the form

$$(1) \qquad v(z,\tau) = \frac{1}{2} \sum_{n=-\infty}^{\infty} v_n(z) e^{j2\pi f_o n\tau} ,$$

where $v_n(z)$ is a complex amplitude weighting function for the nth harmonic of frequency f_o, and τ is the retarded time $\tau = t-z/c$. By substituting this into (21) of chapter 2, the Frequency Domain Solution to Burgers Equation (FDSBE) can be shown to be given by

$$(2) \qquad v_n(z + \Delta z) = v_n(z) + j \frac{n}{4} \left(\frac{\beta 2\pi f_o}{c_o^2} \right) \Delta z \left\{ \sum_{m=1}^{n-1} v_m v_{n-m} + 2 \sum_{m=n+1}^{M} v_m v_{m+n}^* \right\} - (\alpha_o f_n^2) v_n \Delta z .$$

This expression involves two quadratic sums, the first representing accretion of the nth harmonic by a nonlinear combination of other harmonics that have a sum frequency of nf_o. With conjugation, the second quadratic sum may be interpreted as depletion of the nth harmonic harmonics with difference frequencies nf_o. Note that to make the computation realizable, (2) assumes that the solution to Burgers equation can be represented by a finite number of harmonics. When there is no attenuation, (2) is valid only up to the shock distance, and the solution becomes equivalent to Fubini's solution given by (18) in chapter 2. Fenlon (1971) was the first to derive coupled spectral equations that are equivalent to (2). He investigated mono and bi-frequency sources (including cylindrical and spherical spreading. Korpel (1980) presented coupled spectral

18

for arbitrary absorption and dispersion in progressive plane waves. To do this one may make the substitution

(3) $\quad \alpha_o f_n^{\ 2} \rightarrow \alpha_n + jd_n$,

in (2), where α_n is the attenuation coefficient, and d_n is the dispersion coefficient for the nth harmonic. Attenuation may often be modeled by a power law relation, described by

(4) $\quad \alpha_n = \alpha_o f_n^b$,

where α_o is a constant, f_n is the frequency of the nth harmonic, and b is an arbitrary real number. For biological tissue, b is typically between 1.1 and 1.5. The dispersion coefficient may be expressed as

(5) $\quad d_n = n\omega_o \bar{x}(c_n^{-1} - c_o^{-1})$,

and accounts for the deviation of the phase speed c_n of the nth harmonic component from the infinitesimal sound speed of the fundamental c_o.

Haran and Cook (1983) also investigated plane wave nonlinearity using the FDSBE, but used a somewhat different form from that given by (2), which we were unable to verify. Christopher and Parker (1991) also cite a form for the FDSBE that differs from (2). It should be noted that the form of the FDSBE given by (2) is quoted in Hamilton and Blackstock (1998; pp.313-314). We have verified that in the limiting case where there is no attenuation, the numerical results obtained by using (2) reduce to those obtained using the Fubini solution.

The main disadvantage of the FDSBE is that hundreds or thousands of harmonics may be required to accurately propagate pulses or waves which develop shockfronts, and as a result, the computational burden can be large. A promising algorithmic approach to reducing the number of harmonics required for propagation of waveforms with one (and only one) shockfront is that introduced by Pischkal'nikov et. al (1996). The premise of their scheme is that a shockwave may be thought of as a sum of a perfect sawtooth wave and smoothly varying (unshocked wave), which is well represented by only a few (for example 30 or less) harmonics. Because the Fourier transform of a sawtooth wave is exactly known, an infinite number of harmonics may be retained in the spectrum of a

shockwave by approximating higher harmonic amplitudes by the analytic amplitudes from the idealized sawtooth wave.

3.1.2 Time Domain Solutions

In the time domain, we cannot easily incorporate attenuation into finite amplitude wave propagation. The nonlinear equation itself, however, can be solved in the time domain, without attenuation. Two approaches have been taken to the time domain solution to the nonlinear algorithm: (I) an interpolation-based Poisson solution, and (II) Christopher's time domain solution.

The Interpolation-Based Poisson Solution

To describe the nonlinear distortion of a waveform as it propagates from z ro $z+\Delta z$, the Poisson solution (eq. (17) of section 2.3.4) may be written as

$$(6) \qquad u(z + \Delta z, \tau) = u\left\{ z, \tau + \frac{\beta \Delta z}{c_o^2} u(z, \tau) \right\}.$$

Multivalued solutions can be avoided if the step size satisfies

$$(7) \qquad \Delta z < \frac{c_o^2 / \beta}{\max(\partial u / \partial \tau)}.$$

Equation (9) can be numerically implemented by sampling the temporal waveform, and making use of a discrete time-based transformation

$$(8) \qquad \tau_m^{n+1} = \tau_m^n - \frac{\beta \Delta z_n}{c_o^2} u_m^n,$$

where m is the index of the temporal waveform and n represents the nth step Δz_m in z (e.g. Tavakkoli et. al. 1998). The discrete version of the inequality (7) can be written as

$$(9) \qquad \Delta z_n < \left[\tau_m^n - \tau_{m-1}^n \right] \frac{c_o^2 / \beta}{\max(u_m^n - u_{m-1}^n)},$$

Subsequent to this non-uniform, discrete transformation, linear interpolation can be used to resample the waveform, and thus to re-establish a uniform temporal grid. A discussion of the dimensionless form of this algorithm may be found in Hamilton and Blackstock (1998).

Christopher's Time Domain Nonlinear Propagation Algorithm

Christopher (1993) uses a slightly different nonlinear algorithm. It is valid for plane wave nonlinear propagation in a dissipationless medium. His approach is based on the relation

$$(10) \quad u(z + \Delta z) = \frac{u(z)}{1 - \frac{\beta \Delta z}{c_o^2} \frac{du}{dz}},$$

which describes the incremental change in amplitude of the waveform at identical temporal locii after propagating a distance Δz. It is valid for all but very large-amplitude waves ($u \ll c_o/\beta$). He has also derived a more general relationship that is valid for any amplitude. In the discrete implementation of (10), a forward difference du/dt operator is applied to the positive velocity samples, and a backward difference du/dt operator applied to the negative velocity samples. A three point (quadratic) Adams-Bashforth formula (Atkinson, 1978) is used for both the forward and backward difference du/dt operator. For a forward difference computation, the operator is

$$(11) \quad \frac{du}{dt} = \frac{1}{2}\left[3\left(\frac{u(t + \Delta t) - u(t)}{\Delta t} \right) - \left(\frac{u(t + 2\Delta t) - u(t + \Delta t)}{\Delta t} \right) \right],$$

and the backwards difference operator is given by

$$(12) \quad \frac{du}{dt} = \frac{1}{2}\left[3\left(\frac{u(t) - u(t - \Delta t)}{\Delta t} \right) - \left(\frac{u(t - \Delta t) - u(t - 2\Delta t)}{\Delta t} \right) \right].$$

Further precautions are needed to propagate shockfronts. First, shock segments are identified by locating consecutive samples for which there is a change above some threshold level. Next, consecutive shock segments are consolidated into shockfronts, and then propagated as a whole without further steepening. Thus, Christopher's scheme is implicity harmonic-limited, and allows considerable computational savings, while offering great stability, and demonstrating reasonable accuracy.

3.2 Numerical Models of Nonlinear Sound Beam Propagation in 3-Dimensions

There are few analytic solutions to the equations of nonlinear propagation, and such solutions are for very specialized conditions. In general, numerical methods must be used, and these will be discussed under the following headings:

(1) Numerical Solutions to the KZK equation

(2) Time Domain Method of Tavakkoli et. al.

(3) Frequency Domain Method of Christopher and Parker

3.2.1 Numerical Solutions to the KZK Equation

The KZK equation has been solved in a number of ways using time domain, frequency domain, or combined time-frequency domain algorithms. All of the approaches are based on the time-integral of the KZK equation in retarded time, given by

$$(13) \quad \frac{\partial p}{\partial z} = \frac{1}{2c_o^3 \rho_o} \left[\left(\mu_B - \frac{4}{3}\mu \right) \frac{\partial^2 p}{\partial \tau^2} + 2\beta p \frac{\partial p}{\partial \tau} \right] - \frac{c_o}{2} \int_{-\infty}^{\tau} (\nabla_\perp^2 p) d\tau .$$

Combined Time-Frequency Domain Algorithm

Bakhvalov et. al. (1976, 1978a-b, 1979a-c, 1980) used a dimensionless form of (13), and solved for diffraction and absorption in the frequency domain. Their approach calculates nonlinear distortion in the time domain using the method of Godunov (1959) which is based on weak shock theory. In this fractional step / operator splitting approach, they used standard backward difference methods to propagate step by step the effects of diffraction and absorption, and of nonlinearity. Their calculations were restricted to axisymmetric Gaussian, plane and focused sources. Alternative algorithms that solve for attenuation and diffraction in the frequency domain, and nonlinearity in the time domain have been presented by McKendree (1981) and Froysa et. al. (1993).

Frequency Domain Algorithm

The most widely used approach for analyzing periodic signals radiated from circular pistons, both focused and unfocused, is a frequency domain approach first developed by Aanonsen et. al. (1984), and is widely referred to as the Bergen code. They substituted expansion (1) into the KZK equation to get a system of equations, which they then integrated numerically using a simple implicit backward difference scheme. Their work was primarily for nearfield studies. Baker et. al. (1988) verified the accuracy of this numerical KZK solution by comparing with experiment in the case of a CW plane disk radiator in a water medium. Hamilton et. al. (1985) introduced a transformation to

improve the efficiency of the algorithm in the far-field. For focused beams, a modification of the coordinate transformation was introduced by Hart and Hamilton (1988). Other frequency domain studies have investigated radiation from bifrequency (Kamakura et. al. 1989; Naze Tjotta et. al. 1990; Naze Tjotta et. al. 1991), pulsed (Baker and Humphrey, 1992), and rectangular (Kamakura et. al., 1992; Baker et. al. 1995) sources. Averkiou et. al. (1995) used the spectral code developed by Naze Tjotta et. al. (1991) to compare theoretical model predictions with experiments for finite amplitude propagation in water from a focused piston.

Cahill and Baker (1997a,b; 1998) used a non-axisymetric version of the Bergen code, to simulate the acoustic field of a phased array medical scanner for water propagation. They demonstrated that nonlinearity can interact with diffraction in such a way as to move the peak region of intensity off-axis, and to cause the focal region to shift towards the transducer.

Time Domain Algorithm

A first order operator splitting approach introduced by Lee and Hamilton (1995), allows a numerical solution to be implemented in the time domain. Their technique breaks up diffraction, nonlinearity and absorption into separate evolution equations and invokes field propagation using a fractional step marching scheme.

In dimensional coordinates, the operator splitting scheme decomposes the retarded-time integral of the KZK into the following three equations:

(14) $\quad \dfrac{\partial p}{\partial z} = \dfrac{-c_o}{2} \int_{-\infty}^{\tau} (\nabla_{\perp}^2 p) d\tau \equiv L_D \cdot p \qquad$ (Diffraction)

(15) $\quad \dfrac{\partial p}{\partial z} = \dfrac{\beta p}{c_o^3 \rho_o} \dfrac{\partial p}{\partial \tau} \equiv L_N \cdot p \qquad$ (Nonlinearity)

(16) $\quad \dfrac{\partial p}{\partial z} = \dfrac{(\mu_B + \frac{4}{3}\mu)}{2c_o^3 \rho_o} \dfrac{\partial^2 p}{\partial \tau^2} \equiv L_A \cdot p \qquad$ (Absorption)

To first order in terms of the propagation distance Δz, one may show that these equations are independent of each other, so that the total change in pressure can be approximated by the sum of these contributions, i.e.,

(17) $\dfrac{\partial p}{\partial z} = L_N \cdot p + L_A \cdot p + L_D \cdot p$.

As illustrated in Fig. 1, the principle underlying the fractional step algorithm is to first solve the diffraction equation for a plane to plane propagation, then apply absorption, and finally to solve the nonlinearity equation over the distance Δz.
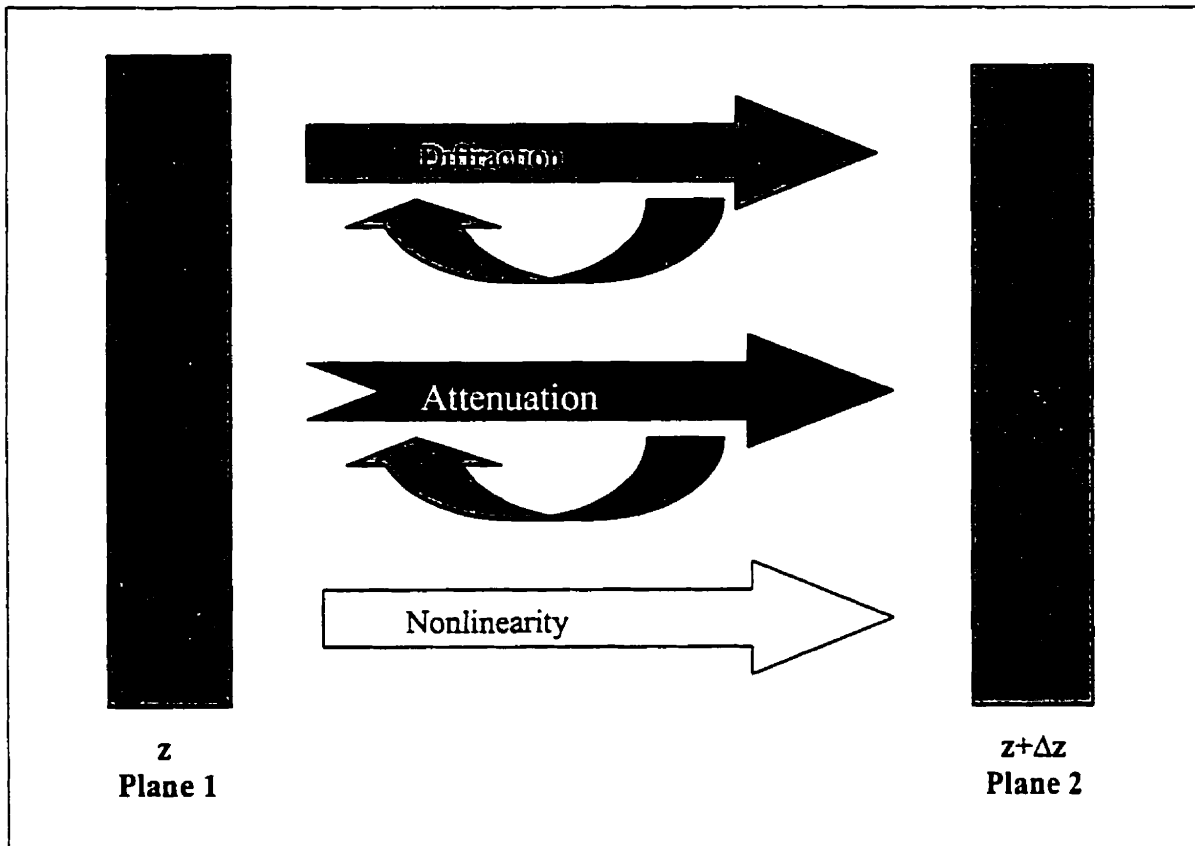
Figure 1 Schematic representing an operator splitting technique. Planes 1 and 2 are an incremental distance Δz apart. By solving for the effects of diffraction, attenuation, and absorption independently over this small step, their combined effects can be well approximated.

The same procedure can be done for the next incremental plane to plane propagation, thus propagating the sound beam in an incremental march over small distances Δz.

The time domain algorithm is well suited to pulsed propagations, and to very large amplitude continuous wave propagation. Of particular note is the work of Averkiou et. al. (1993), who modeled self-demodulation in strongly absorbing fluids, and that of Cleveland et. al., (1996), who investigated the effect of relaxation.

Accuracy and Computational Burden

While KZK methods have been shown to give accurate results for sound beam propagation in water, little work has been done to verify the accuracy of the KZK for other media such as tissue. Computational requirements can become an issue for nonlinear modeling. Baker (1998) comments that the continuous wave field response from an axisymmetric source at moderate drive levels can be run on a personal computer in a matter of minutes. When the drive level is increased, more harmonics are needed, thus incurring more memory and computational time requirements. Pulsed waveforms are also more demanding since a wide spectrum of frequency components must be included. A non-axisymmetric source geometry can cause an order of magnitude increase in the computational burden. The results of Cahill and Baker (1997b) required about 500MB of physical memory and took approximately 40 hours on a DEC alpha 8400 computer.

3.2.2 The Time Domain Method of Tavakkoli et. al.

Tavakkoli et. al. (1998) have developed a time domain numerical model based on the second order operator splitting technique illustrated in Fig. 2. The model avoids the parabolic approximation by using the Rayleigh integral to compute the effects of diffraction. The effects of attenuation and nonlinearity are computed in the time domain over small steps. Attenuation is modeled by a minimal phase FIR filter, which is convolved with the source waveform.

For pulsed propagation, Tavakkoli's method has the advantage of using fairly big Δz steps between propagation planes, but suffers from long computation times for the diffractive steps (~90% of the total CPU time).
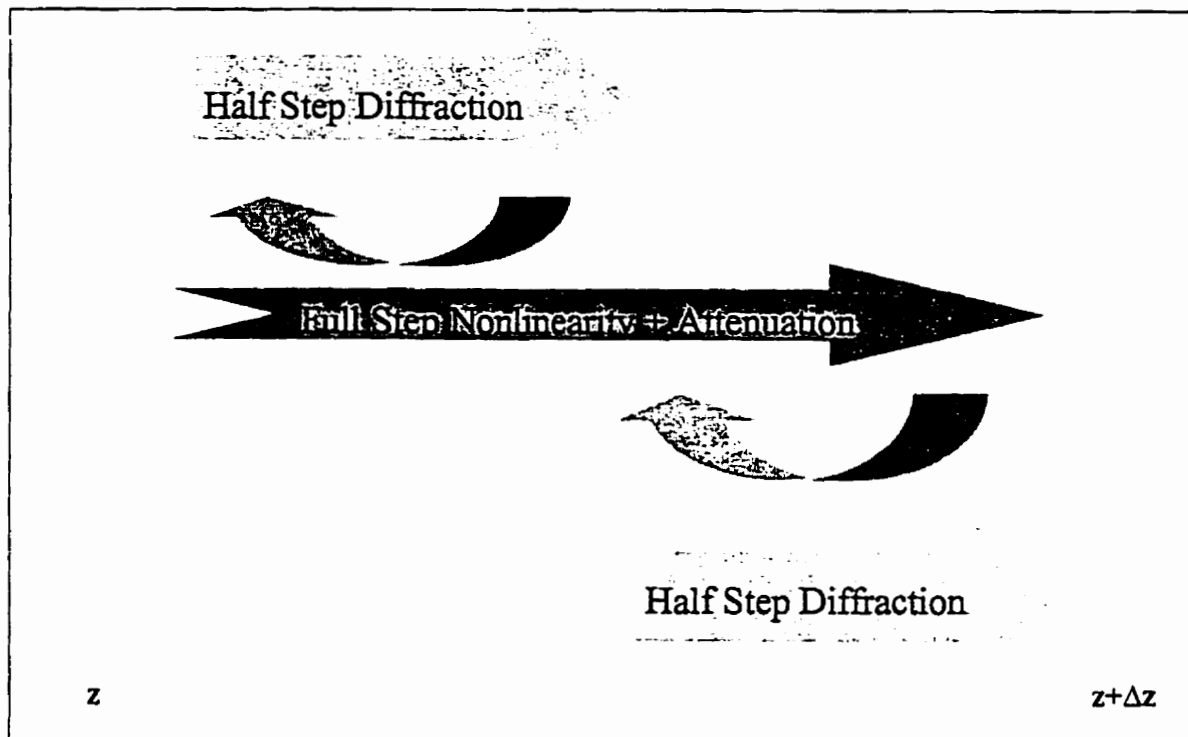
Figure 2 The second order operator splitting method of Tavakkoli et. al. (1998). In this scheme the combined effects of diffraction, attenuation, and nonlinearity are approximated to a second order in the incremental distance Δz.

3.2.3 Christopher's Method

Christopher and Parker (1991) used a frequency domain approach to modeling nonlinear propagation for an axisymmetric geometry. Like other fractional step approaches, they compute the effects of diffraction, attenuation, and nonlinearity over small steps. They used a discrete Hankel transform - based angular spectrum approach to compute diffraction and attenuation. Like the scheme of Tavakkoli et. al. (1998), their diffraction algorithm does not assume the parabolic approximation. For nonlinearity, a frequency domain algorithm similar to the one presented in section 3.1.1 is used. Christopher's

method allows simulation of nonlinear propagation through media with arbitrary
absorptive characteristics, and has impressive computational efficiency. Their approach
has been applied to the modeling of highly focused lithotripter sources (1994), and for
simulation of nonlinear-based imaging (1997).

Chapter 4: A New Approach to Modeling Nonlinear Ultrasound Propagation in Tissue

The previous two chapters have mentioned theoretical and numerical schemes for modeling nonlinear ultrasound propagation. Directional (finite amplitude) sound beam propagation in thermoviscous fluids has been modeled by the so called 'KZK' equation. It was noted that the viscous loss model of the KZK equation leads to an attenuation coefficient with a quadratic frequency dependence, and which does not describe the near-linear frequency relationship of most tissues. Many of the numerical methods based on the KZK equation were restricted to thermoviscous fluids, and thus are not appropriate for modeling finite amplitude propagation in tissue. Although it is possible to model finite amplitude propagation in a tissue medium using the frequency domain solution to the KZK equation, the computational burden can be heavy, especially for pulsed propagation, and non-axisymmetric sources. The methods of Christopher and Parker (1991), and Tavakkoli et. al. (1998) have enabled accurate modeling of nonlinear propagation in tissue. In the approach used by Tavakkoli et. al. the Rayleigh integral is used to compute the effects of diffraction, and is thus computationally burdensome. Christopher and Parker use a fast transform approach to diffractive propagation. Although it affords some computational savings, their approach, like others, is computationally intense for propagation of pulsed excitations, and for non-axisymmteric sources. In this chapter, a new method of modeling is introduced, which not only builds on the strengths of previous algorithms, but which also aims to gain some degree of computational savings compared with these schemes.

4.1 An Evolution Equation for Finite Amplitude Propagation in Tissue

Our approach to modeling propagation in tissue may be viewed as a phenomenological one. We start with a model evolution equation, valid for quasi-plane wave sound beams, given by

(1) $$\frac{\partial v}{\partial z} = L_A \cdot v + L_N \cdot v + L_D \cdot v$$

where L_A, L_N, and L_D are operators representing absorption, nonlinearity, and diffraction respectively, and v is the normal particle velocity.

28

Our hypothesis is that operators L_D, L_A, and L_N exist such that the evolution equation (1) accurately describes finite amplitude propagation in tissue. It is our belief that such a hypothesis is well founded. Partial justification of using (1) is that the KZK equation can be written in a form equivalent to (1) by integrating with respect to retarded time, to obtain (3.22), where the operators are defined by (3.21). We feel that propagation in tissue is likely similar to propagation in thermoviscous fluids, with only attenuation mechanisms being significantly different. Experimental confirmation of this hypothesis stems from the efforts by Tavakkoli et. al. (1998). They used equation (1) as a basis for their model and obtained reasonable agreement with experiments of finite amplitude propagation in a tissue mimicking fluid. Moreover, it can be shown that the approach of Christopher and Parker is equivalent to a first order operator splitting of an equation equivalent to (1). Thus although (1) is not derived from elementary principles of physics as is the KZK equation, there is ample evidence that it can accurately model finite amplitude propagation in arbitrary media, including biological tissue.

4.2 A Second Order Operator Splitting Technique

Our approach to solving (1) will employ an operator splitting scheme so as to solve for the equations of diffraction, attenuation, and nonlinearity separately over small steps. To introduce the operator splitting techniques of this thesis, some notation will first be developed. Consider first the process of diffraction. Given the normal particle velocity field profile $v(x,y,z_1;t)$ across a plane $z = z_1$, we may represent the field profile across plane $z = z_2$ assuming diffractive propagation only (no nonlinearity or attenuation) by introducing an operator $\Gamma_{D,\Delta z}$, such that $v(x,y,z_2;t) = \Gamma_{D,\Delta z}v(x,y,z_1;t)$. The two planes $z=z_1$ and $z=z_2$ are spaced a distance Δz apart. $\Gamma_{D,\Delta z}v(x,y,z_1;t)$ then represents a solution at $z=z_1+\Delta z$ to the diffraction sub-equation

(2) $$\frac{\partial v}{\partial z} = \hat{L}_D \cdot v ,$$

with the initial condition $v=v(x,y,z_1;t)$.

Similarly, we may define propagation operators $\Gamma_{N,\Delta z}$ and $\Gamma_{A,\Delta z}$ for nonlinearity and absorption respectively. There is a relationship between the operators Γ and the operators

L of (1), which will be explained in Appendix A. For now it will suffice to say that $v(x,y,z_2;t) = \Gamma_{N,\Delta z}v(x,y,z_1;t)$ is a solution to the nonlinear sub-equation, and $v(x,y,z_2;t) = \Gamma_{A,\Delta z}v(x,y,z_1;t)$ is a solution to the absorption sub-equation given the initial condition $v = v(x,y,z_1;t)$ on plane $z = z_1$.

As our approach is similar to that of Christopher and Parker (1991), it is important to note that their modeling methodology is equivalent to a first order operator splitting, which may be represented as:

(3) $v(x,y,z_2;t) \equiv \Gamma_{D+A+N,\Delta z}v(x,y,z_1;t) = \Gamma_{D+A,\Delta z}\Gamma_{N,\Delta z}v(x,y,z_1;t) + O(\Delta z^2)$,

where $\Gamma_{D+A+N,\Delta z}v(x,y,z_1,t)$ represents a solution at $z = z_1 + \Delta z$ to (1), and $\Gamma_{D+A,\Delta z}v(x,y,z_1,t)$ represents a solution at $z = z_1 + \Delta z$ to the sub-equation

(4) $\dfrac{\partial v}{\partial z} = L_D \cdot v + L_A \cdot v$

given the initial contition $v = v(x,y,z_1,t)$. In words, (3) says that the combined effects of diffraction, absorption, and nonlinearity can be approximated by one incremental step of combined diffraction and attenuation, followed by one step of nonlinearity. In Appendix A, we will prove the first order nature of this scheme.

Tavakkoli et.al. (1998) proved a second order operator splitting,

(5) $v(x,y,z_2;t) \equiv \Gamma_{D+A+N,\Delta z}v(x,y,z_1;t) = \Gamma_{D,\Delta z/2}\Gamma_{N+A,\Delta z}\Gamma_{D,\Delta z/2}v(x,y,z_1;t) + O(\Delta z^3)$,

which was illustrated in Fig. 2 of chapter 3.

Tavakkoli et. al. used adaptive step sizes – large steps in the nearfield and smaller steps in the focal region. Even for strong pressure amplitudes from a highly focused transducer, the use of only 23 planes out to the focal region sufficed, and impressive agreement with experimental results were reported. In contrast, Christopher's approach required hundreds or thousands of fractional steps out to the focal region of a transducer. Similarly, the finite difference techniques used to solve the KZK equation required relatively fine axial meshing.

In addition to using Tavakkoli's second order operator splitting method, we propose a slight variation of their theorem to allow combination of diffraction and attenuation together. The operator splitting approach we propose may be written as:

(6) $\quad v(x,y,z_2;t) \equiv \Gamma_{D+A+N,\Delta z}v(x,y,z_1;t) = \Gamma_{D+A,\Delta z/2}\Gamma_{N,\Delta z}\Gamma_{D+A,\Delta z/2}v(x,y,z_1;t) + O(\Delta z^3)$

which, like the Tavakkoli (1998) operator splitting, is second order in the small ordering parameter Δz. This operator splitting is illustrated in figure 2.

Half Step Diffraction + Attenuation

Full Step Nonlinearity

Half Step Diffraction + Attenuation

Plane $z=z_1$

Plane $z_2=z_1+\Delta z$
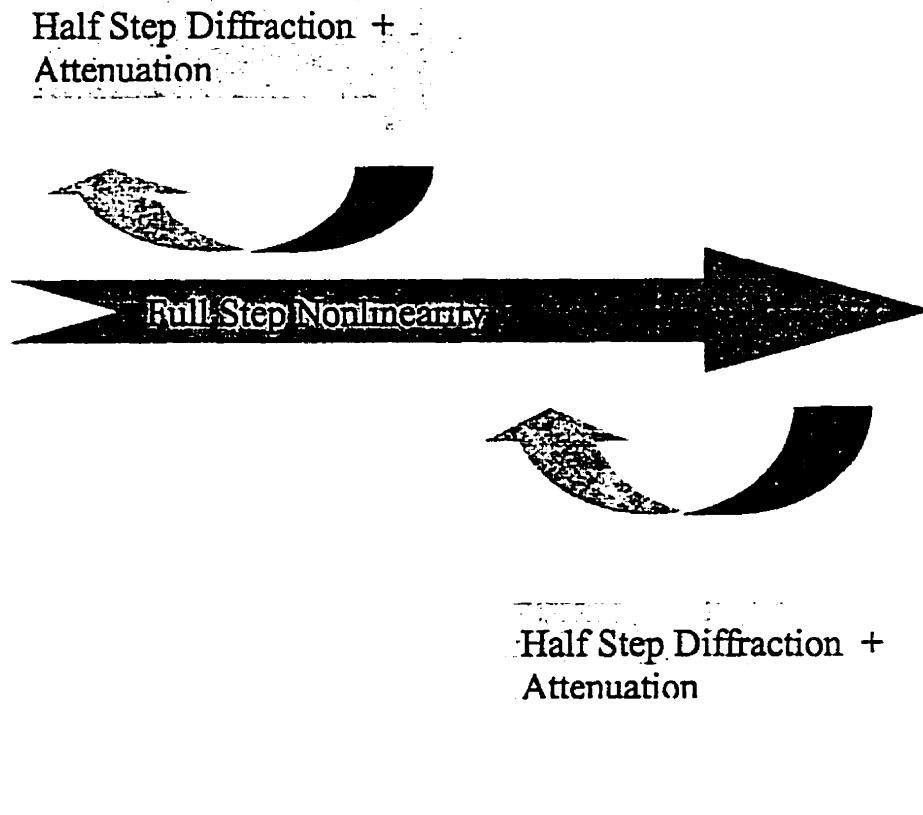
Figure 2 Illustration of the proposed second order operator splitting theorem.

Proof of (6) is provided in Appendix A. It should be noted that both second order operator splitting methods can be used within the context of the KZK equation. Proof of a second order operator splitting algorithm for the KZK equation is also given in Appendix A.

It is hoped that by taking advantage of the larger axial steps which these second order operator splitting schemes allow, and by using faster algorithms for diffraction, considerable computational savings can be obtained.

4.3 Proposed Fractional Step Marching Scheme

To model the nonlinear propagation of a sound beam, our approach will be to divide the region of propagation into parallel planes separated by incremental distances Δz.
The second order operator splitting presented in section 4.2 can be applied to solve for the effects of diffraction, nonlinearity, and absorption over these small steps. Thus, we propose a fractional step marching scheme, which progresses from plane-to-plane along the direction of propagation.

In solving the diffraction sub-equation (2), or the sub-equation combining diffraction and attenuation (4), we may guess that a solution to either of these equations must also be a solution to the homogeneous wave equation, as this is the equation which governs linear propagation phenomena. When the parabolic approximation is made, as is the case for the KZK equation, the solution to the sub-equations are only approximations to the true field which is a solution to the homogeneous wave equation. The approaches of Tavakkoli and Christopher do not make the parabolic approximation, and diffraction is computed exactly.

Like the KZK equation, our model equation (1) of this chapter is only valid for quasi-plane wave sound beams. The quasi-plane approximation assumes that the sound beam is directional and that the angular spectrum is narrow. Thus the nonlinear substep used in a fractional step marching scheme, based on an operator splitting of our model equation is lacking multi-directionality of propagation. It is assumed that the nonlinear propagation

process is strictly in the z (axial) direction. In Tavakkoli's operator splitting approach, both nonlinearity and attenuation are combined together, and thus both processes assume propagation only in the z-direction. In the operator splitting (6) which we prove, absorption and diffraction are combined together. Combining these two effects takes into account the directionality of component ray-paths which are added and attenuated in a linear way. Moreover, the parabolic approximation need not be made and diffraction may be calculated exactly. Because of these reasons, a fractional step marching scheme based on (6) may prove to be more accurate in the near-field than the KZK approach. This prospect will not, however, be investigated, as the very nearfield is of little importance to simulating medical ultrasound systems.

One disadvantage of using a fractional step marching scheme to solve for nonlinear propagation is that modeling errors may accumulate over many fractional steps, and the scheme may become inaccurate at best and unstable at worst. Algorithmic burden, on the other hand is problematic. Often there is an inherent tradeoff between accuracy and computational efficiency, and good judgement must be used in reaching a suitable compromise between the two. The choice of an accurate yet efficient way of computing the effects of diffraction, attenuation, and nonlinearity is thus key to developing a simulation tool for harmonic imaging.

4.4 Choosing Efficient Algorithms for Calculating the Effects of Nonlinearity, Diffraction, and Absorption

One of the prime objectives of this work is to develop a model of nonlinear propagation which is as computationally efficient as possible. With the operator splitting, and fractional step marching schemes presented in sections 4.2 and 4.3, the task of computationally efficient modeling reduces to finding algorithms for diffraction, absorption, and nonlinearity which have minimal computational burdens, and yet are as accurate as possible.

4.4.1 The Choice of a Nonlinear Algorithm

For continuous wave sources, the frequency domain solution to Burgers equation (FDSBE) is a good choice for a nonlinear (plane-wave) algorithm. We use the FDSBE presented in chapter 3, when moderate drive levels are simulated. For very high amplitude excitations, a number of authors comment on the benefits of calculating nonlinearity in the time domain.

The time domain nonlinear algorithm presented by Christopher (1994), and described in section 3.1.2, will be used for pulsed excitation modeling, since it offers great stability, is implicitly harmonic-limited (and thus efficient), and is reasonably accurate.

4.4.2 The Inclusion of Absorption

Absorption can be calculated together with either the diffraction or the nonlinear algorithms. If nonlinearity is modeled in the time domain, we will couple absorption with the diffraction algorithm. If nonlinearity is modeled in the frequency domain, absorption may be included with the nonlinear algorithm (for stability), or with the diffraction algorithm.

4.4.3 The Choice of a Diffraction Algorithm

The choice of an efficient diffraction algorithm was a primary focus of this thesis. Its importance is illustrated by the observation that for the algorithms of Tavakkoli et. al., which used the Rayleigh integral for the diffraction computation, 90% of the CPU time was being used on the diffraction substeps.

Other established methods of computing diffractive propagation include the impulse response method, and the angular spectrum technique. A brief review of these techniques will be provided in sections 4.5 and 4.6.

A suitable diffraction algorithm for the proposed fractional step marching must meet the following requirements:

- Computationally efficient

- Plane to plane

- Valid for non-separable, and non-axisymmetric field distributions. (by non-separable, we mean that a field distribution need not be separable into a product of time and space functions of the form $G(x,y,z)F(t)$).

- Reasonably accurate in the nearfield (because we intend to use a fractional step marching scheme, nearfield inaccuracies may propagate out of control)

- Suitable for a linear phased array, and other transducers with and without apodization.

- Should include the possibility of beam steering.

- Easy to include attenuation, refraction and reflection

- Some way of choosing adequate spatial sampling so as to ensure accurate modeling results

4.5 A Comparative Evaluation of Algorithms for Calculation of Diffraction

Here we consider a few diffraction algorithms and their suitablility for our proposed nonlinear algorithm. Suppose we wish to compute the particle velocity or velocity potential for all points in a plane a distance Δz away from a transducer or source plane at axial coordinate $z = z_o$. Suppose the normal particle velocity distribution of the source plane is $v(x,y,z_o,t)$.

Computation of the velocity or velocity potential will be done discretely, so let us suppose that the x-axis is quantized into N_x discrete values, the y-axis into N_y values, and time into N_t values. (If cylindrical coordinates (r,θ) are used N_x and N_y become N_r and N_θ respectively). We can express the computational complexity of the diffraction algorithms in terms of N_x, N_y and N_t. We will, in particular, investigate the following three methods: (1) The Rayleigh approach (2) The impulse response formalism, and (3) the angular spectrum method.

4.5.1 The Rayleigh Integral

The Rayleigh integral is a mathematical statement of Huygens principle - it is a sum of field contributions from small elements across the source. It is given by

$$\phi(r,t) = \frac{1}{2\pi} \iint_{S_o} \frac{v_n(t - R/c_o)}{R} dS_o ,$$

where ϕ is the velocity potential at the observation point, v_n is the normal particle velocity across the source, R is the distance between the source element and S_o is the surface across the source. Let us consider the computational complexity of the Rayleigh integral.

If we want to calculate the velocity potential at a point on the plane $z=z_I$ for all times of interest, we would evaluate a double integral over the surface of the transducer/source plane. Thus for all times of interest, this would require $N_t(N_x N_y)$ calculations. To do this for all points in the plane $z=z_1$, would require $N_t(N_x N_y)^2$ calculations.

If there is axial symmetry, the Rayleigh double integral reduces to a single integral, and only the radial component of the plane profile needs to be evaluated to represent the entire plane $z=z_I$. Thus the computational complexity for the Rayleigh integral (axial symmetry) is only $N_t N_r^2$.

We are primarily interested in the nonaxisymmetric case, and it is evident that the computational burden due to the Rayleigh integral can be large if planar sampling is dense. Otherwise, the Rayleigh integral satisfies the other requirements given in section 4.4.3.

4.5.2 Impulse Response Formalism

The impulse response of a transducer is, as the name suggests the field response of a perfect impulse excitation:

$$h(r,t) = \iint_{S_o} \frac{\xi_o(x,y)\delta(t - R/c_o)}{2\pi R} dS_o .$$

Here ξ is an apodization factor across the source, and the other variables are the same as those given in the Rayleigh integral. The transient response due to a given excitation may be obtained by convolving the impulse response with the source excitation:

$$\phi(r,t) = v_o(t) * h(r,t).$$

Note that this method assumes that the source velocity $v(x,y,t)$ is separable, i.e. can be written as $v_o(t)\xi(x,y)$ where ξ is an apodization factor. One of the requirements for a suitable diffraction algorithm in the proposed nonlinear propagation algorithm is that the approach be valid for non-separable distributions. To see why this is so, consider a point source which emits a delta-function excitation. The impulse response on a plane a distance away from the transducer will consist of an impulse arriving first at the center of the plane (the point directly normal to point source), followed by impulses arriving later in isochronal rings off axis. The impulse response is therefore given by

$$h(t,z,r) = \delta\left(t - \frac{\sqrt{z^2 + r^2}}{c}\right),$$

which is clearly not separable. Since we are concerned with plane to plane diffractive propagation, it is essential that the method be capable of propagating non-separable distributions. The impulse response formalism is thus discounted from our list of potential candidates for a diffraction algorithm. Nevertheless, we will consider its computational complexity and compare its efficiency with other techniques. If it is computationally efficient, it may be used for the first step propagation from a transducer surface where excitation is separable.

In investigating the computational complexity of this approach, we will consider two situations:

(1) The impulse response function can be evaluated analytically.

In this case, to calculate the velocity potential at a point on the plane $z=z_i$, requires a convolution of the impulse response with the surface velocity of the transducer/source plane. This would require on the order of $3N_t\log_2(N_t) + N_t$ computations if the FFT method of convolution is employed. Thus to evaluate the velocity potential at each point

of the plane $z=z_l$, we would require on the order of $N_xN_y(3N_t\log_2(N_t)+N_t)$ computations. If there is axial symmetry, this reduces to $N_r(3N_t\log_2(N_t)+N_t)$.

(2) The impulse response function cannot be evaluated analytically, and must be computed numerically:

Here, the impulse response function is obtained by evaluating a surface integral over the surface of the transducer/source plane. This would require $N_tN_xN_y$ computations, unless the transducer has axial symmetry, in which case the surface integral would reduce to a single integral (N_tN_r computations). Once we compute the impulse response for a point in the plane $z=z_l$ for all times, we then need to convolve the impulse response with the surface velocity to get the velocity potential at a point in the observation plane. Thus for one point on the plane $z=z_l$, we require $N_tN_xN_y + 3N_t\log_2(N_t) + N_t$ computations. To do this computation for each point in the plane $z=z_l$, we require $N_xN_y(N_tN_xN_y+3N_t\log_2(N_t) + N_t)$ computations, which is of the same order of computational complexity as the Rayleigh formalism, and even slightly more demanding.

There is also a way to compute the impulse response function using only one integral, which we shall call the Tjotta impulse response method (Tjotta and Tjotta, 1982). By this method, one does a coordinate transformation so as to integrate over isochronal ring elements (points equidistant from the observation point). In this case, suppose that the angle to integrate over a single annular isochronal ring is β, and that there are N_β discrete points to sum over. Then for each observation point we require N_β computations to find the impulse response at a single time, and $N_\beta N_t$ computations for N_t times. Once the impulse response has been found for a given observation point, we do a convolution over the source velocity v. This convolution would require $3N_t\log_2(N_t) + N_t$ computations. We then would need to do the identical calculation for all points in the observation plane. Overall, we would thus need $N_xN_y(N_\beta N_t + 3N_t\log_2(N_t) + N_t)$ computations, which is approximately $N_xN_yN_\beta N_t$.

4.5.3 Angular Spectrum Method
The theory of the angular spectrum method will be given later on in the chapter.

It will suffice to mention that for each frequency component of the source excitation, there exists a spatial frequency representation of the source plane. Propagation from one plane to another may be accomplished through use of a transfer function H.

Let us suppose that the surface velocity of the source plane is $v(x,y,z_o,t)$. First we need to perform a FFT to find the frequency domain representation of the velocity $s(x,y,z_o,\omega)$ for each point (x,y) in the source plane. In general, this will require $N_xN_yN_t\log_2(N_t)$ computations. Once $s(x,y,z_o,\omega)$ is found for all points (x,y) in the transducer plane, and for all frequency components ω, the following steps are needed:

For each frequency component ω,

(1) Perform a 2D-FFT on $s(x,y,z_o,\omega)$ to get $S(k_x,k_y; z=z_o)$. ($N_xN_y\log_2[N_xN_y/2]$ computations).

(2) Multiply S by the transfer function $H(k_x,k_y; z_o|z_1)$ defined in section 4.6. (N_xN_y computations).

(3) Perform a 2D-IFFT to obtain the frequency domain velocity $s(x,y,z_1,\omega)$. ($N_xN_y\log_2[N_xN_y/2]$ computations).

Thus we require $N_t[2N_xN_y\log_2(N_xN_y/2)+N_xN_y]$ computations for all the frequency components. (These computations are made once the values for v(x,y,0,t) are computed). Finally, once $s(x,y,z_1,\omega)$ has been computed for all points (x,y) on the plane z=z$_1$, and for all frequencies ω, we do an IFFT on $s(x,y,z_1,\omega)$ enabling the time domain velocity waveform $v(x,y,z_1,t)$ to be obtained. This should be done for all points (x,y) in the plane $z=z_1$ (i.e. $N_xN_yN_t\log_2(N_t)$ computations). Thus in total, we require $2N_xN_yN_t\log_2(N_t)+N_t[2N_xN_y\log_2(N_xN_y/2)+N_xN_y]$ computations.

The angular spectrum method is very computationally efficient compared to the Rayleigh and impulse response methods, given a non-uniform, non-axisymmetric surface velocity on the transducer/source plane.

Below is an example using actual numbers to illustrate this point. Suppose we want to compute the particle velocity for all points in a plane a distance Δz from a

nonaxisymmetric source. Suppose $N_x = N_y = N_t = 512$. The computational efficiencies of the various methods is summarized in table 1.

Table 1 Computational Burden of Various Diffraction Algorithms

Method	# Computations
Rayleigh	3.5184×10^{13}
Impulse response *	3.5188×10^{13}
Tjotta impulse response *	7.2478×10^{10}
Angular spectrum	7.1135×10^{9}

* Only valid for axisymmetric sources

Thus, based on this preliminary analysis, the agular sectrum method is almost 5000 times more computationally efficient than the Rayleigh or impulse response method, and 10 times faster than the Tjotta impulse response method.

Besides being computationally efficient, the angular spectrum method is valid for plane-to-plane propagations – even when the source plane is non-separable. It can be very accurate in the nearfield as will be demonstrated in subsequent chapters. Attenuation, refraction, and reflection can be easily incorporated, and sampling theorems will be developed to ensure accurate modeling results. In short, the angular spectrum method is an ideal choice for modeling diffractive propagation.

4.6 The Angular Spectrum Method: Theory

In the previous section, it was shown that the angular spectrum method showed great promise for efficiently computing the effects of diffraction. Here we consider some background information regarding this useful technique.

The angular spectrum is a widely used technique in optics and is addressed by Ratcliffe (1956), as well as in texts by Gaskill (1978) and Goodman (1968). In acoustics, the angular spectrum methodology has also been well established. Maynard and Williams used it to investigate the possibility of sub-wavelength resolution acoustic holography

(1980), and to compute the field from a plane piston transducer (1982). Stephanishen and Benjamin used the angular spectrum for forward and backward propagations (1982), and Waag et. al. explored windowing and other issues in discrete implementation of the angular spectrum technique (1985). Shafer (1989), and Christopher and Parker (1991) have applied the angular spectrum method to transducer characterization using backpropagation, and nonlinear propagation.

4.6.1 The Spatial Frequency Interpretation of a CW Transducer Excitation

Consider a plane transducer vibrating at a constant frequency f. The acoustic waves propagating away from the transducer surface can be thought of as a weighted collection of wave vectors $\mathbf{k} = (k_x, k_y, k_z)$, each wave vector propagating in a different direction, and each carrying a different weighting, or amplitude. For a wave that is nearly planar, propagating in the z direction, the components $k_x = 0$, $k_y = 0$ will be the most heavily weighted, but weighting will be negligible for large values of k_x or k_y (i.e. vectors pointing away from the direction of propagation). For a pulsating sphere or point source, all wave vectors may be weighted equally as the radiation field produced would be spherically symmetric. We can consider a transducer as a collection of point sources, and the acoustic spatial frequency spectrum as the linear sum of all these point source contributions. Mathematically speaking, for a flat transducer, we can consider the aperature surface $s(x,y,z_o)$ to have a particular spatial frequency spectrum, $S(k_x, k_y)$ given by the two dimensional Fourier transform of the aperature, i.e.,

$$(7) \qquad S(k_x, k_y; z_o) = \Im_{2D}\{s(x,y,z_o)\} = \int\int_{-\infty}^{\infty} s(x,y,z_o) e^{-j(k_x x + k_y y)} \, dx\, dy \, .$$

The distribution S tells us that a particular wave vector $\mathbf{k}=(k_x, k_y, k_z)$ has weighting $S(k_x, k_y)$. Note that for a particular frequency f, a particular wave vector $|\mathbf{k}| = 2\pi f/c$, may be specified by referring only to the (k_x, k_y) components since k_z is given by the relation $k_z^2 = k^2 - (k_x^2 + k_y^2)$.

For a disk transducer, the spatial frequency spectrum corresponds to a *jinc* function, and for a rectangular transducer, the spatial frequency spectrum corresponds to a 2-D *sinc* function.

4.6.2 The Angular Spectrum

We can also write the spatial frequency spectrum as an **angular spectrum**. Given the direction cosines

$$\alpha = cos\theta = \hat{k} \cdot \hat{x} = -k_x/k.$$

$$\beta = cos\psi = \hat{k} \cdot \hat{y} = -k_y/k.$$

$$\gamma = (1-(\alpha^2+\beta^2))^{1/2} = -k_z/k$$

where the symbol '^' denotes a unit vector, we can write

$$(8) \qquad S(\alpha,\beta;z_o) = \int\int_{-\infty}^{\infty} s(x,y,z_o)e^{jk(\alpha x+\beta y)}dxdy .$$

For future note, we will often refer to $S(k_x, k_y)$, given in (7) as the angular spectrum, even though it is technically expressed in terms of spatial frequency vectors, and not direction cosines as is the case for (8).

4.6.3 Diffractive Propagation Using the Angular Spectrum

On a plane a distance Δz away from a harmonically excited transducer, diffractive propagation will alter the spatial frequency spectrum on the transducer surface $S(k_x, k_y; z =z_o)$ to something new, $S(k_x, k_y; z = z_l)$ related once again to the spatial field profile at the plane $z = z_o$ by a Fourier Transform.

There is a linear relation between the field profile at the surface of the transducer, and the field profile on plane $z=z_l$. This linear relation can be thought of as a 2D-transfer function $H(k_x, k_y; \Delta z)$ in the spatial frequency domain, or a point spread function $h(x,y; \Delta z)$ in the spatial domain. Specifically, we may write:

$$s(x,y,z_1) = h(x,y;\Delta z) ** s(x,y,z = z_o)$$

or

$$S(k_x, k_y; z_1) = H(k_x, k_y; \Delta z) S(k_x, k_y; z = z_o)$$

where $\Delta z = |z_1 - z_o|$, and ** denotes two dimensional convolution over x and y.

The form of h and H can be derived analytically, by substituting

$$\Phi(x, y, z) = \frac{k^2}{4\pi^2} \int\limits_{-\infty}^{\infty} \int S(\alpha, \beta : z) e^{-jk(\alpha x + \beta y)} d\alpha d\beta$$

into the homogeneous Helmholtz equation, and solving the resultant second order homogeneous differential equation in S, given the initial condition $S = S(\alpha, \beta : z = 0)$. The transfer function H is thus given by

$$(9) \qquad H(k_x, k_y : \Delta z) = \begin{cases} e^{j \Delta z \sqrt{k^2 - (k_x^2 + k_y^2)}} & for \quad (k_x^2 + k_y^2) \le k^2 \\ e^{-\Delta z \sqrt{k_x^2 + k_y^2 - k^2}} & for \quad (k_x^2 + k_y^2) > k^2 \end{cases}.$$

Thus, given the angular spectrum $S(k_x, k_y; z_o)$ on plane z_o, we can know the angular spectrum on a plane z_1, a distance Δz from plane z_o by the following transfer function relation:

$$(10) \qquad S(k_x, k_y; z_1) = H(k_x, k_y; \Delta z) S(k_x, k_y; z_o)$$

The field profile on the plane z_1 can then be found by taking the inverse 2-D Fourier transform of the above result. The sequence of steps used to compute the angular spectrum is illustrated in Fig. 2 below.
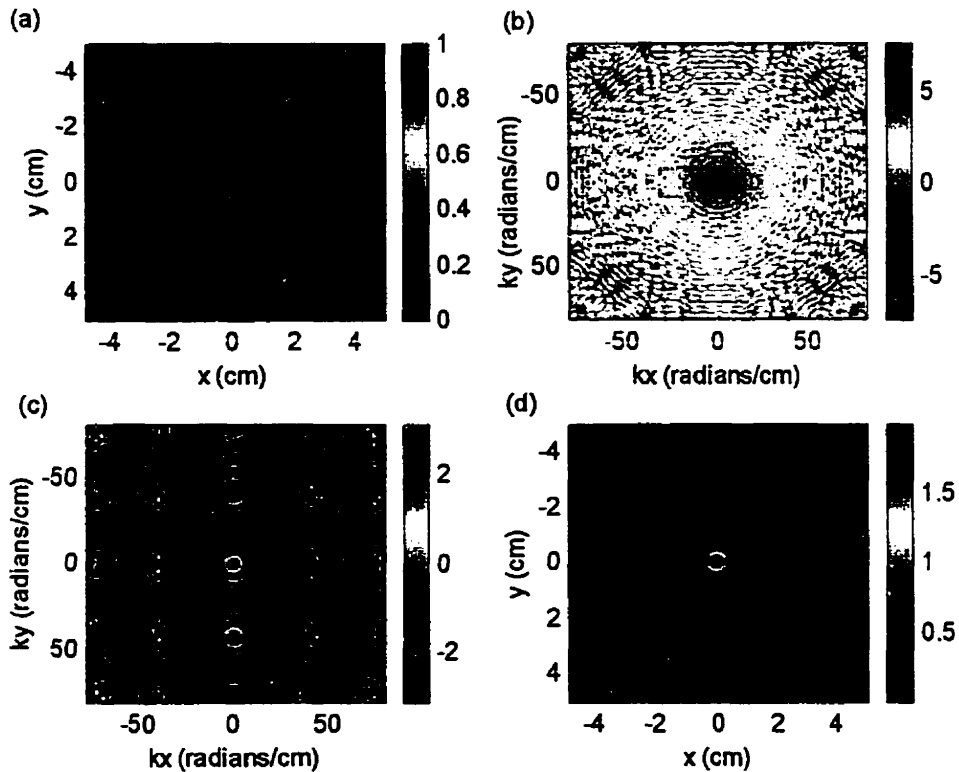
Figure 2 Illustration of the angular spectrum approach to diffractive propagation. (a) is the normal velocity profile (m/s) of a plane piston of radius 1cm. It transmits a CW excitation at 5 MHz. (b) is the spatial frequency representation of the source (c) is the argument of the transfer function H, and (d) is the normal velocity field profile at $z=a^2 \lambda$

The transfer function H can be thought of as a complex phase weighting, that governs Huygen's principle of wave superposition. The ultrasonic field from a source may be thought of as a collection of constituent waves - each with its own directionality and magnitude. The angular spectrum is a mathematical description of the magnitude of such directional components. The field across an observation plane, a distance Δz away from the transducer is characterized by how these constituent waves interfere with each other. The superposition of the constituent waves at a point on the observation plane depends on the relative phase between the wave components. The transfer function H is the mathematical mechanism whereby each component wave is assigned a phase. After these components are shifted by their assigned phase, they are added together linearly in a sum, which, is given mathematically by the inverse 2-D Fourier transform of (10).

An alternative to an angular spectrum based - description of diffractive propagation is a spatial one. The point spread function $h(x,y;\Delta x)$ which relates the field profiles between planes separated a distance Δz apart is obtained by taking the inverse Fourier transform of the transfer function H, and is given by

$$h(x,y:\Delta z) = -\frac{ze^{jkR}}{2\pi R^2}\left(jk - \frac{1}{R}\right)$$

where

$$R = \sqrt{x^2 + y^2 + \Delta z^2}$$

Thus, given the field profile $s(x,y,z_o)$ on a plane z_o, we can know the angular spectrum on a plane z_1 a distance Δz away from z_o by the following 2-D convolution relation:

$$s(x,y,z_1) = h(x,y;\Delta z)**s(x,y,z_o) .$$

We can think of the point spread function $h(x,y;\Delta z)$, as the field profile or response on plane $z=z_o$ given a one point source at $(x_o,y_o,z=0)$ is harmonically excited with frequency f. H is the Fourier transform of h, and represents a spatial frequency domain version of the response due to a point source excitation.

Pressure and Normal Particle Velocity

It should further be noted that other field variables may be used for diffractive propagation, such as pressure, or normal particle velocity. For example, normal particle velocity u is a useful parameter to define the profile across the transducer surface. The normal particle velocity distribution across a surface z_1 a distance Δz from the transducer, then is given by

$$u(x,y,z_1) = h(x,y;\Delta z)**u(x,y,z_o)$$

where h is the point spread function. Equivalently, this could be written as

$$u(x,y:z_1) = \Im_{2D}^{-1}\{H(k_x,k_y;\Delta z)U_z(k_x,k_y;z_o)\}$$

where U denoted the 2D-Fourier Transform of u, and H is the transfer function. Similar expressions may be written for pressure field to pressure field diffractive propagation.

If we want to know the pressure, or velocity potential at a plane a distance Δz away from the transducer, given the normal particle velocity on the source plane (transducer surface), however, we need a different form for H and h.

For example, suppose we want to compute the pressure over a plane z_1 a distance away from the transducer:

$$p(x,y,z_1) = u(x,y,z=0) ** h_{u \to p}(x,y:\Delta z)$$

The point spread function $h_{u\text{->}p}$ is in this case given by

$$h_{u \to p}(x,y:\Delta z) = -j\omega\rho g(x,y,\Delta z) = -j\omega\rho \frac{e^{jkR}}{2\pi R}$$

where g is the point source Greens function and

$$R = \sqrt{x^2 + y^2 + \Delta z^2}$$

It can also be shown that the transfer function $H_{u\text{->}p}$ is given by

$$H_{u \to p}(k_x, k_y : \Delta z) = -j\omega\rho G(k_x, k_y : \Delta z) = \frac{\omega\rho e^{j\sqrt{k^2-(k_x^2+k_y^2)}\Delta z}}{\sqrt{k^2 - (k_x^2 + k_y^2)}},$$

where G is the Fourier transform of the Greens function. Using $H_{u\text{->}p}$ can be numerically troublesome because of the singularity for $k_z=0$ (Maynard and Williams, 1982), and the use of $h_{v\text{->}p}$ may be a better alternative. The forms of $h_{v\text{->}\phi}$ and $H_{v\text{->}\phi}$ are equal to those of $h_{v\text{->}p}$ and $H_{v\text{->}p}$ divided by a factor of $-j\omega\rho$.

Chapter 5: Numerical Implementation of the Angular Spectrum Method

In Chapter 4, a new scheme was proposed to numerically evaluate finite amplitude ultrasound propagation. The proposed methodology was based on a second order operator splitting. Diffraction, absorption, and nonlinearity are solved separately over small incremental steps, and the field profile is marched along in a plane-to-plane fashion using a fractional step marching scheme. The choice of an efficient and accurate diffractive propagation algorithm suitable for such a modeling scheme is important considering previous models suffer from computational bottlenecks in the diffraction portion of the propagation algorithm. The angular spectrum method was shown to be a good candidate for such an algorithm. Discrete implementation of the angular spectrum scheme involves sampling and windowing issues which are nontrivial. In this chapter, we consider diffractive propagation from non-axisymmetric sources. The reader is referred to Appendix B for the slightly different analysis needed for radially symmetric sources.

5.1 Numerical implementation of the Angular Spectrum Method in cases where there is no radial symmetry

In cases where the transducer has radial symmetry, Christopher and Parker's (1991) approach to diffractive propagation using the DHT may be used. Their approach, along with some general insights into the use of the angular spectrum approach for cases with radial symmtery, is discussed in Appendix B. They argue that the principles behind their algorithm can easily be extended to non-axisymetric sources by using the 2DFFT in place of the DHT. In fact, Christopher (1999) implemented a nonaxisymmetric version of his FSC algorithm, using the 2D-FFT. However, he used axial increments of 20 per cm, which is a subwavelength step size. Our intention is to exploit the second order operator splitting introduced in Chapter 4 to enable the use of much larger step sizes, while concurrently saving computational cost. Christopher's use of subwavelength distances for the angular spectrum likely elicited small wraparound errors. For large-step diffractive propagation, however, there are some unfortunate problems which will require careful analysis. First, however, we will formally introduce the notation, theorems, and

algorithms associated with the 2D numerical implementation of the angular spectrum method.

5.1.1 Notation

There are two approaches one may take to implement the angular spectrum method numerically. One approach, which we shall call the frequency sampled convolution (FSC) algorithm, involves sampling the propagator function H in the spatial frequency domain. The other method, called the spatially sampled convolution (SSC) approach, is to sample the point spread function h in the spatial domain. These approaches have different consequences, which will be discussed in due course. In doing so, will first describe the SSC algorithm.

To accurately implement the 2D SSC algorithm numerically, we must choose an adequate sampling scheme. Thus we must specify the sampling intervals Δx and Δy, as well as specify the spatial extent of the transform domain. Given a field distribution $s(x,y)$ over an infinite extent source plane $z = z_o$, we must choose a finite truncation of s. If the source plane is coincident with the transducer surface, then the normal particle velocity will naturally be of finite extent. However, if we are considering the case of plane to plane diffractive propagation, and the source plane is actually some distance from the transducer, then the field profile across the source will be of infinite extent, and must be truncated and windowed. Windowing issues will be dealt with in section 5.7. We shall denote the desired spatial extent of the source in the x and y directions by $\pm X_s$ and $\pm Y_s$. The spatial extent of the source plane should be chosen so that the bulk of the field energy across the plane is contained within these boundaries. Now we must sample $s(x,y)$ over the interval $[\pm X_s, \pm Y_s]$, with sampling intervals Δx and Δy. Let N_{Xs} be the number of samples over $0 < x < X_s$, and N_{Ys} be the number of samples over $0 < y < Y_s$. The sampling should adequately capture the planar variations in the source distribution, as determined by the 2D-Nyquist Theorem.

Next assume that we wish to find the diffracted field profile across a plane $z = z_1$ a distance Δz away from the source. Again, the diffracted field profile on the observation

plane may be of infinite extent, however, we must choose a finite window in which we desire correct results. Call the x and y spatial extents of the observation plane $\pm X_o$ and $\pm Y_o$ respectively.

The point spread function h must also be sampled with adequate sampling out to some finite extent. The point-spread function h is of infinite extent, and must be truncated. The required convolution is only numerically realizable if both s and h are of finite extent. Note that h must be sampled out to at least [X_o + X_s, Y_o + Y_s] to be able to get accurate results out to the extent of interest, [$\pm X_o$, $\pm Y_o$]. Denote this extent as [T_x, T_y]. Let N_{Tx} be the number of points spanning $0<x<T_x$, and let N_{Ty} be the number of points spanning $0<y<T_y$. With this notation (see Fig. 6), the convolution becomes

$$(5) \qquad s_d[m,n] **h_d[m,n] = \sum_{j=-N_{Ys}}^{N_{Ys}-1} \sum_{k=-N_{Xs}}^{N_{Xs}-1} s_d[j,k]h_d[m-j,n-k],$$

for $-N_{Tx}<m<+N_{Tx}-1$, and $-N_{Ty}<n<+N_{Ty}-1$. Correct results are obtained in the region $-N_{Xo}<m<+N_{Xo}-1$, $-N_{Yo}<n<+N_{Yo}-1$, with aliasing errors dominating the region exterior to this.

$T_x \geq X_s + X_o$ (spanning N_{Tx} points) is the extent to which h is sampled

X_s (spanning N_{Xs} points) is chosen so as to contain the bulk of the energy in the source plane

y

x

Source Sampled in this Region

h sampled in this region. This is also the extent of the transform space.

$T_y \geq Y_s + Y_o$ (spanning N_{Tx} points) is the extent to which h is sampled

Y_s (spanning N_{Ys} points) is chosen so as to contain the bulk of the energy in the source plane

(b)

$T_x \geq X_s + X_o$ (spanning N_{Tx} points) is the extent of the transform space.

X_o (spanning N_{Xo} points) is the extent to which correct results are desired in the observation plane.

y

x

Correct Field Profile in this region of the Observation Plane

Convolutional wraparound artefacts exist throughout this region

$T_y \geq Y_s + Y_o$ (spanning N_{Ty} points) is the extent of the transform space.

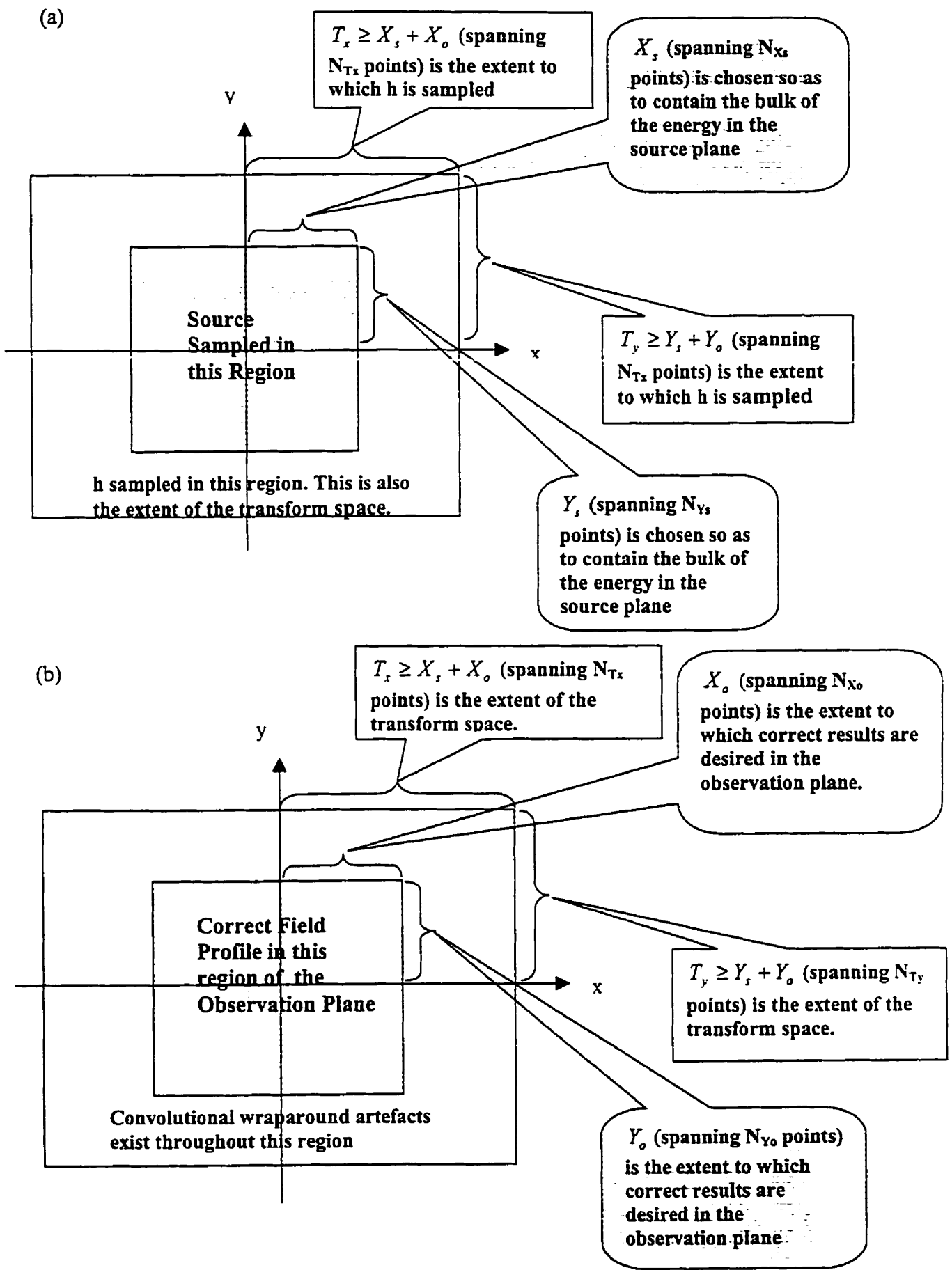Y_o (spanning N_{Yo} points) is the extent to which correct results are desired in the observation plane

Figure 6 The notation and variables used in the 2D-FFT based angular spectrum algorithm for (a) the source plane and (b) the observation plane.

5.1.2 The 2D SSC Algorithm

The convolution (5), may be implemented in a computationally efficient way using the 2D-FFT as follows:

Having chosen $[T_x, T_y]$, and $[\Delta x, \Delta y]$, and sampling the sequences s and h as outlined above,

1. Zero pad $s[m,n]$ out to $[N_{Tx}, N_{Ty}]$. If s is of infinite extent, first use a tapered window to taper the edge discontinuities from truncation to zero. This will prevent edge artefacts in the convolution. Call the zero padded (and tapered) window $s_p[m,n]$.

2. Take the 2D FFT of both h_d and s_p and call the results H_d and S_p, respectively.

3. Take the 2D IFFT of the product $H_d \times S_p$.

4. The correct result of the convolution can be found by extracting the central $[N_{Xo}, N_{Yo}]$ core results of the inverse transform. The results outside this core have wraparound error.

5.1.3 The 2D FSC Algorithm Using the 2D FFT

Spatial frequency sampling of H may be used as an alternative to the spatial sampling (SSC) methodology. The spatial frequency domain extends across the region $[-k_{xmax} < k_x < k_{xmax}, -k_{ymax} < k_y < +k_{ymax}]$, where $k_{xmax} = \pi/\Delta x$, and $k_{ymax} = \pi/\Delta y$. There are N_{Tx} samples across $[0, k_{xmax}]$, and N_{Ty} samples across $[0, k_{ymax}]$. The sampling intervals in the spatial frequency domain are defined by $\Delta k_x = \pi/T_x$, and $\Delta k_y = \pi/T_y$.

The 2D FSC algorithm can be described as follows:

1. Having chosen $[T_x, T_y]$, and $[\Delta x, \Delta y]$, sample the sequences s, as outlined above.

2. Sample the point spread function in the frequency domain by sampling the analytic transfer function H in the frequency domain with discrete spatial frequency sampling defined above. Call this sampled version H_d.

3. Zero pad $s[m,n]$ out to $[N_x, N_y]$. If s is of infinite extent, first use a tapered window to taper the edge discontinuities from truncation to zero. This will prevent edge artefacts in the convolution. Call the zero padded (and tapered) distribution $s_p[m,n]$.

4. Take the 2D FFT of both s_p, scale it by a factor $1/\Delta x \Delta y$, and call the result S_p.

5. Take the 2D IFFT of the product $H_d \times S_p$.

6. The correct result of the convolution can be found by extracting the central $[N_{Xo}, N_{Yo}]$ core results of the inverse transform. The results outside this core have wraparound error.

5.1.4 A Note Regarding the Implementation of the 2D-FFT Using Established Algorithms

Most 2D FFT algorithms assume that the matrices to be convolved are not centred about the origin, but rather have their lowest indices [1,1] coincident with the origin ($x=0, y=0$). Thus, before using most 'black-box' 2D FFT algorithms, we must first shift the sequences so their bottom edge coincides with the origin. After using the 2D FFT algorithm, the sequences must be shifted back so that they are centered about the origin. This shifting process can be accomplished by a function (called fftshift2 in MATLAB), which swaps quadrants I and III and II and IV.

5.2 Accurate Sampling of the Point Spread Function h for the Case of Single Step CW Diffractive Propagation

The Nyquist theorem demands that the maximal frequency content of the point spread function h ultimately dictates the sampling we should use in the spatial domain. Thus, by looking at H, the frequency domain representation of h, we can get a picture of what kind of sampling Δx and Δy we need in the spatial domain.

Inside the radiation circle,

$$(6) \qquad k_x^2 + k_y^2 = \left(2\pi f/c\right)^2,$$

the transfer function $H(k_x, k_y)$ has magnitude 1, and tapers off to zero exponentially beyond it. Thus if we choose a threshold for the maximal frequency content $[k_{xmax}, k_{ymax}]$ of h as being slightly beyond the radiation circle, (i.e. $k_{max} = 2\pi f/c + \varepsilon$, where ε is a small amount), the point spread function will be well represented, and the 2D FFT of h will have negligible wraparound error. This can be understood by considering that the transform of h would be equivalent to an aliased version of H infinitely wrapped around itself with period $[2\pi f/c + \varepsilon, 2\pi f/c + \varepsilon]$. It is the evanescent portion of H which will be aliased back into the spectrum, and since the evanescent tails are typically negligible, the

wraparound errors associated with H_d will be negligible. Thus the SSC algorithm using the 2D FFT will be accurate. Note that the sampling defined by the Nyquist threshold $[k_{xmax}, k_{ymax}]$ corresponds to a rate of slightly better than $\lambda/2$ sampling.

If the propagation distance Δz is very small (less than a wavelength), the evanescent tail of H will be significant, and sampling at intervals of $\Delta x \sim \lambda/2$ will not suffice. In this case, one might consider a much denser sampling, or, alternatively, sampling the transfer function H in the spatial frequency domain.

5.3 Accurate Sampling of the Transfer Function H

Sampling the transfer function H in the spatial frequency domain in 2-D somewhat more subtle than Christopher's axisymeteric (1-D) treatment. The crux of the problems are associated with what one might call circle-square issues.

Consider the following three cases.

1. The radiation circle is completely within the spatial frequency (transform) domain

2. The radiation circle is only partially within the spatial frequency (transform) domain

3. The spatial frequency domain is completely inside the radiation circle

With cases (1) and (2) at least part of the radiation circle is within the transform domain. In general, these situations are not ammenable to spatial domain sampling of H. This is because the radiation circle corresponds to a region of H where there is an abrupt change, and very dense oscillations, and cannot be adequately sampled. Sampling the point spread function h in these cases is the appropriate route. For case (1), adequate sampling of h is guaranteed, since the radiation circle is contained within the transform domain, and wraparound error from the evanescent tail of H is negligible. For case (2), h must be sampled at $\lambda/2$ or better, even though this may not be the sampling scheme for the source. The 2D-FFT of h may, however be truncated to the extent of the angular spectrum of the source, enabling the computation to be done.

In case (3), where the radiation circle is completely beyond the finite-extent spatial frequency domain, the oscillations of H can be adequately sampled, given the Nyquist rate of the most rapidly varying portion of the 2-D transfer function H (within the finite spatial frequency domain).

Suppose that we wish to sample H, and we wish to do so by sampling out to $[k_{xmax}, k_{ymax}]$, which is within the radiation circle. We may ask what sampling $[\Delta k_x, \Delta k_y]$ do we need to adequately represent the oscillations of the transfer function? The answer comes from the Nyquist theorem, and is based on an analysis of the highest frequency of oscillations of H contained within the transform domain. The highest frequency oscillations will be at the corner of the transform domain, since we know the oscillations become more dense close to the radiation circle. We can use the 2-D Taylor expansion of the argument of H in the epsilon neighborhood of $[k_{xmax}, k_{ymax}]$ to express H to first order as

$$H(k_x, k_y) \approx e^{j(\beta_x k_x + \beta_y k_y + \text{constant})},$$

thus giving an estimate $[\beta_x, \beta_y]$ of the maximum frequency of oscillations of H in the transform domain.

Given that

$$H(k_x, k_y; \Delta z) = e^{-j\Delta z \sqrt{k^2 - (k_x^2 + k_y^2)}}$$

is the transfer function for the frequency f (and $k = 2\pi f/c$), we may define a function g, such that

$$g(k_x, k_y) = \Delta z \sqrt{k^2 - (k_x^2 + k_y^2)}$$

Expanding this as a Taylor's series about (k_{xmax}, k_{ymax}), to first order

$$g(k_x, k_y) \approx g_n(k_{xmax}, k_{ymax}) + (k_x - k_{xmax})\frac{\partial g}{\partial k_x}\bigg|_{\substack{kx\,max \\ ky\,max}} + (k_y - k_{ymax})\frac{\partial g}{\partial k_y}\bigg|_{\substack{kx\,max \\ ky\,max}}$$

The desired sampling rate, which will determine Δk_x is

$$\beta_x = \left.\frac{\partial g}{\partial k_x}\right|_{k_{x\max},k_{y\max}} = \left.\frac{\Delta z k_x}{\sqrt{k^2-(k_x^2+k_y^2)}}\right|_{k_{x\max},k_{y\max}} = \frac{\Delta z k_{x\max}}{\sqrt{k^2-(k_{x\max}^2+k_{y\max}^2)}},$$

and a similar result can be obtained for β_y. Thus the sampling rate Δk_x is given by

$$(7) \qquad \Delta k_x \le \frac{\pi}{2\beta_x} = \frac{\pi\sqrt{k^2-(k_{x\max}^2+k_{y\max}^2)}}{2\Delta z k_{x\max}},$$

and a similar result is obtained for Δk_y. All of the above analysis assumes that the transform domain is completely within the radiation circle.

Essentially, we can use such a scheme where the extent of the angular spectrum of the source is well contained within the extent of the domain, or at least the bulk of the energy is contained within the transform domain. This will be the case for field distributions which are relatively smooth, and slowly varying in the spatial sense. Thus the nearfield of a source would be a poor candidate for using this scheme, and sampling h would likely be a better choice.

5.4 The Limitations of the Ray Theory Truncation for 2-D Diffractive Propagation

The idea of the ray theory truncation, described in Appendix B, is to limit the maximum spatial frequency extent based on the maximal angle between the source and the edge of the plane where correct results are desired. Truncation in the spatial frequency domain can reduce the computational requirements for the SSC and FSC algorithms. The ray theory truncation may be used to truncate the product $H \times S$, and thus decrease the size of the matrix on which to perform the inverse 2D-DFT. However, may be unprofitable if the 2D-FFT is used, which requires that the matrix be of size $2^n \times 2^m$ points (where n and m are integers). The ray theory truncation may not be used to decrease the spatial sampling of s or h directly, as this may incur serious aliasing errors in the convolution.

5.5 Sampling of the Transducer Surface

5.5.1 Sampling in the Spatial Domain vs. the Spatial Frequency Domain

Sampling of the aperature may be difficult due to the abrupt edges associate with the transducer surface. A course sampling of the aperature results in poor nearfield accuracy of not only the angular spectrum method, but also the Rayleigh method, and the impulse response method. The farther the observation plane from the source, the more accurate the computed field profile (based on the given gridding scheme) will be. Reasonably accurate results may be obtained for observation planes which are in the farfield of each sampling element. Nearfield inaccuracies may be a source of instability for a plane-to-plane fractional step nonlinear propagation algorithm, which we intend to develop. Nearfield errors may propagate incrementally in the marching scheme, and so it is important, if at all possible to secure reasonably accurate nearfield results. One way of ensuring nearfield accuracy is to use an extremely dense gridding scheme. This however comes at the expense of greater computational burden.

An attractive alternative, proposed here, is to use sample the analytic transform of the aperature in the frequency domain, when the analytic transform is known. This is possible for disks, rectangles, and, in the next section, an analytic representation of a linear phased array will be presented. The advantage of sampling the aperature in the spatial frequency domain is that an effectively infinitesimal spatial sampling can be obtained, thus eliminating aliasing artefacts associated with sampling an abrupt edge.

For phased arrays, an optimal design for eliminating grating lobes involves using elements whose inter-element spacing is less than $\lambda/2$. Should we sample the transducer in the spatial domain, very fine mesh would be needed to define the small detail present. Alternatively, sampling the transducer in the spatial frequency domain, has an additional advantage of using moderate sampling rates for representing the angular spectrum of a source.

The angular spectrum only needs to be defined out to a spatial frequency k_{max} of slightly better than $k_o = 2\pi f/c$, since after a step of diffractive propagation, the transfer function H

will filter all spatial frequencies beyond the radiation circle. In fact, we have found that sampling the aperture in the spatial frequency domain, can give very accurate results - even in the nearfield.

5.5.2 An Analytic Representation of a Linear Phased Array in the Spatial Frequency Domain

Here we give an analytic expression for the 2D Fourier Transform of a linear phased array. Consider a phased array composed of N elements of height H, and width W. Suppose the inter-element spacing is s, and the distance from the center of one element to the center of an adjacent element is $d = W+s$. The length of the array is $D = (N-1)d+W$. Supposing that N is even, the aperature function may be written as:

$$(8) \qquad s(x,y) = \xi(y) \sum_{n=-N/2}^{N/2} A_n E(x-nd,y)e^{j\phi_n} ,$$

where A_n is an apodization factor for the nth element, $e^{j\phi_n}$ is a phase delay for element n, and ξ represents the complex phase delay and apodization of a lens applied to the elevation plane of the entire array and used for additional focusing. Here the function $E(x,y) = \text{rect}(x/W)\text{rect}(y/H)$. Taking the Fourier Transform of the aperature function, we get

$$(9) \qquad S(k_x,k_y) = \Im\{\xi(y)rect(y/H)\} \sum_{n=-N/2}^{N/2} A_n \frac{\sin(Wk_x)}{Wk_x} e^{-jndk_x} e^{j\phi_n} .$$

If $\xi = 1$ (i.e. there is no lens), the expression becomes

$$(10) \qquad S(k_x,k_y) = \frac{\sin(Hk_y)}{Hk_y} \sum_{n=-N/2}^{N/2} A_n \frac{\sin(Wk_x)}{Wk_x} e^{-jndk_x} e^{j\phi_n}$$

If a lens is used, the y-component of the Fourier Transform may be difficult to evaluate analytically, but can be numerically calculated. Alternatively, Wu and Stepinski (1999) give an expression, based on an extension of the angular spectrum approach to curved radiators, for a linear array with a cylindrically concave surface. Yet a further technique for diffractive propagation from array transducers is to use a non angular spectrum technique for the first step, such as the impulse response method of Ullate and San Emeterio (1992), which is appropriate for calculating the transient near-field of phased array transducers. The angular spectrum method could then be applied in a plane to plane fashion following this first step propagation.

5.6 Results of One Step Diffractive Propagation from a CW Source

5.6.1 Plane Piston Transducer

To verify the accuracy of our angular spectrum method, the field of a plane piston

transducer was compared with the lateral profile computed with the Rayleigh integral.

Our approach shows good agreement in the farfield, at a^2/λ. Figs. 7(a) and (b) show the

comparison at the axial distance a^2/λ.

(a)

lateral distance (cm)

(b)

(c)
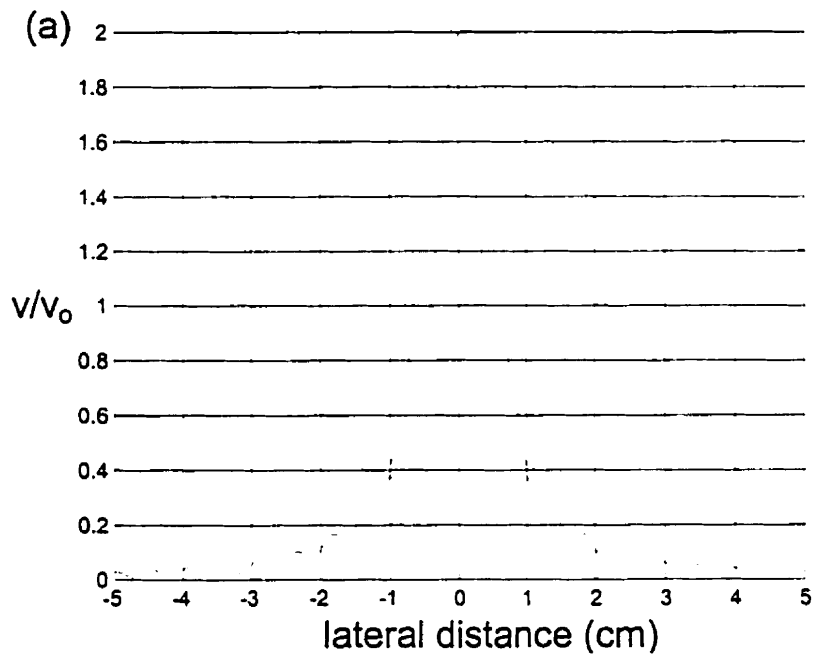
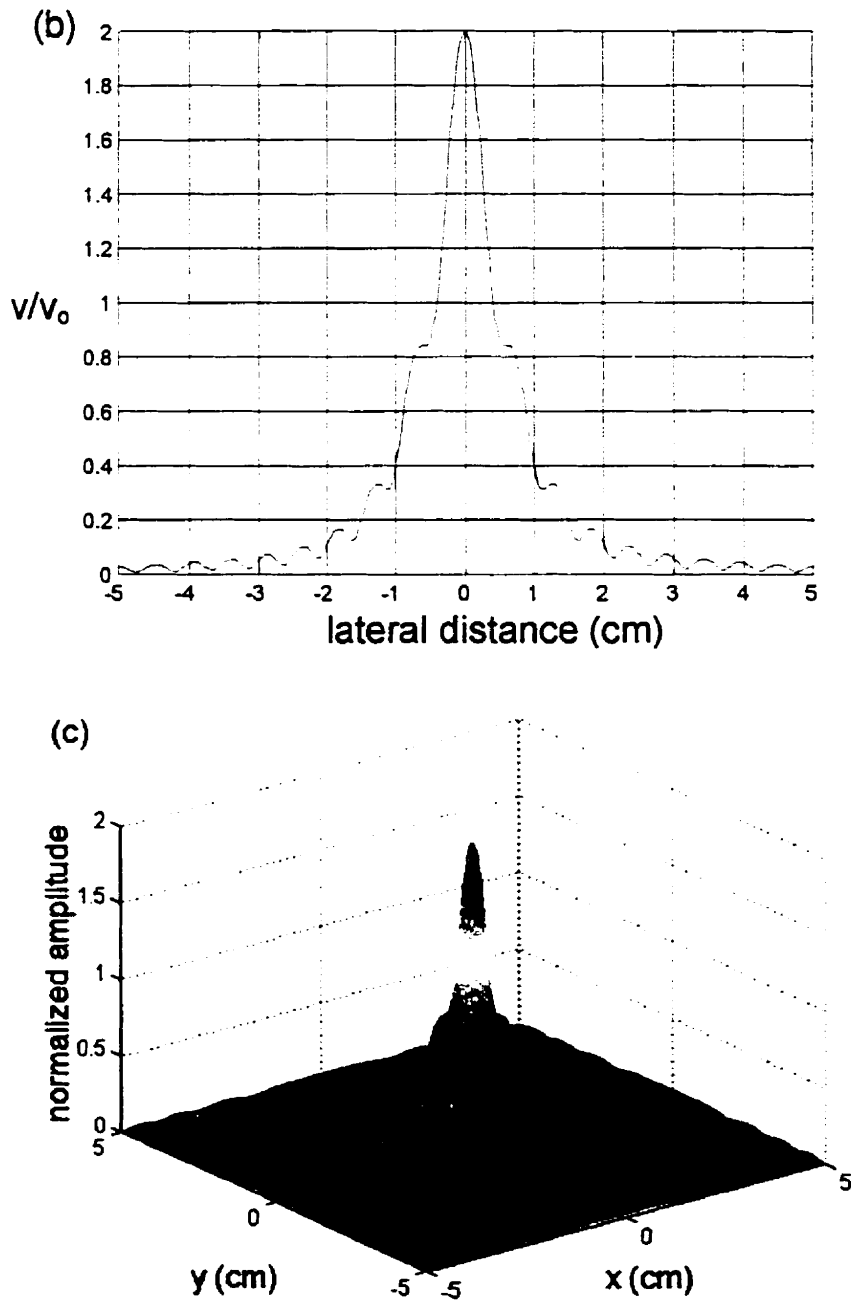
Figure 7 Lateral field profile at $z = a^2/\lambda$ from a plane piston (a=1.9cm) operating at 3MHz. The field amplitudes have been normalized relative to the magnitude of the source excitation. (a) Obtained using the Rayleigh integral. (b) & (c) Obtained using the angular spectrum approach.

5.6.2 Linear Array

Diffraction from a linear array using the angular spectrum method with spatial frequency domain sampling outlined in section 5.6.2 was simulated. The array had 16 elements, and was of height H=2cm, width W=λ/2, and had inter-element spacing s=λ/4. It used no focusing or apodization, and was excited at f= 1 MHz, with a normal particle velocity of 1cm/s. The lateral field profile was computed at a distance $z=\pi(H/2)^2/\lambda$ away from the transducer. The results are shown in Fig. 8(a).

To assess the accuracy of the technique, results were compared with a calculation based on the Fresnel approximation. The expression used was (Crombie et. al., 1997)
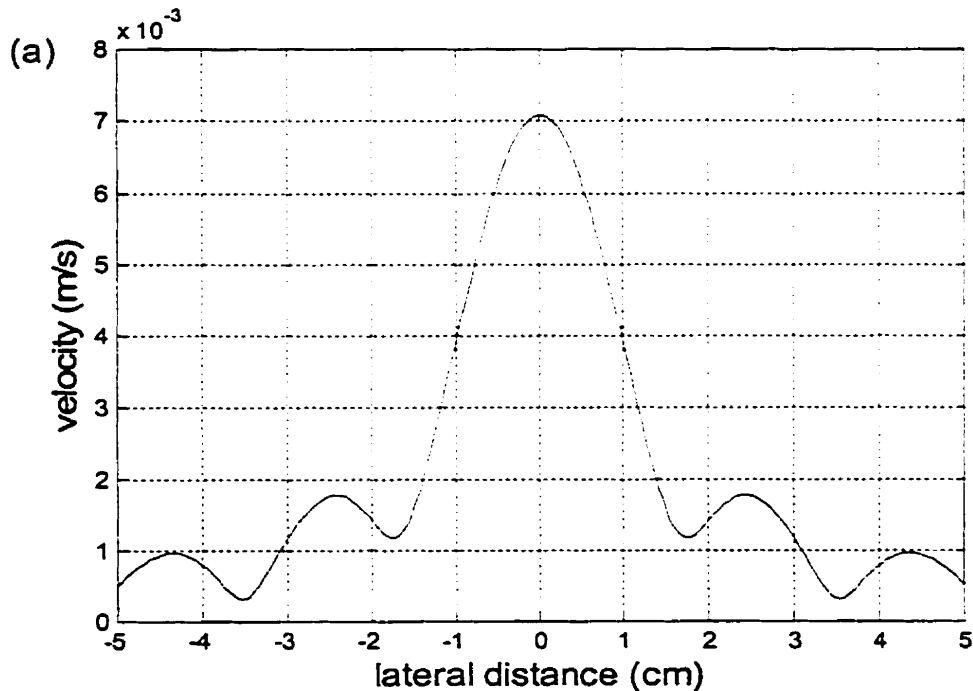
$$v(x_o, y_o, z; \omega) \approx -v_o \left(\frac{z}{4R}\right) e^{-jkz} \Pi_x \Pi_y ,$$

where

$$\Pi_x = erf[\sigma(W - 2x_o)] - erf[-\sigma(W + 2x_o)], \quad \Pi_y = erf[\sigma(H - 2y_o)] - erf[-\sigma(H + 2y_o)],$$

and where $\sigma = \sqrt{\dfrac{-j\pi}{4\lambda z}}.$

Results of this calculation are shown in Fig. 8(b). Note the close agreement between the two methods.
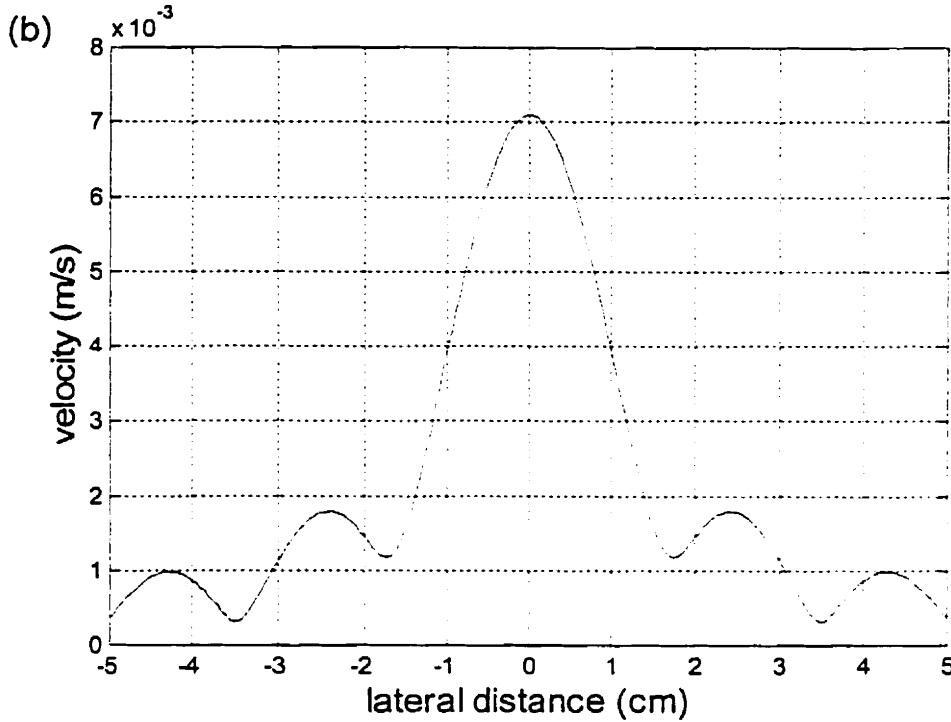
(a)

Figure 8. The normal particle velocity lateral field profile of a linear array with no focusing or apodization using (a) the angular spectrum method and (b) the Fresnel approximation. The relevant parameters are: N=16 elements, H=2cm, f=1MHz, W=$\lambda/2$, s=$\lambda/4$, z=$\pi(H/2)^2/\lambda$, v_o = 1cm/s.

5.7 Multistep Diffractive Propagation and Windowing Issues

For plane-to-plane diffractive propagation, the infinite-extent fields must be truncated. To eliminate the associated edge artefacts, we have used a radially symmetric cosine-tapered window, that is unity out to a cutoff region, and then tapers down to zero at the truncation region, following a cosine-trend. Truncation and windowing are important aspects of our model, yet have the distinct disadvantage that some energy may be lost in the plane-to-plane diffraction algorithm.

5.8 Results for Multistep CW Linear Propagation

5.8.1 Plane Piston Transducer

To assess the accuracy of the multistep diffractive propagation algorithm, we simulated the continuous field response from a plane piston transducer, and compared the axial profile with the known analytic curve. As shown in Fig. 9(a), the agreement between our algorithm and the analytic solution are in excellent agreement. Fig. 9(b) shows the field

distribution of the transducer over a plane defined by the lateral and axial coordinate axes. The dark region near the edges of the beam profile are due to windowing.
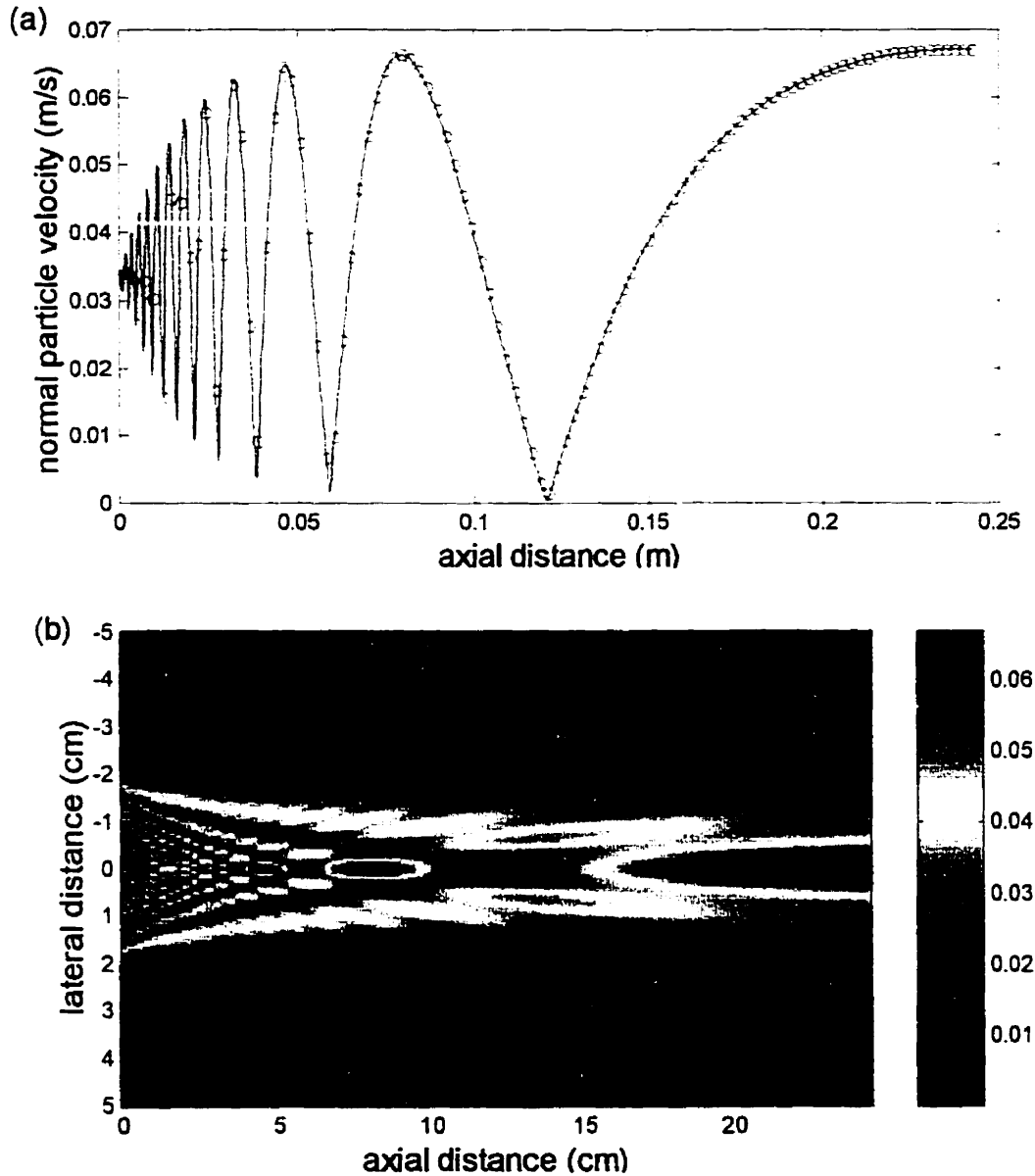

Figure 9 (a) shows the axial normal particle velocity profile of a plane piston transducer of radius a = 1.9cm, frequency f=1MHz, and initial pressure P_o = 50kPa. The solid line is the analytic profile, and the circles are the result of the multistep angular spectrum method. (b) Showing the field profile along the lateral xz-plane out to the distance a^2/λ. For this simulation, the aperature was sampled in the frequency domain. The amplitude units are m/s.

5.8.2 Linear Phased Array

The field profile for a linear phased array with no elevation focusing is illustrated in Figs.10(a) and (b) below. The angular spectrum method appears to be well suited to simulate the field profiles of even complex, non-axisymmetric geometries.
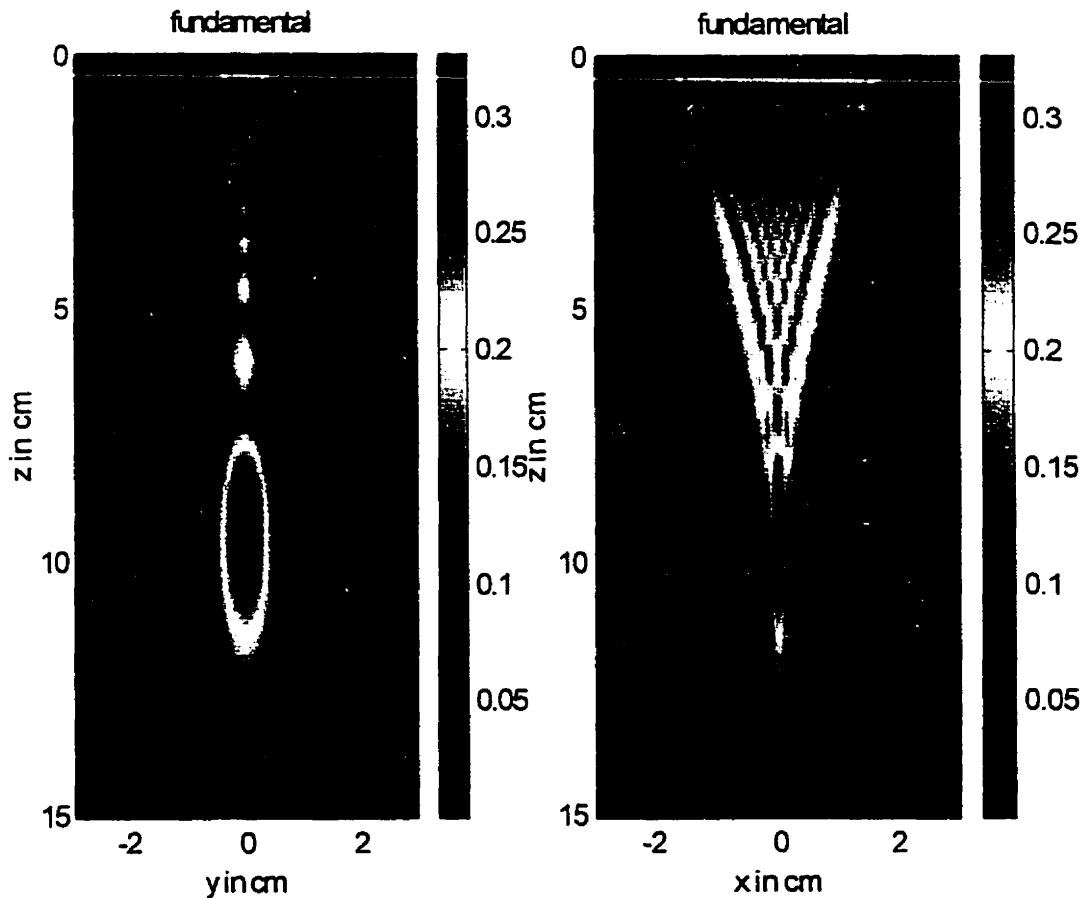

Figure 10 (a) The normal velocity field profiles from a linear phased array (a) in the elevation plane (b) in the azimuthal plane. The parameters are: _f_=2 MHz, _N_ = 64 elements, _F_ = 10 cm, P_o = 347kPa, height 1cm, and length = 3.7cm. Note that this is a finite amplitude signal level. Propagation was in tissue, with α = 0.3 dB/cm and b = 1.1.

5.9 A Note Regarding Beam-steering and the Angular Spectrum Method

Although this thesis will not attempt to model beam-steering from phased array transducers, we mention how it might be accomplished. We suggest that a non-angular spectrum technique, such as the impulse response method of Ullate and San Emeterio (1992) be used to calculate the first-step linear field profile across a plane normal to the

direction of propagation. Subsequent to this first step, the angular spectrum approach could be used for the incremental plane-to-plane propagations.

5.10 Pulse Propagation

So far in this chapter, we have discussed the numerical implementation of the angular spectrum method for monofrequency sources. In considering pulsed sources, the source waveform must be broken up into frequency components. Each frequency component will have its own angular spectrum, and may be propagated separately using a propagator function appropriate for the distance and frequency in question. When choosing the size of the mesh over the source and observation planes, sampling at slightly better than the Nyquist rate of the highest frequency present in the spectrum should be used. This corresponds to $\lambda/2$ sampling, where λ is the wavelength of the peak frequency component. Pulsed propagation will be considered more fully in Chapter 7.

5.11 Conclusions Regarding Diffractive Propagation of Non-axisymmetric Sources

Given a planar field distribution as a source, the angular spectrum method may be used to diffractively propagate this source to a plane a distance Δz away.

- The source plane must be sampled at at-least the Nyquist rate of the CW frequency ($\lambda/2$) or the 2D-Nyquist rate of the distribution, whichever is lower.

- If the angular spectrum of the source is very narrow, the FSC algorithm may be used. This is because otherwise potentially dangerous undersampling of H for extreme spatial frequencies will be weighted by negligible values from the angular spectrum of the source.

- Once the sampling rate for the source is decided upon, we must decide how to sample the propagator function. The choice of sampling intervals for the source determines the extent of the spatial frequency domain.

- If the extent of the spatial frequency domain is completely contained within the radiation circle, the FSC algorithm may be used. The theorem in section 5.4 tells us what sampling intervals are needed within the spatial frequency domain to adequately

sample H. These spatial frequency domain sampling intervals, in turn determine the spatial extent to which the source should be zero padded.

- If the extent of the spatial frequency domain completely contains the radiation circle, spatial sampling of h is better. Because the radiation circle is contained within the transform domain, adequate sampling of h in the spatial domain is guaranteed.

- If the radiation circle is only partially contained within the transform domain, h must be sampled at a rate slightly better than the source. the sampling rate being slightly better than $\lambda/2$ (so as to increase the spatial frequency extent of h to completely encompass the radiation circle). Upon taking the Fourier Transform of h, the resulting angular spectrum may be truncated to match the spatial frequency extent of the source.

- The ray theory truncation may be used to truncate the product $H \times S$, and thus decrease the size of the matrix on which to perform the inverse 2D-DFT. This however may be unprofitable if the 2D-FFT is used, which requires that the matrix be of size $2^n \times 2^m$ points (where n and m are integers). The ray theory truncation may not be used to decrease the spatial sampling of s or h directly, as this may incur serious aliasing errors in the convolution.

- Frequency Domain sampling of transducer surfaces may prove to be more accurate in near-field computations, and may offer computational savings.

With the above approach, accurate results for continuous wave propagation were obtained, as verified by comparison with other methods.

Chapter 6: Modeling Finite Amplitude Propagation from Continuous Wave Sources

A propagating finite amplitude wave will distort due to convective and nonlinear effects. This distortion gives rise to harmonics not present in the initial spectrum, and thus in modeling nonlinear propagation, each of these harmonic components must be accounted for. The general approach we propose to modeling nonlinear progression has been outlined in chapter 4. This chapter will give greater attention to the details of our proposed scheme when the excitation signal is narrowband. In particular, we will comment on our choice of operator splitting approaches, the choice of nonlinear algorithm, and we will investigate modifications in the angular spectrum algorithm needed to propagate harmonics generated in nonlinear propagation. Approaches used to validate our algorithm will be explained, and results of our modelling will be compared with published data.

6.1 Choice of Operator Splitting Scheme

For continuous wave sources propagating in tissue, attenuation is expected to greatly reduce the amplitudes of harmonics generated in the nonlinear propagation process. It is anticipated that retention of only a few harmonics may be necessary for propagation at excitations levels typically used for diagnostic imaging. Frequency domain algorithms lend themselves nicely to nonlinear propagation when only a few harmonics are required.

The general idea behind the proposed modelling methodology is to solve for the effects of diffraction, attenuation and nonlinearity separately over small steps. As explained earlier, this can be accomplished by using an operator splitting approach with a fractional step marching scheme. In selecting an operator splitting technique, two second order schemes were presented in Chapter 4 which are suitable for simulation of finite amplitude propagation in tissue for CW sources. One of these schemes was originally presented by Tavakkoli et. al. (1998), and consists of an incremental half step of diffraction, followed by a whole step of nonlinearity and attenuation, followed by an additional half step of diffraction. The other approach was to first do a half step of combined diffraction and

attenuation, followed by a full step of nonlinearity, and finishing with a half step of combined diffraction and attenuation.

The choice of these operator splitting schemes may be based on whether it is desirable to combine diffraction and attenuation together, or whether combined nonlinearity and attenuation is preferred.

Our chosen diffraction algorithm, the angular spectrum approach, is inherently a frequency domain algorithm. It may save some computation time to calculate the effects of nonlinearity in the frequency domain, since this approach would bypass the need to transform the spectra back into the time domain. Because of this reason, and because of the computational efficiency afforded by needing only a few harmonics, the FDSBE is an attractive algorithm for CW nonlinear propagation. The FDSBE, allows the numerical evaluation of the combined effects of nonlinearity and attenuation. The inclusion of attenuation in the nonlinear algorithm is attractive for the sake of stability of the nonlinear substep, as it will tend to dampen higher harmonics. This may be particularly crucial when large substeps, (made feasible due to the second order nature of the operator splitting scheme) are chosen. If the FDSBE is used, the operator splitting scheme presented by Tavakkoli et. al. (1998) would be the natural choice to use in the fractional step marching scheme. Such a scheme has been implemented by us with moderate success. It should however be noted that the other second order operator splitting scheme has also been implemented with accurate results.

6.2 The Nonlinear Substep

The accuracy and reliability of our nonlinear propagation algorithm will greatly depend on the accuracy and reliability of its substituent algorithms. In particular, the algorithm for the nonlinear substep should be not only accurate, but also stable. Often times in numerical modeling, instability is an undesirable product of nonlinearity. We consider here validation of our nonlinear algorithm which will be implemented in the fractional step NLP algorithm.

6.2.1 Validation of the FDSBE Algorithm

To verify the accuracy of our FDSBE algorithm, we simulated plane wave nonlinear propagation in a dissipationless medium, and compared the harmonic trends with that of the (analytic) Fubini solution, presented in Chapter 3. This comparison (shown in Figs. 1(a) and (b)) is, of course, not valid beyond the shock distance. Fig. 1(c) shows typical harmonic trends of a plane acoustic wave propagating in liver.
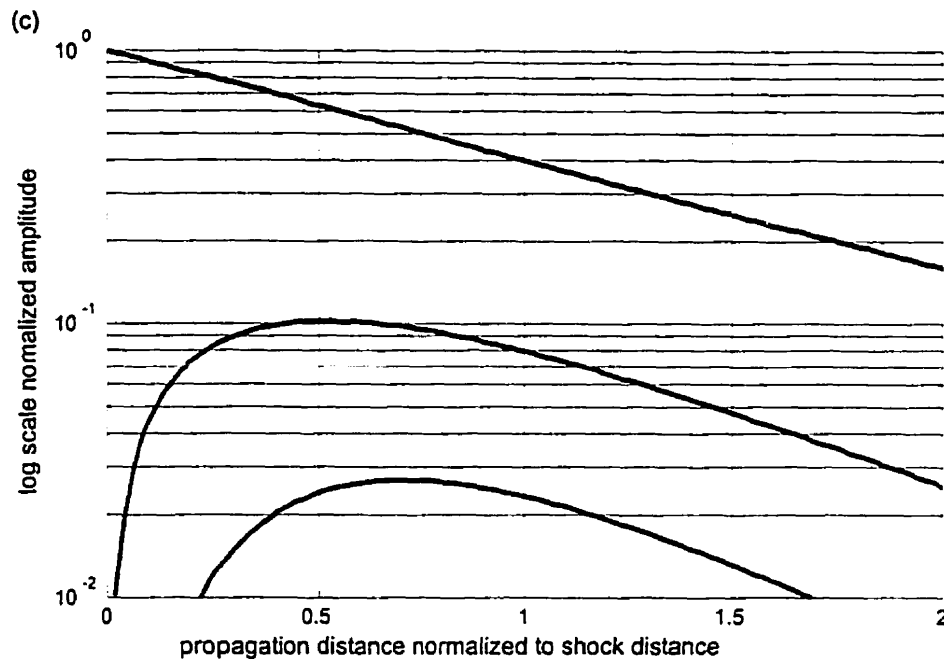
(a)

(b)
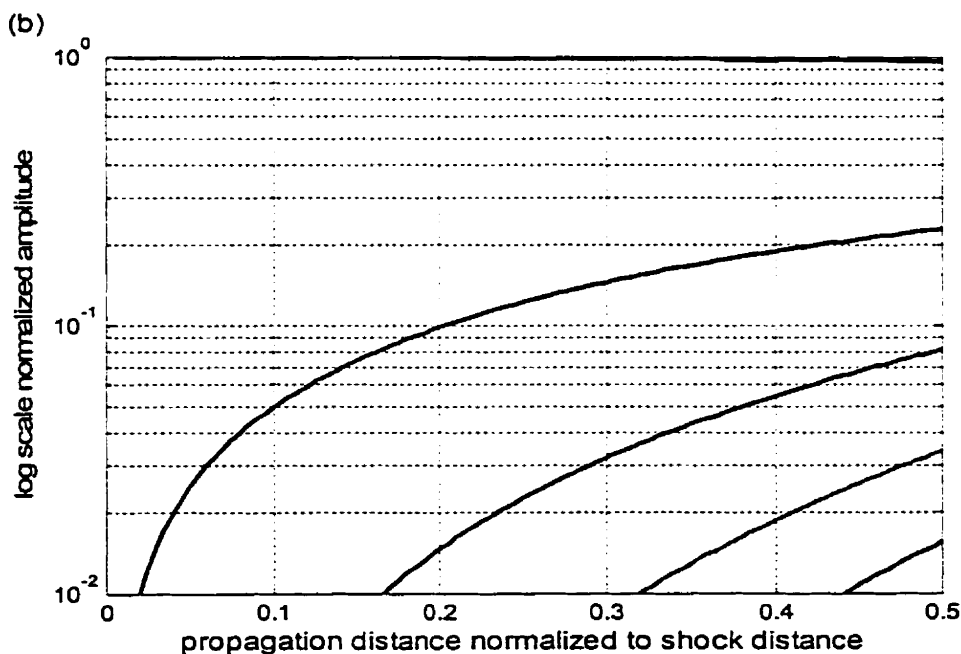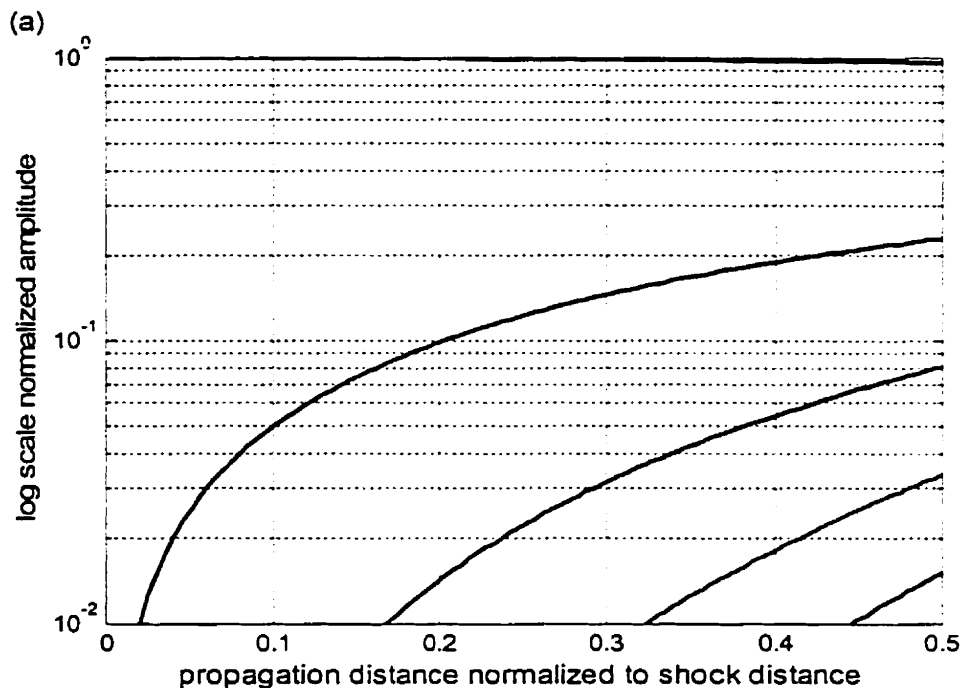
Figure 1 (a) The propagation curves of the first 5 harmonics (f = 1MHz ... 5MHz) using the FDSBE in a dissipationless medium. (b) The Fubini solution. (c) Nonlinear plane wave propagation in tissue for the first three harmonics, assuming an attenuaton coefficient of 0.3dB/(cm MHz), (i.e. a linear frequency dependence of the attenuation) using the FDSBE. The source amplitude for all three plots was 0.1m/s, and the nonlinear parameter β was 3.5.

6.2.2 Stability of the Plane Wave Nonlinear Algorithm

Unfortunately, the FDSBE has complex stability properties which are not well understood. The algorithm involves a finite number of harmonics, and so propagation of temporal waveforms which develop shockfronts may be troublesome if insufficient harmonics are retained. Trivett and Van Buren (1984) have investigated the accuracy of the algorithm for varying numbers of harmonics.

Step size is an important factor in contributing to the stability of the algorithm. If the steps used in the FDSBE algorithm are too big, the algorithm incorrectly extrapolates the nonlinear distortion, causing instability problems. Christopher and Parker (1991) found that limiting the step increments to a certain size resulted in stable computations. In particular, their step sizes were no larger than the distance over which the highest harmonic might be attenuated by a factor of 0.7. We will call this the 0.7 rule. Although

it seems counter-intuitive to consider step sizes which limit attenuation, the issue is more with regards to the nonlinearity. The FDSBE cannot handle large changes robustly. Our work confirms the general utility of the 0.7 rule for the plane wave FDSBE algorithm. We did, however, notice that the rule did not always apply when diffraction present. Some instabilities were observed for moderate amplitude wave propagation in water. Fewer problems were encountered for tissue propagation.

Each nonlinear substep may be broken down into smaller substeps to allow the 0.7 rule to be implemented. Larger step sizes, however, were still retained for the diffraction substeps, and thus some of the instabilities we noticed may have been for cases where the large step size of diffraction perturbed the subsequent application of the nonlinear algorithm. Further investigation of stability for our approach is recommended for future work.

For shock wave propagations, hundreds or thousands of harmonics may be needed, greatly increasing the computation time of the FDSBE algorithm. Specifically, computational complexity on the order of N^5, where N is the number of harmonics retained. Christopher and Parker used a harmonic limiting scheme whereby artificially high attenuation was applied to higher harmonics, thereby allowing shockfront propagations to be carried out reasonably accurately with 50-100 harmonics. Because we are primarily concerned with nonlinear propagation in tissue, attenuation may work naturally to our advantage in this regard, and so artificial ramping of the attenuation for higher harmonics was not considered in this work. The scheme proposed by Pischal'nilov et. al. (1996) may also be useful for shock wave propagations, but was not considered here, as shock waves are not anticipated in tissue for amplitudes used in diagnostic medical ultrasound.

6.3 The Diffractive Substep

A diffraction algorithm suitable for integration into the CW NLP algorithm must account for diffractive propagation of frequency components generated due to nonlinearity. The angular spectrum method has been shown to be an attractive approach to the calculation of diffraction. It remains to be shown, however, how the angular spectrum approach can

be applied to nonlinear propagation within the context of the second order operator splitting scheme. In particular, choosing a planar sampling grid may be a non-trivial task. For each harmonic profile, it must further be decided whether to use the FSC or SSC approach to calculate diffraction.

For simplicity, let us presume that each harmonic profile has an identical planar sampling scheme. Moreover, although it is possible to use an adaptive gridding scheme, we found it simpler to use the identical gridding scheme for each plane along the direction of propagation.

Intuitively, one might presume that the sampling intervals Δx and Δy which are needed to represent planar distributions in propagation of harmonics would be at most $\lambda_N/2$, where λ_N is the wavelength of the highest harmonic. Although this is the rate needed to adequately sample the point spread function h for step sizes $\Delta z > \lambda$, the harmonic profile itself may be much smoother than this Nyquist rate requires.

In the work of Christopher and Parker (1991), it was found that reasonable modeling results could be obtained by sampling at rates far less than the Nyquist rate of the highest harmonic. In fact, they observed that for focused field propagations involving up to 50 harmonics, a radial sampling rate of 4 times the Nyquist rate of the fundamental has given very good results. For unfocused fields, 1 or 2 times the Nyquist rate of the fundamental worked very well. Like them, we can confirm of the adequacy of the sampling rate by examining the radial profiles of the highest harmonics. If the radial sampling rate is insufficient, then these profiles will loose coherence.

Selection of a lateral sampling rate for the harmonic profiles of the planes, essentially reduces to an educated guess. If increasing the sampling rate across the lateral profiles of the harmonics does not significantly produce different results, one may surmise that a convergent solution has been reached and that sampling is adequate.

Once lateral sampling rates have been chosen, each harmonic profile must be propagated an incremental distance using either the FSC or the SSC algorithms. Based on the analysis in the previous chapter, there is a reliable way of choosing whether to sample h or to sample H. If the radiation circle of the nth harmonic is completely contained within the discrete transform domain, sampling of h should be done at the rate determined by the gridding of the harmonic distribution itself. If the radiation circle is partially contained within the transform domain, once again h should be sampled, however, sampling should be done at the Nyquist rate of the nth harmonic ($\lambda_n/2$) or better - even if it requires sampling at a different rate that the source field. Sampling H may be done when the radiation circle is exterior to the extent of the spatial frequency domain and when all the oscillations of H contained within this domain may be adequately sampled by the spatial frequency sampling scheme of the source.

Suppose that the source plane harmonic profiles are sampled at a rate γ times the Nyquist rate of the fundamental, where γ is a real number, typically between 1 and 4. For harmonics $n > \gamma$, the discrete spatial frequency transform domain will be completely inside the radiation circles $k_x^2 + k_y^2 = k_n^2$. For some harmonic $n_H > n_\gamma$ and above, it will be possible to sample H at the same rate as the angular spectrum of the source. For harmonics $n_H - 1$ and below, sampling H is not advisable since there may be convolutional wraparound errors which may give erroneous results of the FSC algorithm. Exceptions to this hypothesis may be in situations where either the propagation distance is small compared to the harmonic wavelength, or where the angular spectrum of the source plane is very narrow. The minimum harmonic n_H for which sampling H is reliable can be obtained from the theorem given in section 5.4. Equation (7) in this section, may be re-written as

(1) $$\Delta k_x \leq \frac{\pi \sqrt{k_n^2 - (k_{x\,max}^2 + k_{y\,max}^2)}}{2 \Delta z k_{x\,max}},$$

where $k_n = nk = 2\pi n f/c$ is the magnitude of the wave vector for the nth harmonic.

We can solve equation (1) for n to find the minimum harmonic, n_H, for which frequency domain sampling of H will give accurate results, given the chosen sampling extents and gridding. This minimum harmonic is given by

$$(2) \qquad n_H = \sqrt{\left(2\Delta z \gamma \Delta k_x / \pi\right)^2 + 2\gamma^2} \,,$$

where

$$\gamma = k_{xmax} / k_o \,.$$

6.3.1 The Virtual Source Interpretation of Nonlinear Harmonic Generation, and the Danger of Using a Ray Theory Truncation

As a finite amplitude sound beam progresses through space it interacts with itself in a nonlinear way. In the process, harmonics as well as sum and difference frequencies are generated. One way of thinking about the harmonic generation process is to consider that there are virtual sources along the path of the sound beam, emitting harmonic frequencies. With this oversimplistic, yet useful concept, one may immediately see the danger in using a Ray Theory Truncation. Virtual sources some distance from the transducer may emit harmonics which will contribute to the field profile at the observation plane. The angle subtended by the edge of the observation plane and the virtual source will be greater than the angle θ_{max} determined by the ray theory (see Fig. 5-4). Thus restricting the spatial frequency extent over the observation plane by a ray theory truncation may lead to inaccuracies. For this reason, we chose not to implement the ray theory truncation in our NLP algorithm.

6.3.2 Summary of the Diffraction Algorithm for CW Nonlinear Propagation

Our version of the diffraction algorithm for propagating multiple frequency harmonics can be summarized as follows:

- Assume that sampling the harmonic source planes at γ times the Nyquist rate will adequately represent the angular spectra of the highest harmonic. This determines the maximal extent of the transform space in the spatial frequency domain k_{xmax} and k_{ymax} as well as the spatial sampling intervals Δx and Δy. For simplicity, we take equal x and y coordinate sampling lengths.

- Choose the maximal extent $[X_o, Y_o]$ of the observation plane which one desires correct results. Again, for simplicity, let $X_o = Y_o$. Moreover, consider for simplicity that the sampling extent $[X_s, Y_s]$ of the source plane is the same size as the region of interest in the observation plane. Thus, $X_s = X_o$ and $Y_s = Y_o$.

- Choose the maximal extent of the spatial domain transform space: $T_x \geq X_o + X_s$, and $T_y \geq Y_o + Y_s$. (We can, moreover choose $T_x = T_y$). This choice establishes the extent to which the source plane must be zero padded. It also establishes the spatial frequency domain gridding Δk_x and Δk_y.

- Note that the radiation circle of the harmonics $n_\gamma > \gamma$ are contained within the spatial frequency transform domain.

- Determine the desired step size Δz between planes. Note that a constant step size algorithm will be the most computationally efficient since the propagator functions would only need to be computed once.

- For harmonics n_H (given by Eq. (2)) and above, sample H in the spatial frequency domain with the sampling prescribed by $\Delta k_x = \pi/T_x$ and $\Delta k_y = \pi/T_y$.

- For each of the harmonics $n = 1, \ldots, (n_H-1)$, sample h. For harmonics $1 \ldots n_\gamma$, the sampling of h should be done with the intervals Δx and Δy used to sample the source plane. For harmonics $n_\gamma \ldots n_H-1$, sample h with intervals determined by the Nyquist rate of the nth harmonic ($\lambda_n/2$) or better.

- The product $S_d \times H_d$ can be truncated in the spatial frequency domain to γk, which is the spatial frequency extent determined by the sampling $\Delta x, \Delta y$ of the harmonic source planes.

6.4 Scheme for testing the Diffraction algorithm for harmonics

Testing that the diffraction algorithm will perform satisfactorily when integrated in the NLP algorithm is important because the high frequency harmonics generated in nonlinear propagation need to be propagated accurately. Such a test is difficult to devise because there is no known gold standard to test whether a particular harmonic generated after a nonlinear substep is being propagated properly in the subsequent diffractive substep.

Our approach to testing the diffraction algorithm is to quantitatively assess the accuracy of linear propagation of several frequencies from a large piston source – where harmonics are not generated due to nonlinear propagation, but rather originate from the source directly. The astute reader will be cautious of such a test. Having selected a sampling rate γ at between 1 and 4 times the Nyquist rate of the fundamental, it may be that the angular spectrum for harmonics $n > \gamma$ extend beyond the extent of the spatial frequency domain – thus incurring wraparound error. Indeed, even after diffractive propagation, where the angular spectrum S is tapered by a transfer function H, the extent of the angular spectrum may still extend out to the radiation circle of the nth harmonic, which is exterior to the spatial frequency domain for $n > \gamma$. For large sources and focused sources, however, the sound beam will be fairly directional, and the angular spectrum may be narrow – such that the bulk of the energy will be contained within the extent of the spatial frequency domain. This is the motivation for using a large disk.

Results of our multistep diffraction algorithm for a large disk radiating several harmonics was compared with results of another diffraction technique of known accuracy, where the frequencies were propagated one by one, and not all together. Harmonic profiles of the two techniques are compared in Fig. 2.
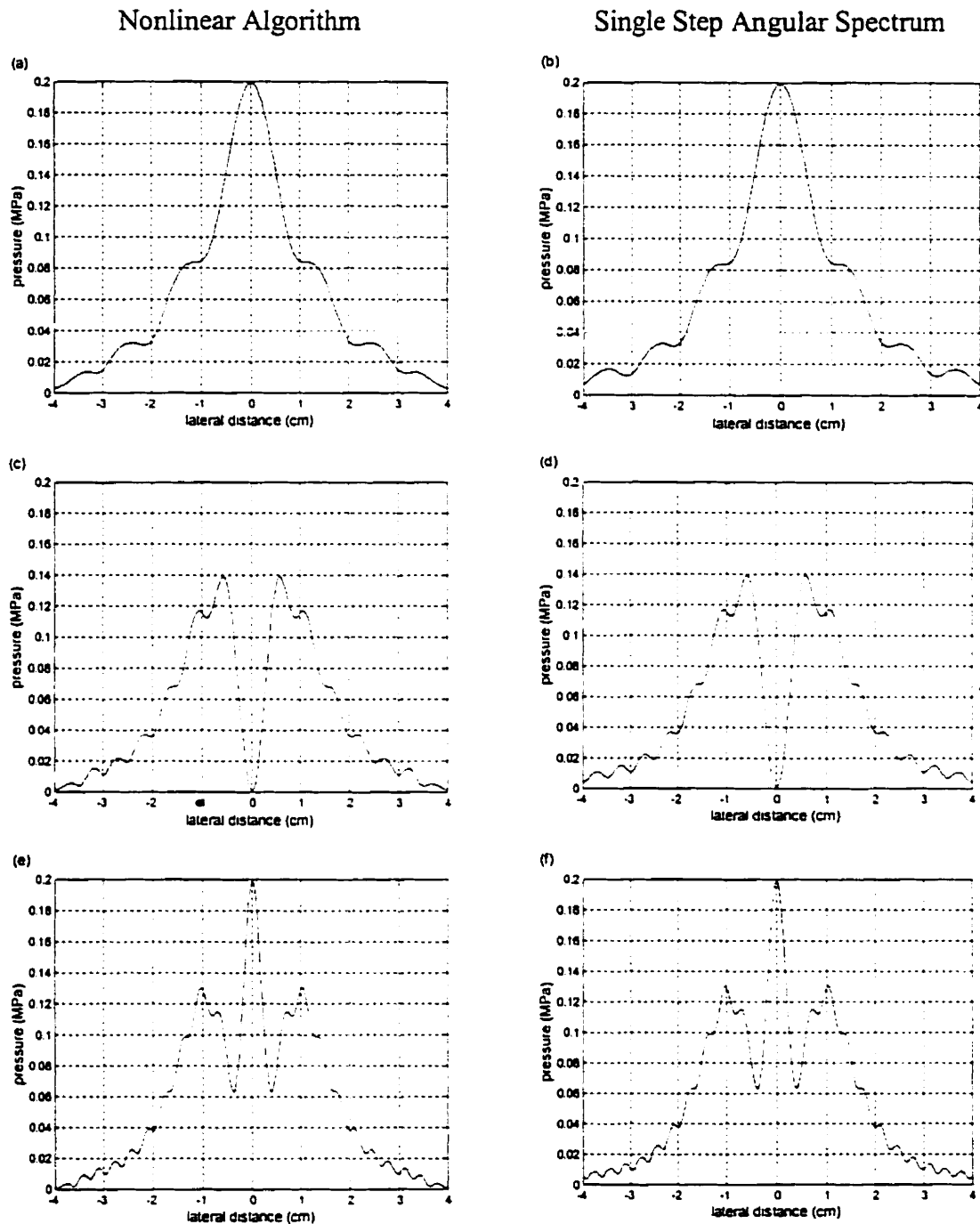
Nonlinear Algorithm   Single Step Angular Spectrum

Figure 2 The figures on the left are lateral profiles of a disk of radius 1.9 cm using our nonlinear propagation algorithm, with β=0, and harmonics of 1,2, and 3 MHz being transmitted from the source. The figures on the right are lateral profiles of frequencies *f* = 1, 2, and 3 MHz, respectively using a 'Gold Standard' one-step angular spectrum method which has been cross verified with the (slower) Rayleigh integral method. This comparison is to verify that the proposed sampling scheme for the diffraction algorithm can accurately propagate multiple frequency harmonics. The parameters for the results on the right are: #planes = 10, pressure amplitude of each frequency component = 100 kPa, axial distance at which the profiles were computed = a^2/λ_o, where λ_o is the wavelength of the 1MHz signal. Sampling was done at 1.1 times the Nyquist rate of the fundamental.

6.5 Coding of the NLP Algorithm

The entire nonlinear propagation algorithm was coded in MATLAB v.5.3. All efforts were used to avoid loops in the code, as MATLAB is an interpretive language, and handles loops very slowly. However, array operations are a forte of MATLAB, and most algorithms could be vectorized to take advantage of MATLAB's optimized array processing capabilities. Software exists to compile MATLAB code into C/C++, however, this route was not taken since run times were reasonable enough in the MATLAB environment.

6.6 Verification of the NLP Algorithm

6.6.1 The NLP Algorithm with Vanishing β

An important test to validate the nonlinear propagation algorithm is that the algorithm successfully simulates linear propagation, when $\beta = 0$. Results identical to those in figure 2(a) were obtained when a 1.9 cm disk radiating at 1MHz was simulated.

6.6.2 Comparison with KZK Modeling and Experimental Data for Propagation in Water

Although our primary interest is in nonlinear propagation in biological tissue, modeling water propagation should also be attainable. Water has weak absorptive characteristics, while maintaining a non-negligible nonlinear properties. Our model was used to compute the CW response from a plane disk transducer of radius 1.9cm, operating at 2.25 MHz. The source pressure was only 100 kPa. Baker (1988) obtained experimental and theoretical fields which we use to compare with our results in Fig. 3 and 4. Also shown in Fig. 5 is a comparison with results reported by Christopher's (1991).
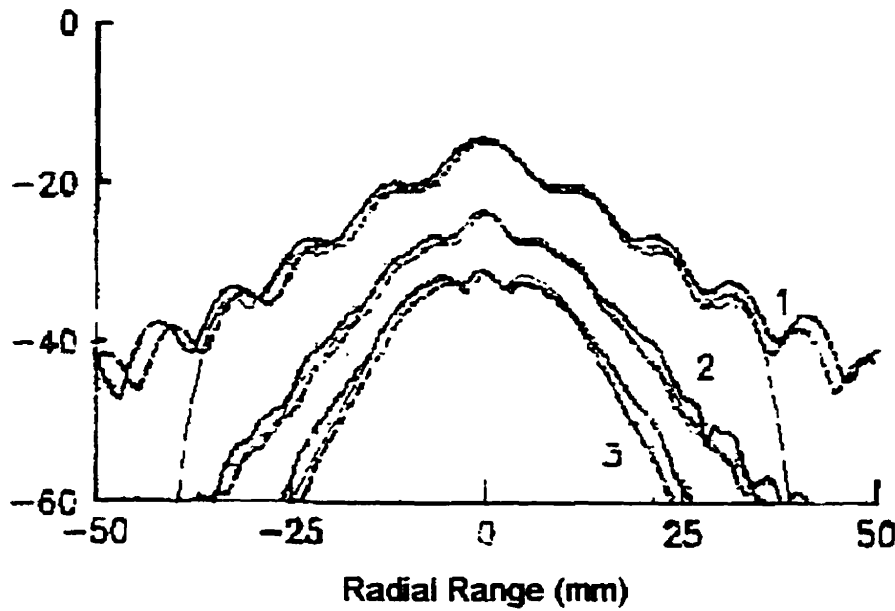
Figure 3 Comparison of our results (colored lines) with Baker's experimental results (solid lines) and KZK modeling (dashed lines) for the first three harmonics. The curves represent the lateral pofiles at 50 cm in water from a 1.9 cm radius piston at 2.25 MHz.
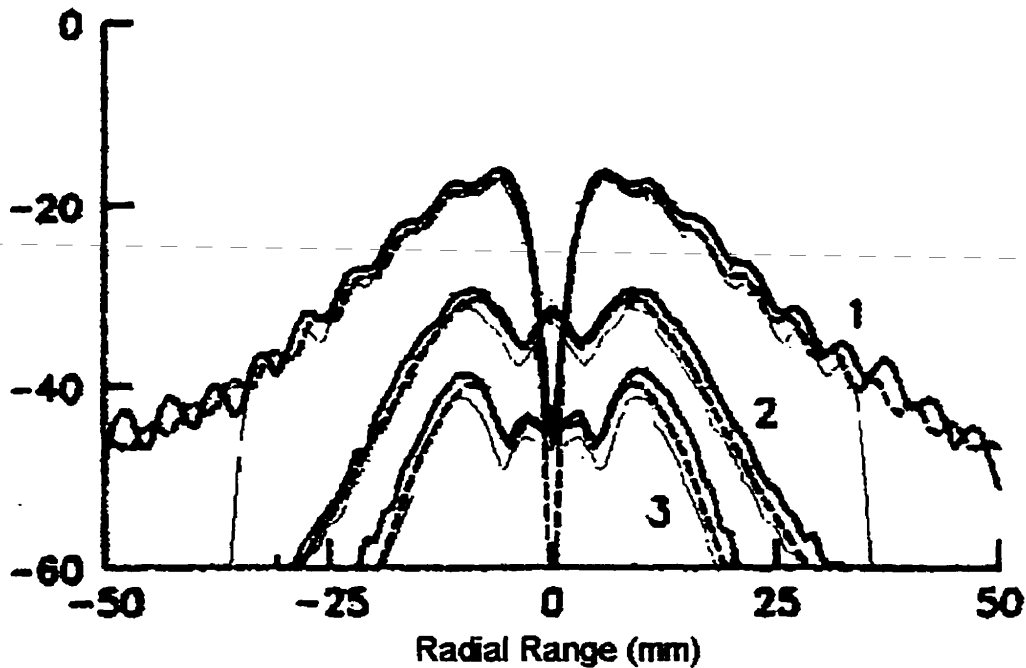

Figure 4 Lateral profile at z = 275 mm of the first three harmonics produced from a 1.9 cm plane piston transducer, radiating at 2.25 MHz. The colored lines are the results from our model, the black solid line is experiment (Baker, 1988), and the black dashed line is results of KZK modeling (Baker, 1988).
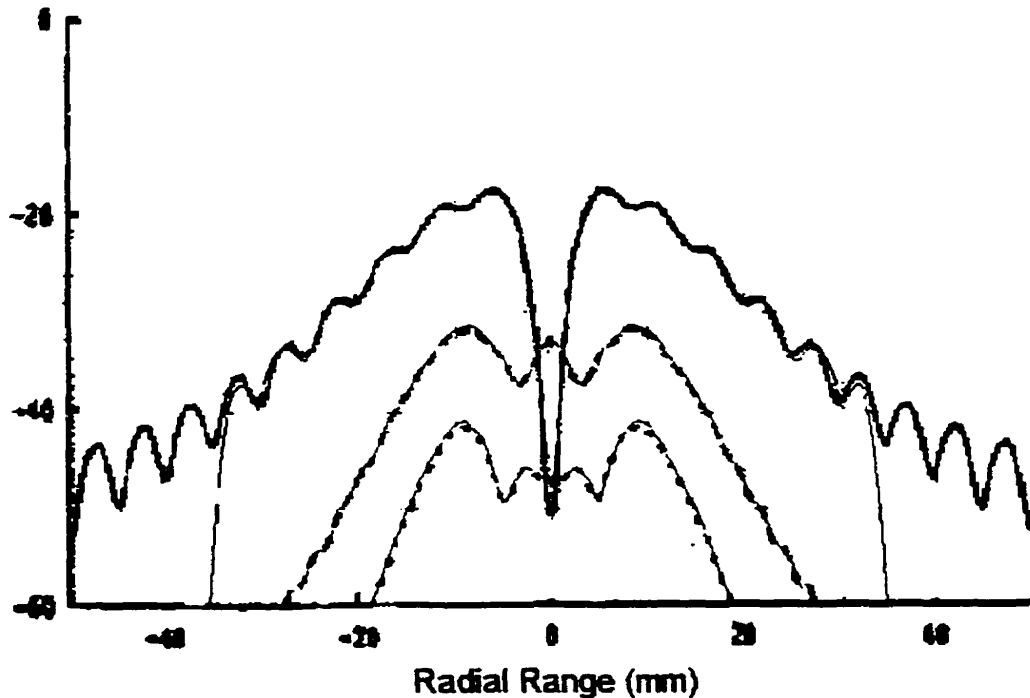
Figure 5 Comparison with the modeling results of Christopher (1991) for the same paramters as given in Fig. 2.

Our simulations for Figs. 3-5 used only 20 propagation planes. In contrast, Baker used a smaller step size in his finite difference code corresponding to over 1000 planes. Christopher, too uses small steps (often 20 per cm) thus requiring hundreds or thousands of increments. The second order operator splitting scheme of our approach appears to offer a fundamentally new way of improving the computational efficiency while maintaining accuracy.

Note the overall close agreement between our results published data. It may be observed in Figs 3-5 that the lateral profile of the fundamental drops off at around 35mm on either side of the mainlobe. This is due to the windowing we applied to the propagation planes. A further observation is that the 3rd harmonic is slightly lower than the experimental and KZK results in Fig. 4, but in very good agreement with Christophers results shown in Fig. 5. This may be due to the use of the plane impedance relation we used to relate normal particle velocity with pressure. Both our method and Christopher's technique used normal

particle velocity in the NLP algorithm. The plane impedance relation is less accurate in the nearfield, and may give rise to a source of error.

It is interesting that that in Figs. 4 and 5, the on axis fundamental level is actually below the levels of the harmonics. Moreover, the levels of the harmonics are fairly high overall. In Fig. 3, the second harmonic is less than 10dB down from the fundamental, even out to about 20 mm off axis. This is encouraging with regards to harmonic imaging, since extracting the harmonic signals may be very challenging if the signal level is too low. One might worry more about signal levels in tissue propagation, since tissue is typically a strongly attenuating medium. In the next section we show some encouraging modeling which demonstrates the signal level of harmonics in tissue is also promising.

6.6.3 Comparison with KZK Modeling for Propagation in Tissue

Modeling nonlinear propagation in tissue may be considered less of a computationally burdensome task than simulating nonlinear propagation in water. This is because attenuation works to dissipate the energy buildup of higher harmonics. Averkiou et. al. (1997) have simulated nonlinear propagation from a focused disk in a liver-like medium using a KZK modeling approach. We use our model to compare with his results. For these simulations, the source, operating at 2 MHz, had a radius of 1 cm and a focal length of 10cm. In our modeling approach, we did not sample the aperature in the spatial frequency domain. Instead, we implemented sampling of the aperature in the spatial domain, where we modeled the focused disk as a plane disk with a complex phase weighting function $e^{jk\sqrt{d^2+r^2}}$, where d is the focal distance. This is not an exact technique, but rather is equivalent to a Fresnel approximation. For the modeling results in Figs. 7 and 8, only 20 propagation planes were used with a lateral sampling of 2.1 times the Nyquist rate of the fundamental. For Fig. 6, more propagation planes were used so as to capture the axial variations of the harmonics. The deep nulls which are seen in Averkiou's results, but not in ours may be due to higher axial sampling on their part, and less axial sampling on our part.
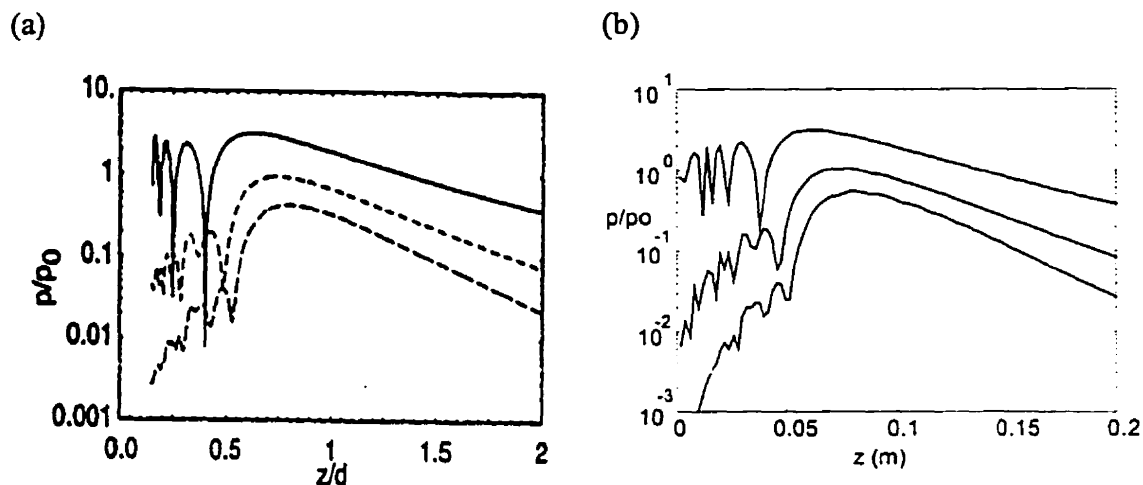
(a)

(b)

Figure 6 Axial profile of a 1 cm radius focused disk transducer operating at 2 MHz in liver. $\alpha = 0.3$dB/cm, $c = 1486$ m/s, and $\beta = 5.0$. (a) Results of KZK modeling by Averkiou et. al. (1997) (b) Results obtained with our algorithm.
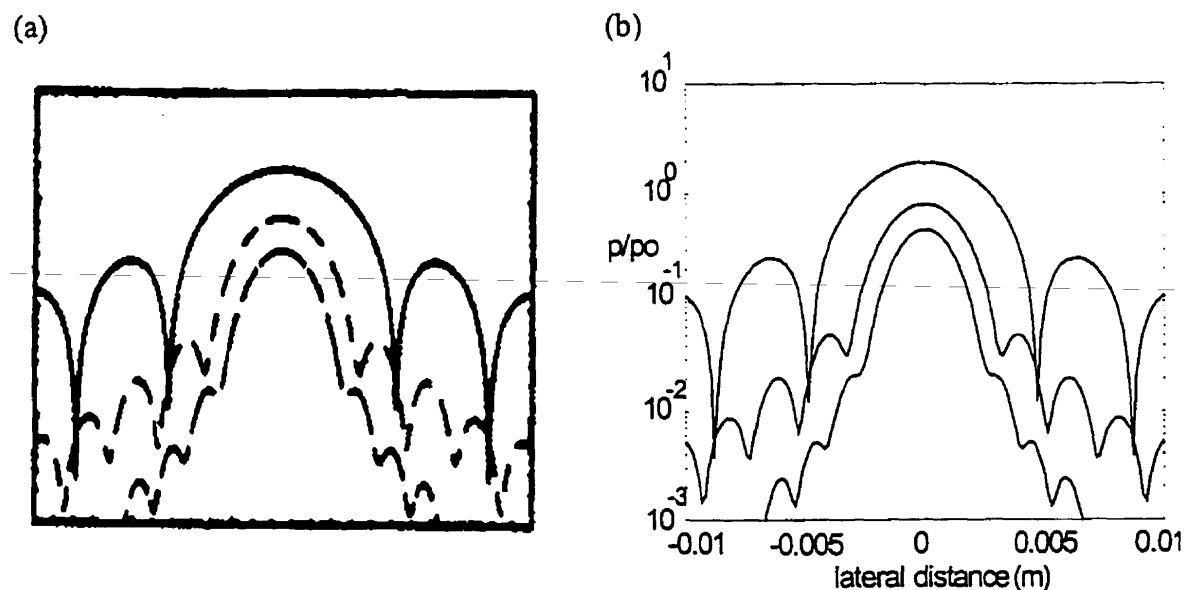
(a)

(b)

Figure 7 Lateral profile of first three harmonics at the focal distance. (a) From Averkiou et. al., (1997). (b) Results from our model. The parameters are the same as for Fig. 6.
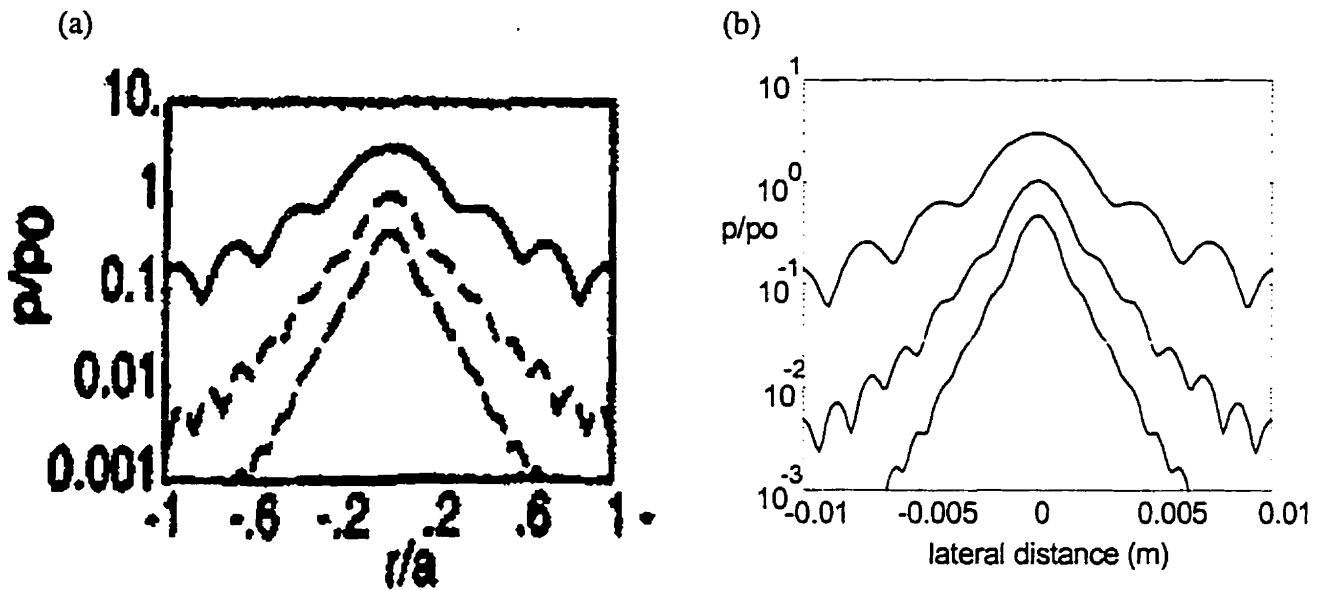
(a)

(b)

Figure 8 Lateral profile of the first three harmonics at 0.7 of the focal distance. (a) From Averkiou et. al. (1997). (b) Results from our model. Parameters were the same as for Fig. 6.

Note that in the axial profile (Fig. 6) the harmonic build-up due to nonlinearity occurs as the beam propagates, and that the signal is not well formed in the extreme nearfield. This can be advantageous for imaging, where surface inhomogeneities would otherwise perturb the coherence of the fundamental signal. Because harmonics are primarily formed after these surface regions, their utility for imaging deeper structures is more robust compared with using the fundamental.

Note also that there is a prefocal shift of the last maximum of the fundamental curve. This occurs because energy is being depleted from the fundamental to feed the generation of higher harmonics. Such a shift may be accounted for in designing a tissue harmonic imaging system.

In the lateral profiles, as for water propagation, the harmonic sidelobes fall off more quickly than the fundamental sidelobes. This is a major factor in the attraction of using

harmonics for imaging. Lower sidelobes may mean an improvement in the signal to clutter ratio. One reason that harmonic sidelobes are lower may be that harmonic generation is amplitude dependent. Where the fundamental level is highest (in the mainlobe region) the harmonic level will also be high, but when the fundamental level is lower (in the sidelobe regions), the harmonic levels drop off rapidly. Propagation in tissue may actually work to our advantage in this regard. In the mainlobe region, nonlinearity will dominate over attenuation if the signal is strong enough, however, in the sidelobe region, attenuation may dominate over nonlinearity, and the harmonic sidelobes will fall off very rapidly.

The lateral profile of the fundamental is still very similar to the profile one would see in pure linear propagation. Note the classic Bessel directivity of the fundamental at the focus. Sidelobe oscillations called fingers may be seen in the harmoinic profiles and are characteristic of nonlinear propagation. They have been noted by a number of authors, including Averkiou (1997).

Finally it should be noted that the second harmonic level is still quite high (only 9dB down from the fundamental at the focus), even for low amplitude excitation, and for propagation in tissue. As noted, generation of sufficient harmonic levels is important for realizing the feasibility of signal detection for harmonic imaging.

6.7 Nonlinear Propagation in Tissue from a CW Linear Phased Array

So far, the nonlinear propagation results presented have been those of radially symmetric transducers. Having verified the accuracy of the algorithm we are in a position to demonstrate the nonlinear field response of a linear phased array. Here we consider a linear phased array with no beam-steering, no apodization, and no lens in the elevation plane. We have used the spatial frequency domain sampling approach outlined in section 5.7.2. The array considered had 64 elements of width $\lambda/2$, and spaced $\lambda/4$ apart, where the operating frequency was 2MHz. Elements were of height 1cm, and the array was phased such that the focal distance was 10cm. The length of the transducer was 3.7 cm,

and the continuous wave excitation was of amplitude 347 kPa. Propagation was in a liver-like medium with β=5 and α_0 = 0.3dB/cm at 1MHz. Shown in Fig. 10 are the azimuthal (x-z) and elevation (y-z) planar distributions. As expected, the harmonic mainlobes are much narrower than the fundamental. Moreover, as may be seen in Fig. 9, the harmonic sidelobes drop off extremely fast compared with the fundamental. In the elevation plane, even when no lens is used, the harmonic profiles are narrower. In phased array B-mode imaging, fundamental sidelobes have been known to be particularly troublesome, causing clutter artefacts. For harmonic sidelobes, however, it seems that attenuation dominates over nonlinearity, and thus clutter artefacts may be reduced by using the harmonic signal.

There is notable harmonic buildup off axis before the focal region which may be troublesome for imaging purposes. Moreover, the last maximum in the focal region seems to be slightly closer to the transducer than the 10 cm mark which we would expect.
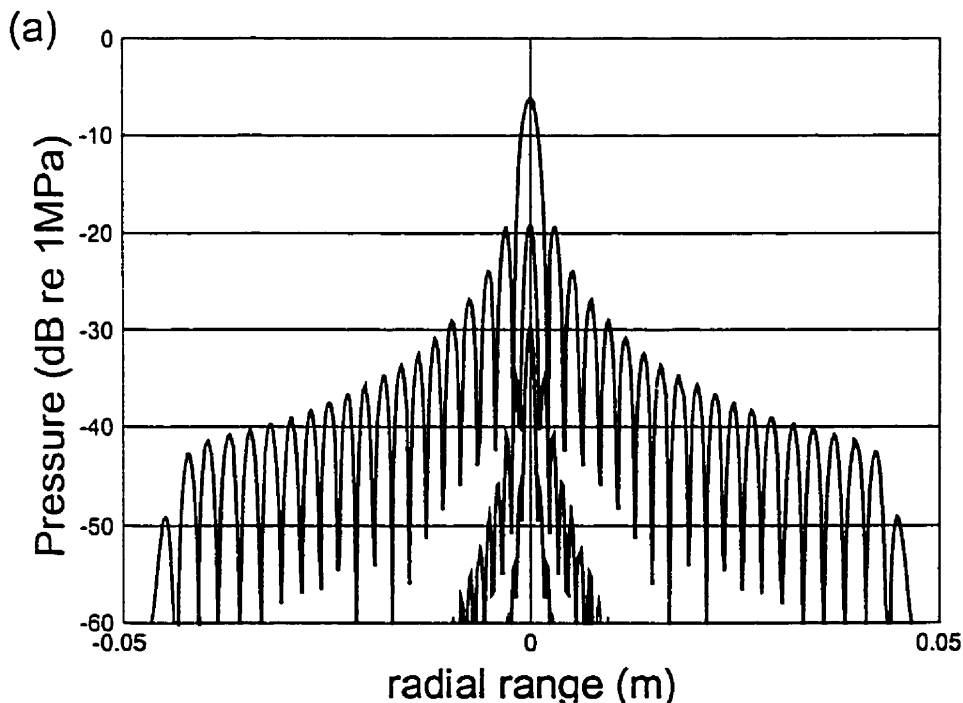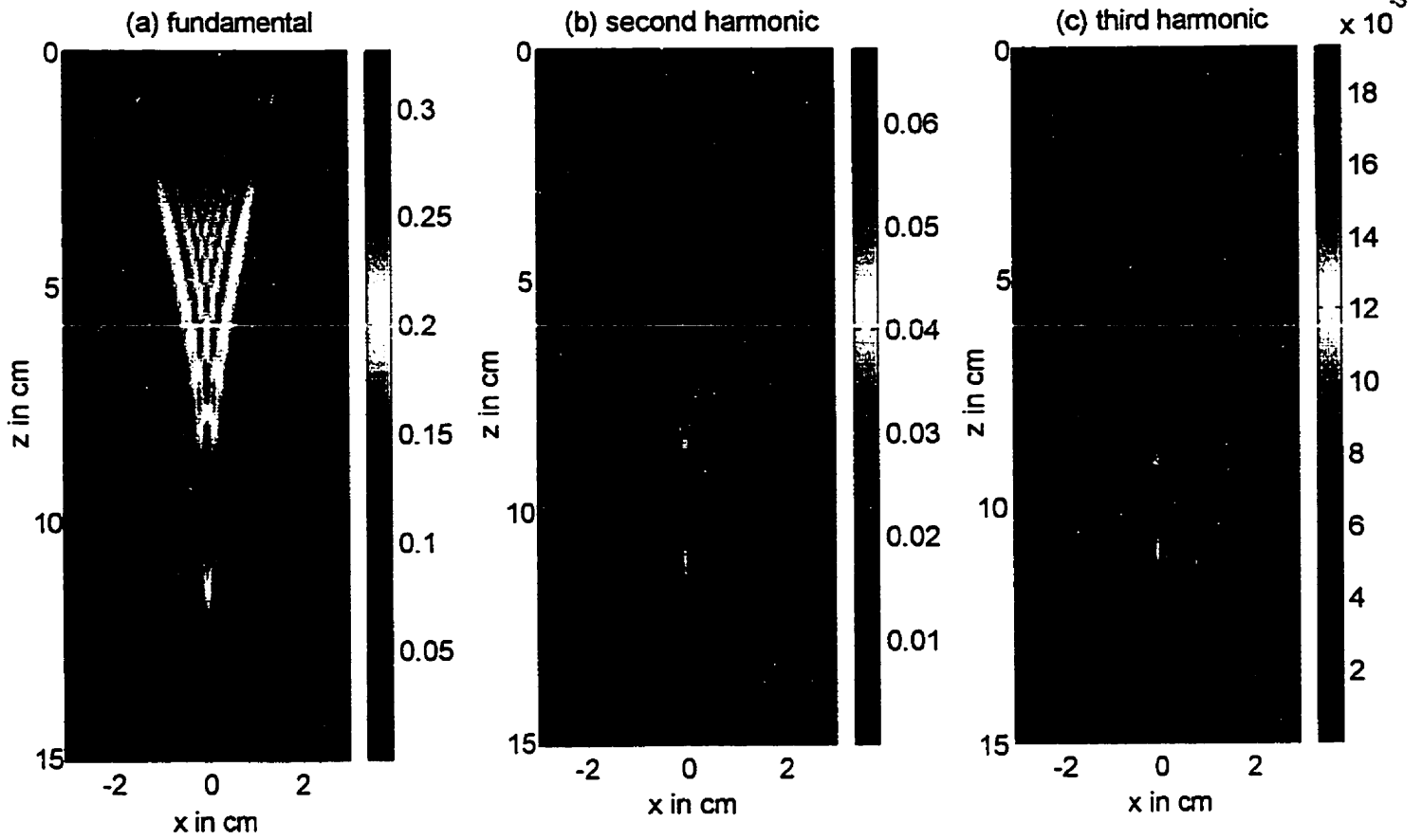

Figure 9 Lateral profile of first three harmonics of a linear phased array.

(a) fundamental   (b) second harmonic   (c) third harmonic

(d) fundamental   (e) second harmonic   (f) third harmonic $\times 10^{-3}$
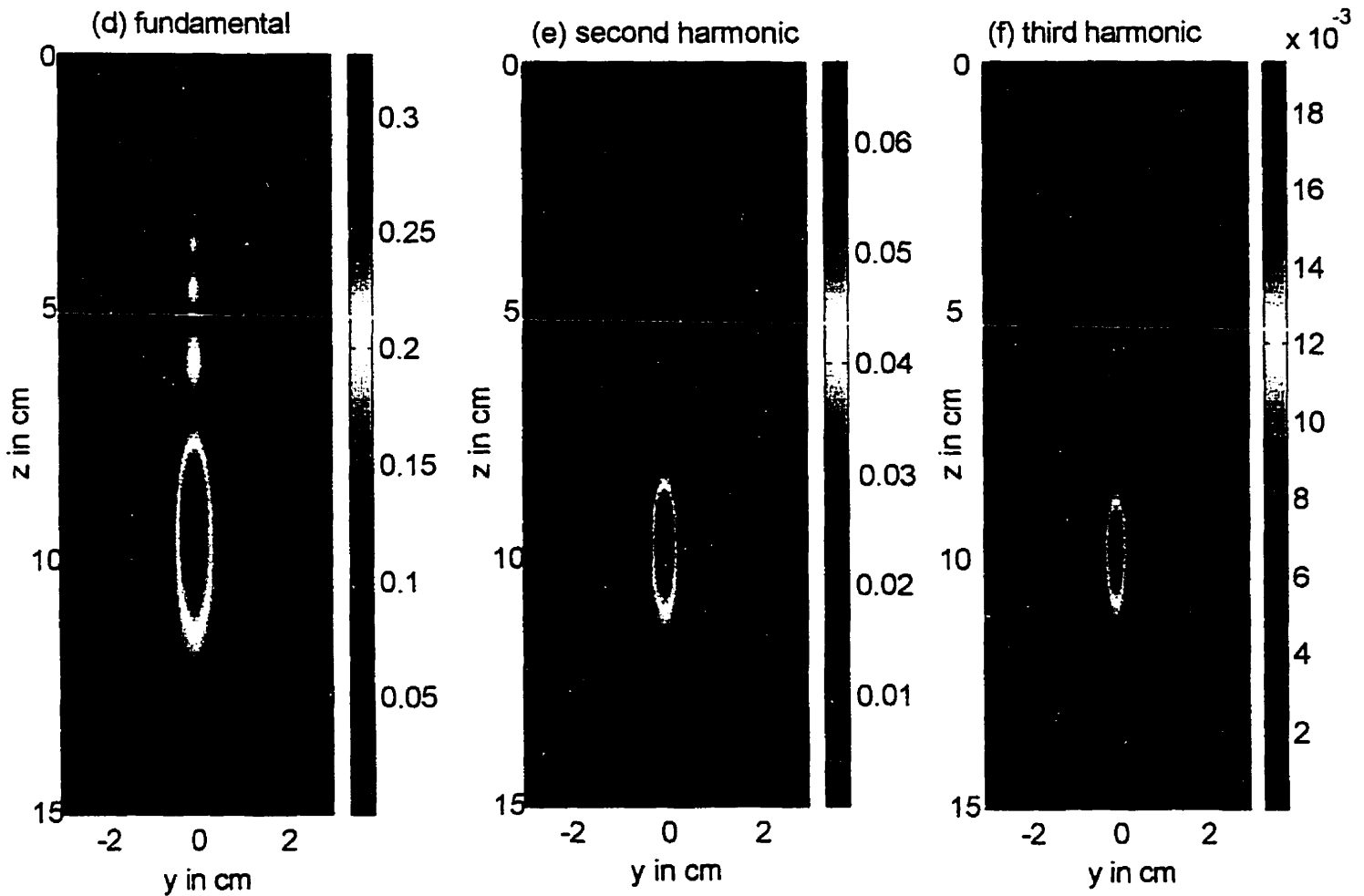
Figure 10 (a)-(c) Azimuthal plane and (d)-(e) elevation plane harmonic profiles from a 2 MHz linear phased array propagating in a liver-like medium. The array had 64 elements of hight 1cm, and was 3.7cm in total length. The elements were $\lambda/2$ across, and spaced $\lambda/4$ apart, where $\lambda = c/f$. The focal length was 10cm. The tissue was assumed to be characterized by $\beta=5$, $\alpha_0 = 3$ dB/(cm MHz), and b=1.1. No lens was used to focus the transducer in the elevation plane.

Factors Affecting Speed

One of the largest factors affecting the computational burden of the NLP algorithm is the lateral extent and sampling of propagation planes used. Because our model may handle non-axisymmetric sources, a 2D grid of sample points must be used to represent each propagation plane. Increasing the number of samples from 512 x 512 to 1024 x1024, for example, produces a large increase in computation time. For a given aperature size,

simulating the field response of a higher frequency is more computationally demanding than that of a lower frequency. This is because higher frequencies require denser sampling.

The other major factor affecting the speed of the algorithm is the number of harmonics included. Luckily, for tissue, we can attain reasonable results with only a few harmonics. For water, there is less attenuation, and, in general, more harmonics are needed.

# Chapter 7: Nonlinear Propagation of Pulsed Ultrasound

As noted earlier, when the excitation is pulsed, more frequency components are needed in the initial spectrum, and thus both the nonlinear substeps and the diffractive substeps are burdened by a computational load much greater than in the narrowband case. Efficient modeling of nonlinear propagation of wideband signals requires a slightly different approach than that used for CW excitation as outlined in the previous chapter. In this chapter we intend to develop a methodology appropriate for pulsed excitation.

7.1 Choice of the Nonlinear Algorithm

Use of the FDSBE algorithm is far less attractive for pulsed excitations than for continuous wave excitations. In Chapter 6 it was noted that the computational complexity of the FDSBE was on the order of N^5, where N is the number of frequency components used. For pulsed sources hundreds or even thousands of frequency components may be needed to accurately sample the temporal variations of a wideband signal. Artificial absorption of higher harmonics has been used in the continuous wave case to limit the harmonics created due to nonlinearity. However, such as scheme when applied to pulsed waveforms, may cause unnatural distortion. Most investigators agree that using a time domain nonlinear algorithm is a much more attractive option. For diffraction, our intention is to use the angular spectrum method, as this approach has shown great computational savings over the Rayleigh method. The disadvantage, then, of using a time domain nonlinear operator is that we will need to transform back and forth between time and frequency domains for each substep in the NLP algorithm. Not only will this process take additional time, but such numerical book-keeping will likely incur some errors. However, the computational savings to be won by using a time domain nonlinear algorithm, may outweigh any potential time losses or inaccuracies due to the transform algorithms.

Of the two time domain algorithms for nonlinear plane wave propagation presented in Chapter 3, we selected the algorithm developed by Christopher, as it is very stable, is computationally efficient, and is reasonably accurate. To verify the accuracy of our code, we compared our Time Domain Solution to the Nonlinear Equation (TDSNE) with the

Fubini solution in the pre-shock region for a sinusoidal excitation. The two methods compared well (Figs. 1(b) and (c)), although discrepancies may be observed when the step size Δz is too large (Fig. 1(a)). The TDSNE also captured relatively well the dynamics of plane wave nonlinearity of pulsed sources (Fig. 2). Both step size and sampling frequency of the waveform play an important role in the accuracy of the nonlinear substep. When this algorithm is integrated into the fractional step NLP algorithm, multiple nonlinear substeps may be needed for each large diffractive substep. This is especially the case if large substeps are used.
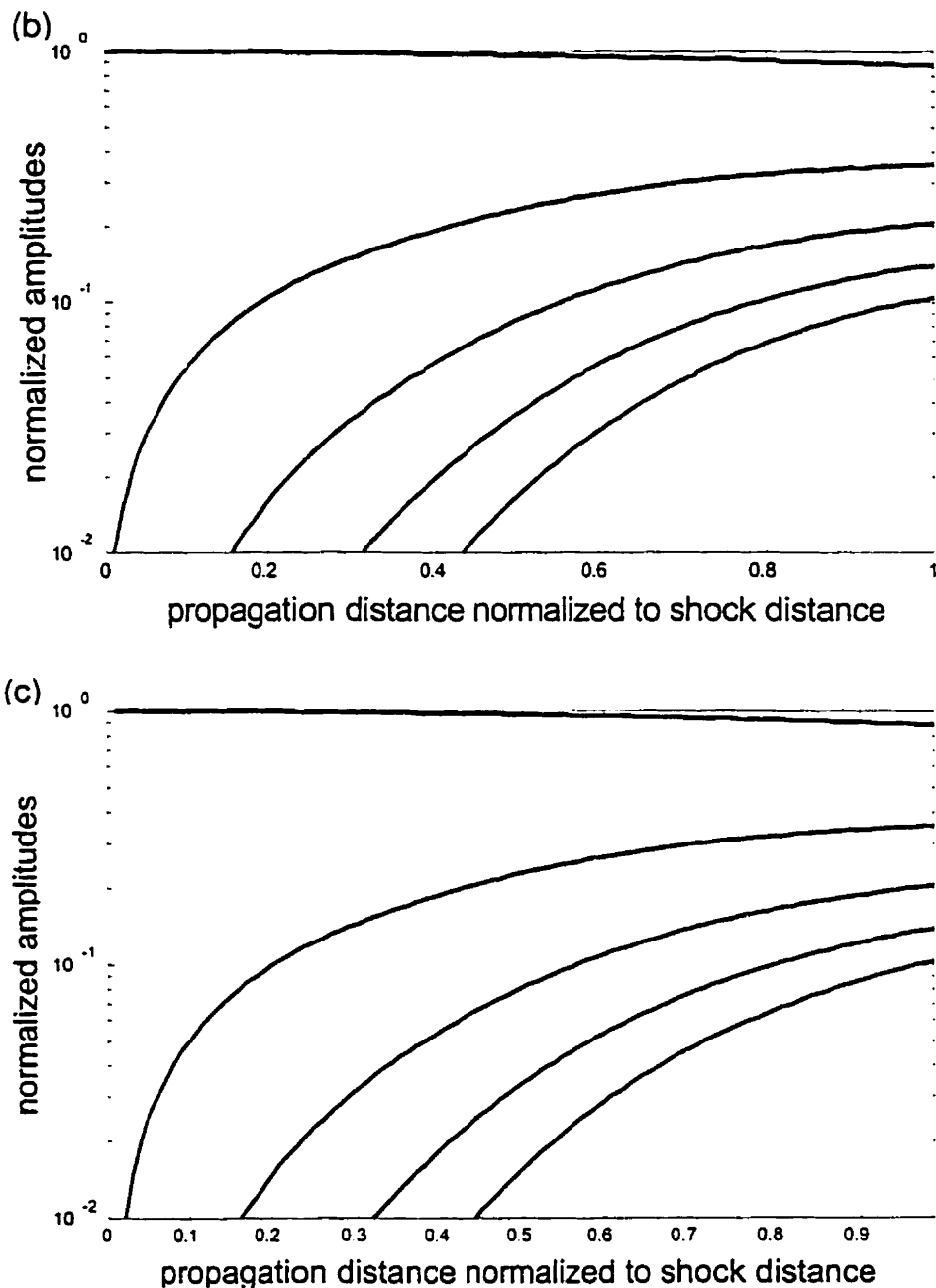

(a)
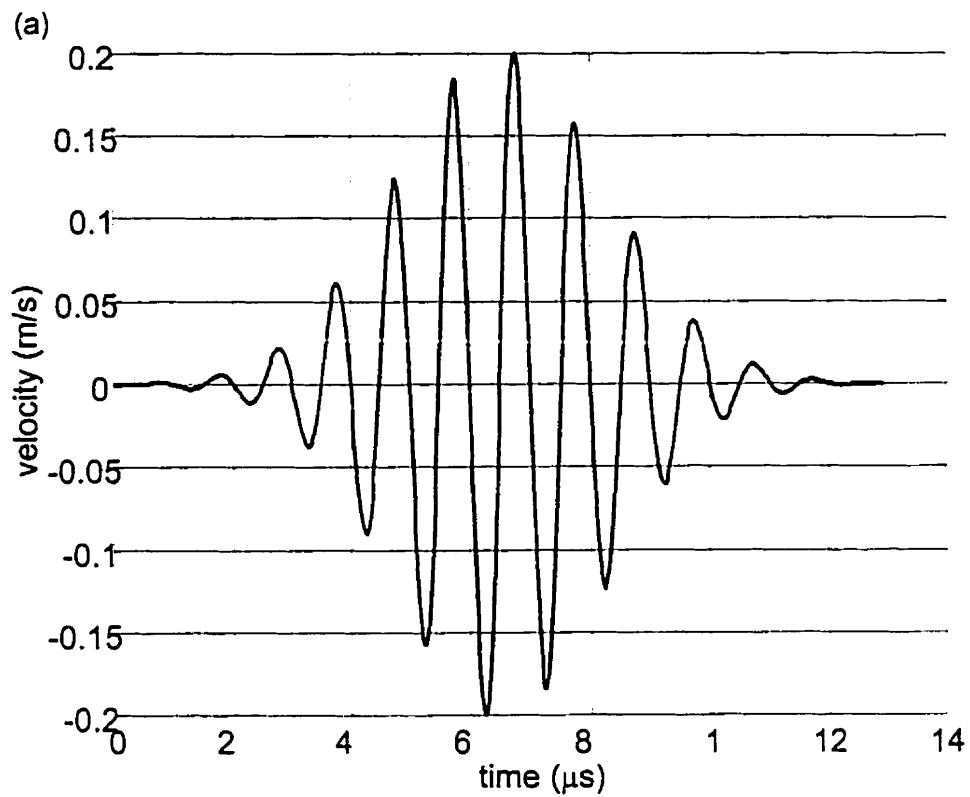
propagation distance nomalized to shock distance
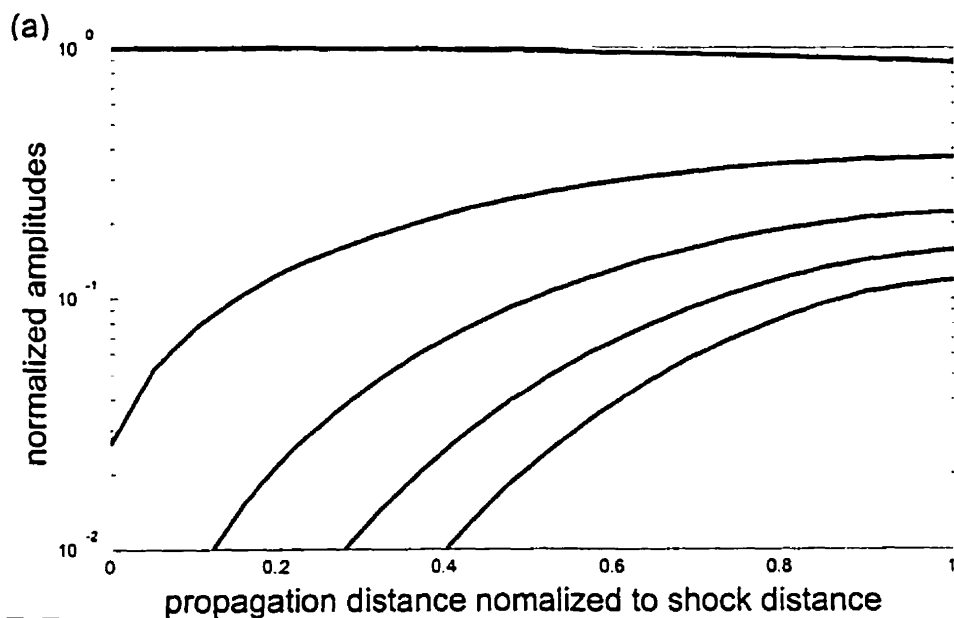
Figure 1 The harmonic profiles from the time domain nonlinear algorithm for plane wave propagation with (a) 20 harmonics and 20 Δz steps. (b) with 20 harmonics and 100 Δz steps compared with (c) the Fubini solution out to the shock distance. Note that there are some discrepancies in (a) due to insufficient step size.

(a)

(b)

(c)

(d)
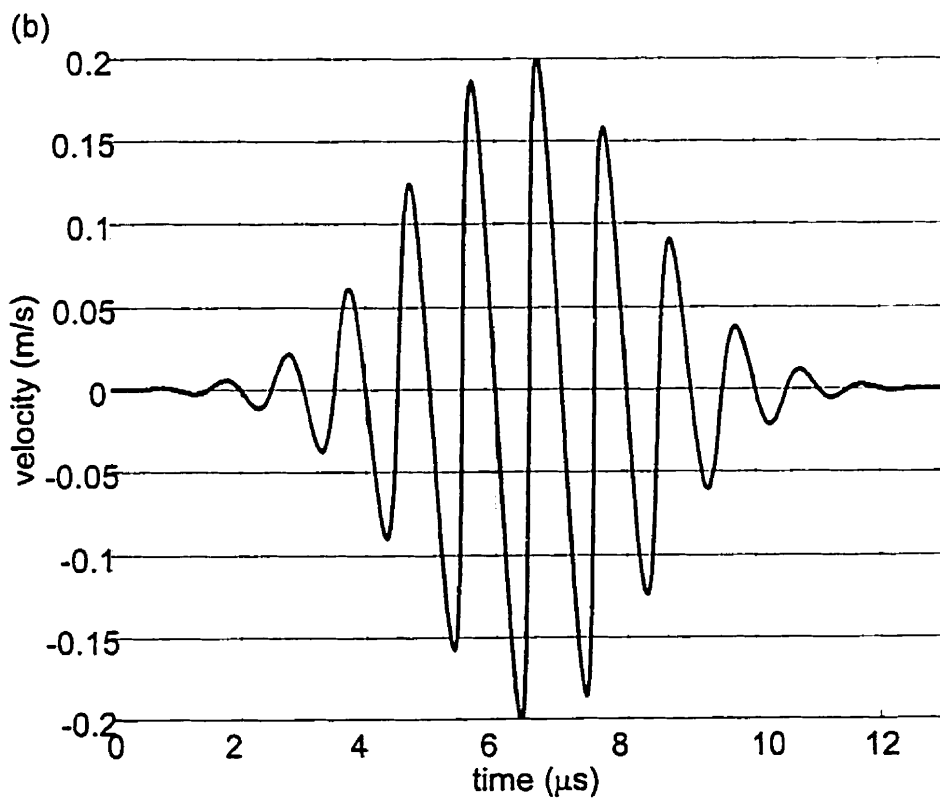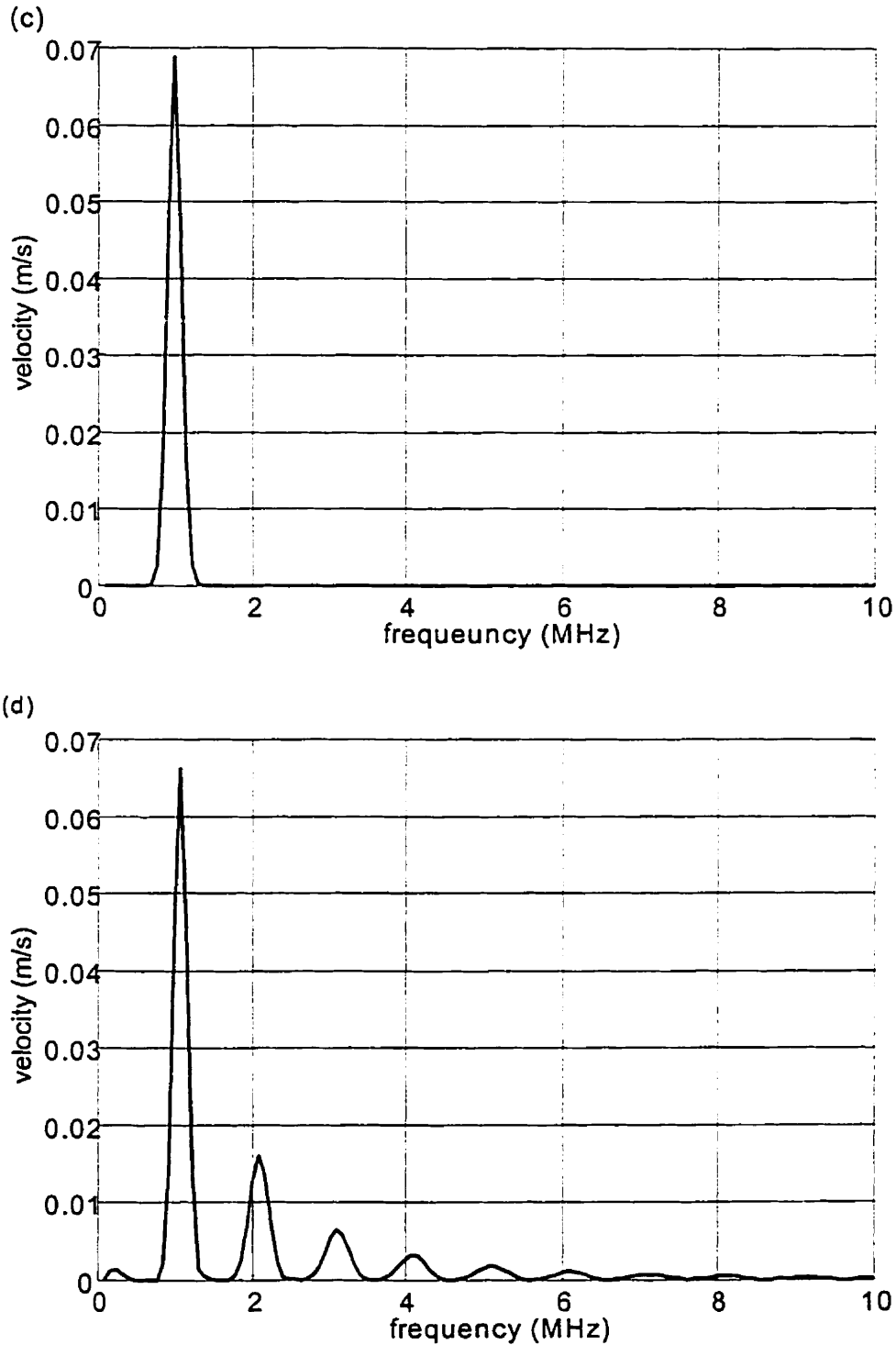

Figure 2 Plane wave pulse propagation. (a) Initial waveform (bDistorted waveform after propagating 0.7 of the shock distance (c) Initial spectrum of the waveform, and (d) spectrum of the distorted waveform corresponding to 0.7 of the shock distance.

7.2 Choice of Operator Splitting Methods

In Chapter 6 we selected the second order operator splitting method of Tavakkoli et. al.
(1998) to implement the fractional step marching scheme of the NLP algorithm. In large
part this choice stemmed from the hope that by combining absorption with the nonlinear
substep the FDSBE would be more stable. For pulsed sources, we have opted to evaluate
nonlinearity in the time domain, and there is no obvious way to include attenuation in the
TDSNE algorithm. One option would be to evaluate nonlinearity and attenuation step by
step over very small intervals (smaller than the diffractive substeps which may be used in
the NLP algorithm). Another alternative is to calculate the attenuation with the diffractive
substep. The TDSNE is fairly stable, so the absence of attenuation in the nonlinear
substep will not greatly affect the stability of the NLP algorithm. Moreover integration of
attenuation in the diffraction algorithm is relatively easy. By modifying the propagator
functions h and H to include absorptive effects,

$$H_a(k_x, k_y, \Delta z) = H(k_x, k_y, \Delta z) \times \exp\left\{ \frac{-\alpha f^n \Delta z}{\cos[\sin^{-1}(c\sqrt{k_x + k_y} / f)]} \right\}$$

and

$$h_a(x, y, \Delta z) = h(x, y, \Delta z) \times \exp\left(-\alpha f^n \sqrt{z^2 + r^2}\right)$$

attenuation may be accounted for in a very computationally efficient way. In light of our
choice to combine the effects of attenuation and diffraction, the operator splitting scheme
we choose to implement is not that presented by Tavakkoli et. al., but rather the new
scheme proposed in section 4.2, and illustrated in Fig. 2 of chapter 4. In this scheme, the
combined effects of diffraction and attenuation are propagated over an incremental half
step, followed by a full step of nonlinearity, and finishing with a half step of attenuation
and diffraction.

7.3 The Diffraction Substep

A few key matters need to be addressed when deciding on a diffraction algorithm for nonlinear pulse propagation: sampling of the propagation planes, choosing between the FSC or SSC algorithms for each discrete spectral frequency, selection of temporal sampling and determining an adequate temporal extent to the signal. We will deal with the later two issues first.

7.3.1 Sampling the Temporal Signal

Sampling of any temporal signal should be done at a rate equal to or greater than the Nyquist rate, which is defined to be twice the rate of the highest frequency component in the spectrum. If a pulse has center frequency f_0 and bandwidth Δf, then the sampling rate should be at least $f_{Nyquist}=2(f_0+\Delta f/2)$.

For a finite amplitude pulse, harmonics will be generated during nonlinear propagation which are not present in the initial spectrum. Because it is difficult to anticipate the complex interaction between diffraction, attenuation, and nonlinearity, selection of a sampling rate becomes nontrivial.

For nonlinear propagation in tissue, it is likely that attenuation will filter high frequencies generated due to nonlinearity. Based on our experience from CW propagation in tissue, it is expected that no more than 5-10 harmonics of the center frequency may be required for the kinds of amplitudes allowed in diagnostic imaging. Thus, we should choose the sampling frequency to be 5-10 times the Nyquist rate $f_{Nyquist}=2(f_0+\Delta f/2)$ of the initial spectrum.

7.3.2 Temporal Extent of the Signal

To avoid temporal aliasing of the signal in our plane-to-plane fractional step marching scheme, a sufficiently long temporal window, or pulse repetition interval (PRI) must be used in the initial signal. To choose an adequate temporal window, both linear and nonlinear effects must be considered.

Linear Analysis

Consider a piston transducer of radius a, and consider that we wish to send a pulse from the transducer where the pulse has duration σ. Now consider that we observe the waveform at a point (x,y) on a plane a distance z away from the source.

The time marking the beginning of the observed waveform will be given by the shortest transit time between the transducer and the observation point. The time marking the end of the observed waveform is given by the longest transit time between the transducer and the point plus the length of the pulse.

If (x,y) is in the shadow of the transducer, (i.e. $r = (x^2 + y^2)^{1/2} \leq a$) the time duration of the observed waveform is given by:

$$T_p = \left\{ \sigma + \frac{\sqrt{(r+a)^2 + z^2}}{c} \right\} - \frac{z}{c}$$

For a given z, T_p is maximal for $r = a$. At $r = a$, T_p is maximal for $z=0$.

Thus, the absolute longest duration the pulse could be is given by:

$$T_p = \sigma + \frac{2a}{c}$$

If (x,y) is not in the shadow of the transducer, the length of the pulse is given by

$$T_p = \left\{ \sigma + \frac{\sqrt{(r+a)^2 + z^2}}{c} \right\} - \frac{\sqrt{(r-a)^2 + z^2}}{c}$$

which is maximal for any given r when $z=0$, and in which case, once again we have:

$$T_p = \sigma + \frac{2a}{c}$$

Should we want to ensure that a pulse is adequately represented in the frequency domain, we would then need sampling given by the Nyquist theorem:

$$\Delta f \leq \frac{1}{2T_p}.$$

If an insufficient temporal extent is used for pulsed propagations, the waveform at the observation point may be aliased. The closer the observation plane to the source, the

greater the extent of a temporal window is needed to prevent aliasing errors. A plot of the required temporal window versus axial distance from source is shown in Fig. 3.
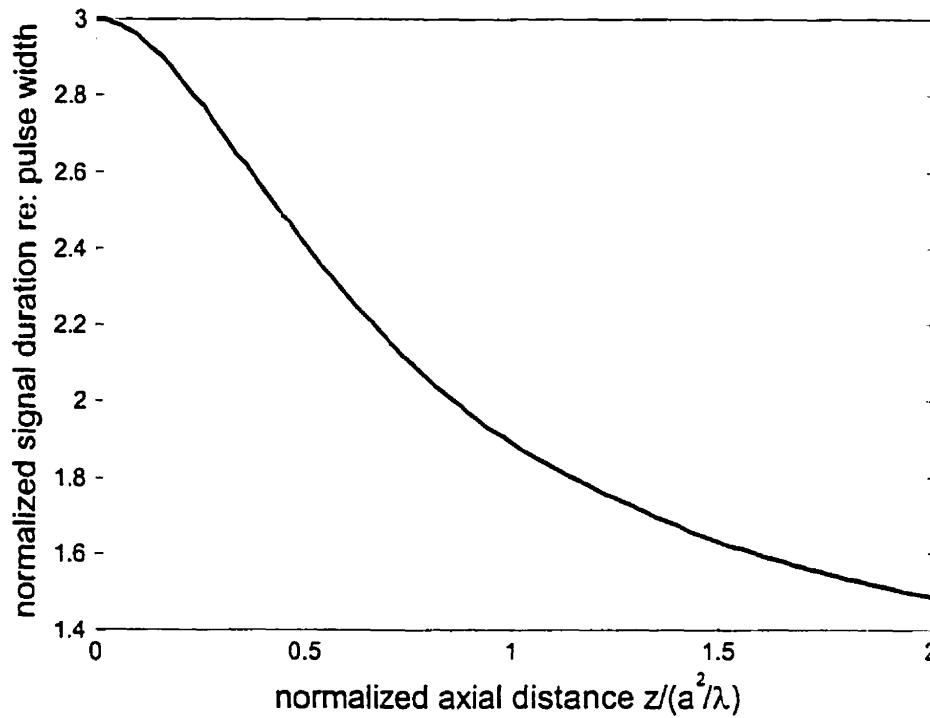

Fig. 3. Pulse duration required to avoid temporal aliasing as a function of axial distance for a 1.5 cm radius disk, and a pulse width of 10 μs.

Nonlinear Analysis

A peculiar phenomenon occurs in nonlinear propagation, where difference frequencies accumulate in a spectral region below the fundamental band of the signal. This phenomemon has been coined "self demodulation" by Averkiou (1993) and others. In highly absorptive media, attenuation may moreover filter out a good deal of the spectral frequencies above this demodulated band, and thus produce a signal which is of lower frequency than initially transmitted. This self-demodulation phenomenon can sometimes be accompanied by signal elongation. If the temporal extent of the pulse is shorter than the resultant pulse lengthening, wraparound error may occur. It is our experience, however, that the temporal window required for the linear analysis of the previous section

is more than adequate to accommodate the small degree of pulse lengthening and self-demodulation which occurs in nonlinear propagation through tissue.

7.3.3 Lateral Sampling of the Propagation Planes

For linear propagation of a pulse using the angular spectrum method we might presume that planar sampling should be done at a rate equal to or better than the Nyquist rate of the highest spectral component f_{max} (thus $\Delta x < \lambda_{min}/2$. where $\lambda_{min} = c/f_{max}$). For unfocused sources, it may well be that such dense spatial sampling is not needed farther away from the transducer, and a ray theory truncation may enable reduction of this sampling rate.

For finite amplitude propagation, harmonic profiles may vary more spatially than the fundamental profiles, and greater sampling may be needed. Borrowing insight from the CW investigations, a good guess for spatial sampling of unfocused sources may be at 1 to 2 times the Nyquist rate of the highest spectral component, f_{max}, in the initial spectrum. For focused sources between 2 and 4 times this Nyquist rate may be more appropriate.

7.3.4 Sampling of the Propagator Functions

After temporal and spatial sampling schemes have been chosen, and the axial intervals between propagation planes selected, the techniques outlined in chapters 5 and 6 may be used to choose a sampling scheme for the propagator functions. For each frequency component $f_n = nf_s = n/T_p$, the choice of sampling either the spatial point spread function h or the frequency domain transfer function H, once again hinges on whether the corresponding radiation circle for the given frequency is wholly or partly contained within the discrete spatial frequency domain. Suppose that lateral field profiles are sampled at ζ times the Nyquist rate of the highest spectral component $f_{max} = f_c + \Delta f/2$. This corresponds to a rate of $\gamma = \zeta f_{max}/f_s$ times the rate of $f_s = 1/T_p$. We may define an index

$$n_H = \sqrt{(2\Delta z \gamma \Delta k_x / \pi)^2 + 2\gamma^2} \ .$$

such that for frequency components f_n up to n_H-1, the point spread function should be sampled. For $n \geq n_H$, sampling of the transfer fucntion H may be employed. For $n < \gamma$, the sampling of h should be done with the intervals Δx, Δy used to sample the source plane.

For each frequency component f_n such that $\gamma < n < n_H - 1$, the point spread function h should be sampled with at least the Nyquist rate of f_n (i.e. $\Delta x = \lambda_n/2$).

7.4 Verification of the Diffraction Algorithm

To verify the diffraction algorithm, we simulated the pulsed response of a plane piston transducer and compared with the waveforms obtained from the impulse response method. Specifically, a 1cm disk transmitting a pulse with a peak amplitude 1cm/s, a center frequency of 1MHz, and 50% bandwidth (figure 4(a)) was simulated. Excellent agreement was obtained, as shown in figures 4(b) and (c). The observation point for these figures was on axis at a distance of a^2/λ_o, where λ_o is the wavelength of the center frequency.
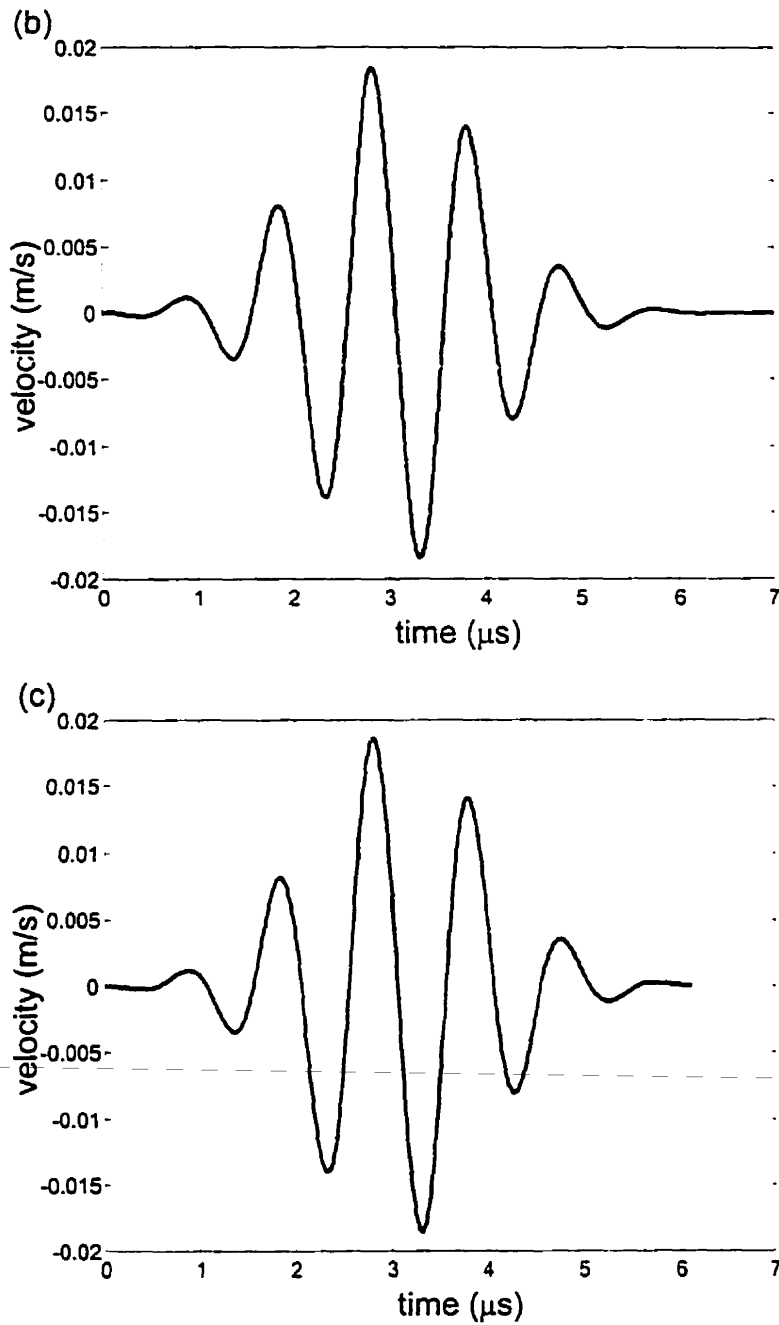
(a)

(b)

(c)
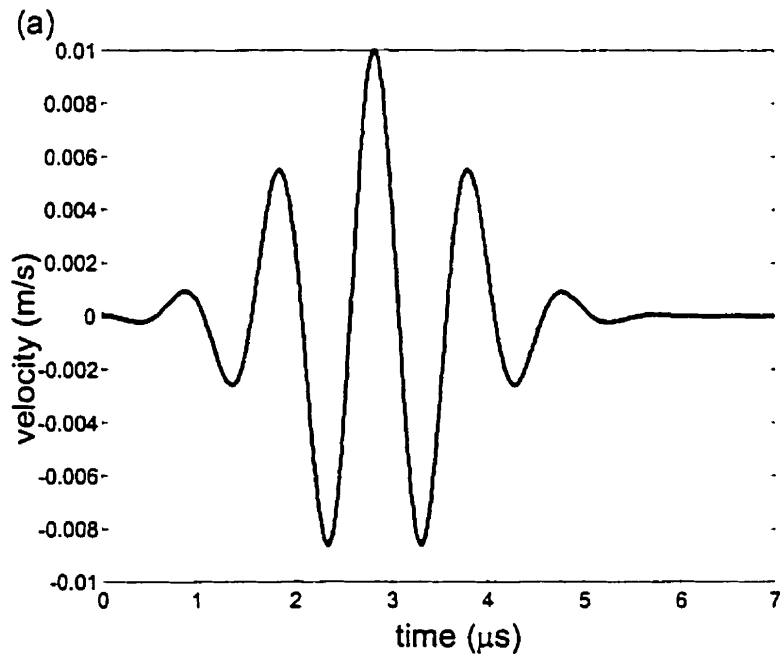
Fig. 4 Comparison of small signal diffraction calculations (a) Initial pulse waveform calculated using (b) our angular spectrum approach, (c) the impulse response technique. For a disk transducer at a^2/λ_o.

7.5 Verification of the NLP algorithm

Having verified the accuracy of the nonlinear plane wave algorithm, and the diffraction algorithm, verification of the full nonlinear propagation (NLP) algorithm was performed with a few key tests:

7.5.1 The Quasi-CW Limit

For a long quasi-continuous wave pulse, the pulsed nonlinear propagation algorithm should behave like the continuous wave algorithm of chapter 6. To this end we compare the results of Averkiou et. al. (1997), with our own modeling technique for a focused disk propagating 100 cycles of a 2 MHz sine wave in a liver-like media. We used 25 propagation planes, where each plane was divided up into 5 substeps for the nonlinear algorithm. In this comparison, shown in Fig. 5, there are some discrepancies. A complete explanation for these discrepancies is not understood, however, it is hypothesized that the step size may be too large to account for the complex interaction between diffraction and nonlinearity.
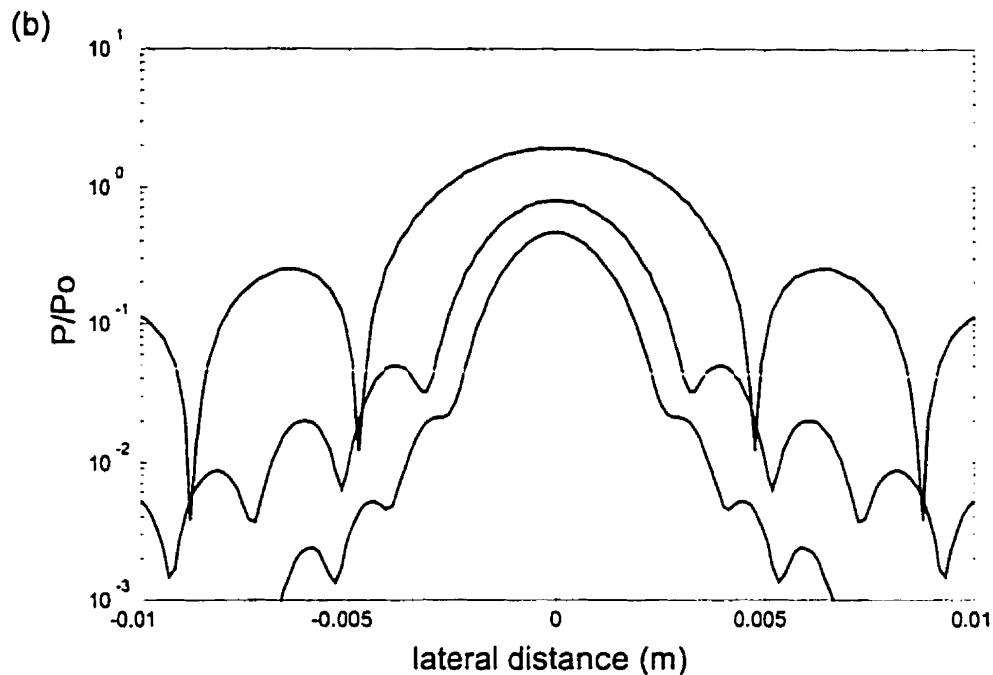
(a)

(b)
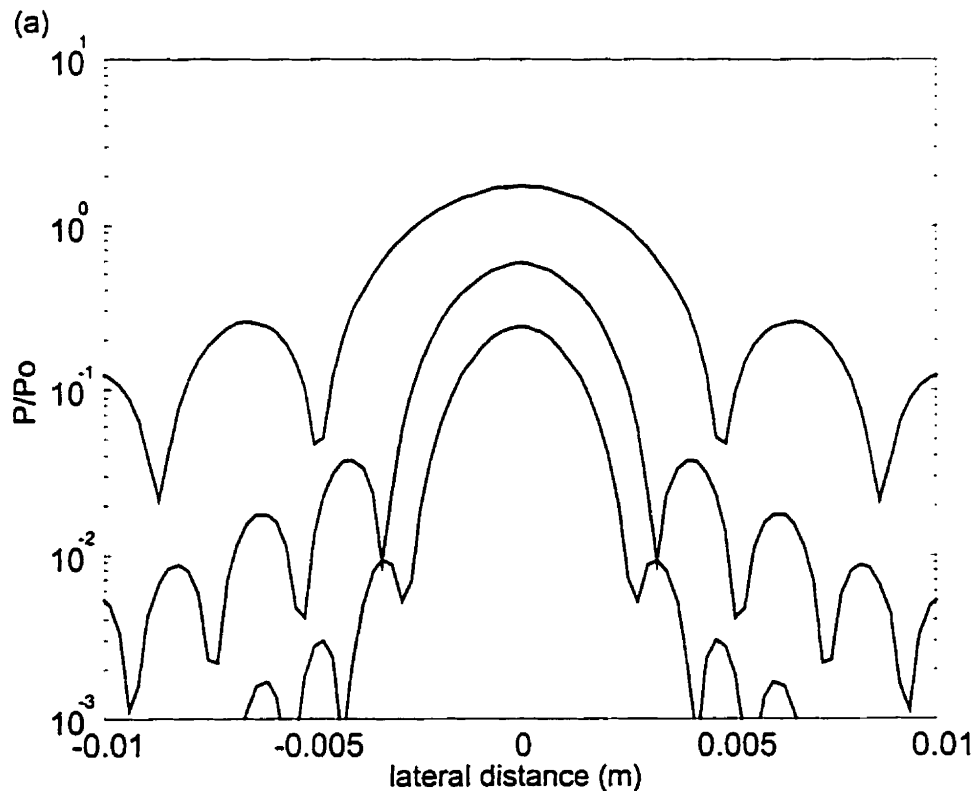
Fig. 5. Comparison of the new NLP algorithm for pulsed sources (a) in the quasi-CW limit with the NLP algorithm (b) of the previous chapter. Shown are the lateral harmonic profiles of a 2MHz fundamental signal at the focal distance (z=10cm) of a concave disk. Both results may be compared with Averkiou et. al. (1997).

7.5.2 The Linear Limit

In the limit where β approaches zero, the nonlinear algorithm should behave in a linear way. For this test we try to reproduce the linear propagation results of figure 4(c) above. The result of our algorithm, shown in figure 6 is in excellent agreement with the result obtained by the impulse response method.
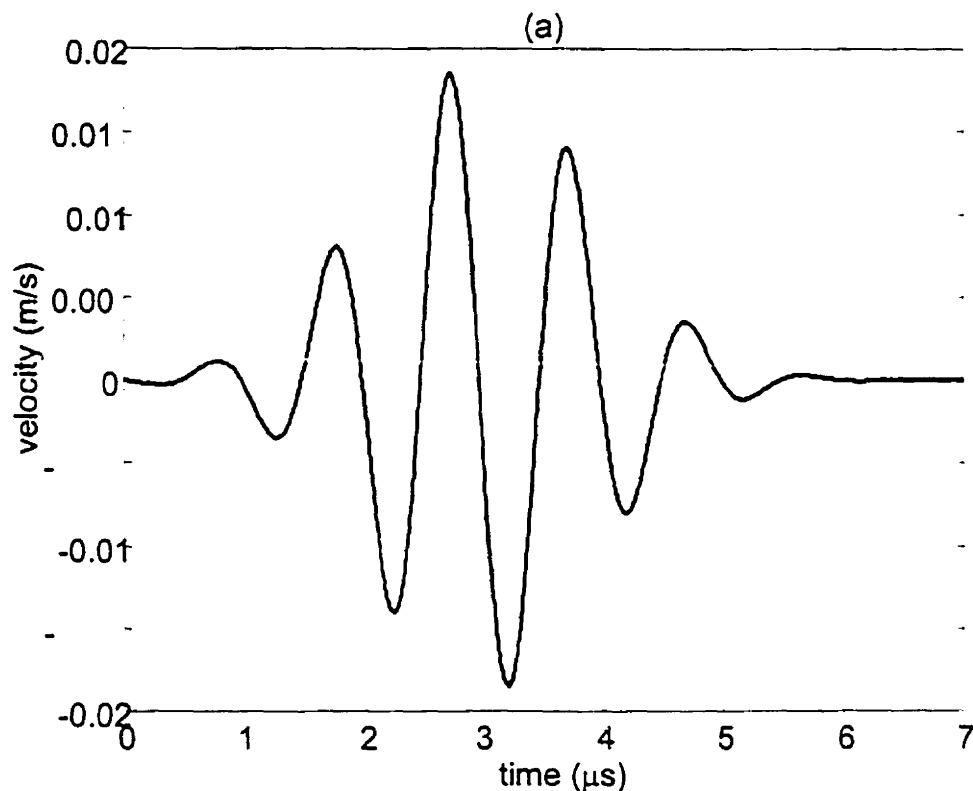
Fig. 6. The observed waveform computed using our pulsed NLP algorithm in the limit of vanishing β. This result may be compared with Fig. 4(c).

7.6 Qualitative Analysis of Nonlinear Pulse Propagation

Our model demonstrates unique characteristics of nonlinear propagation, including wavefront steepening, and harmonic generation. Figs. 7(a) and (b) demonstrate these characteristics. Note in Fig. 7(a) that there is an interesting asymmetry in the envelopes of the positive and negative portions of the waveform. This asymmetry is a trademark of the interaction between diffraction and nonlinearity, and has been seen in water propagation, as described by Hamilton (chapter 8 of Hamilton and Blackstock, 1998). This asymmetry may be significant with respect to standards in medical ultrasound. Current standards limit the Mechanical Index (MI), which is a measure of the peak negative pressure divided by the square root of the center frequency. The MI is used as gauge to judge the liklelihood of cavitation bioeffects (Apfel and Holland, 1991), and is currently based on linear analysis. The amplitude asymmetry shown in Fig. 7 may suggest a more careful

analysis of standards, to account for nonlinear effects. Averkiou and Hamilton (1997) have shown that the negative pressure is often maximized before the focal region of the transducer, and thus particular attention should be directed to monitoring possible adverse cavitation phenomena in the prefocal region. Their simulations, however, were for water propagation. It is hoped that future investigations using this model for tissue may shed additional light on the important area of standards.
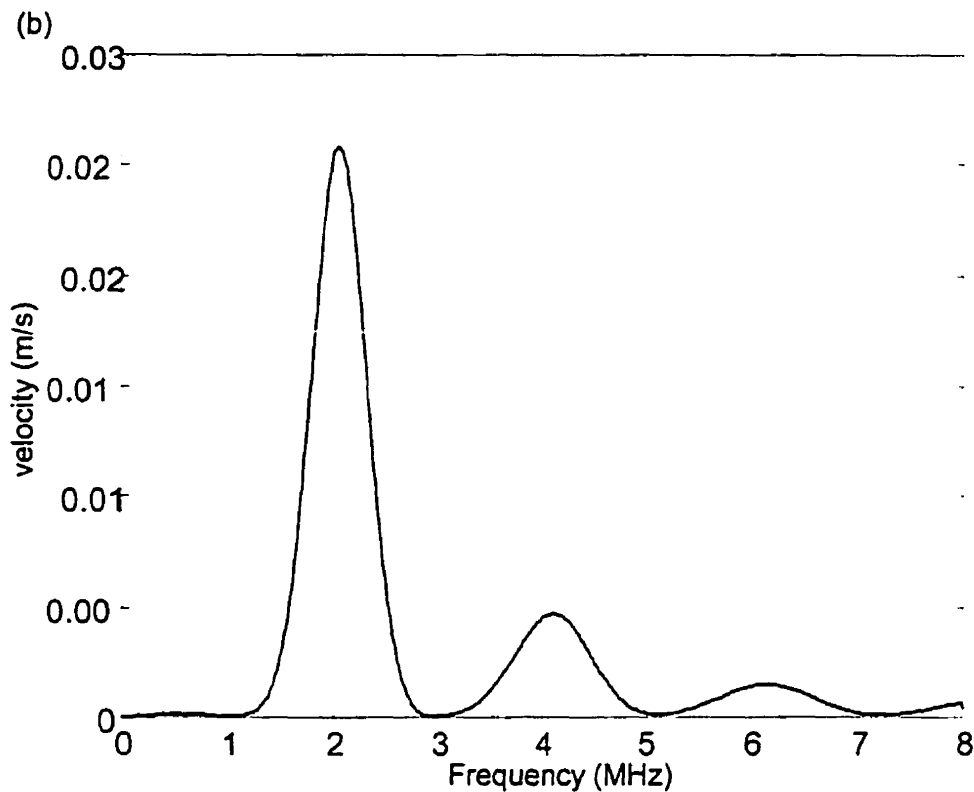
(a)

(b)
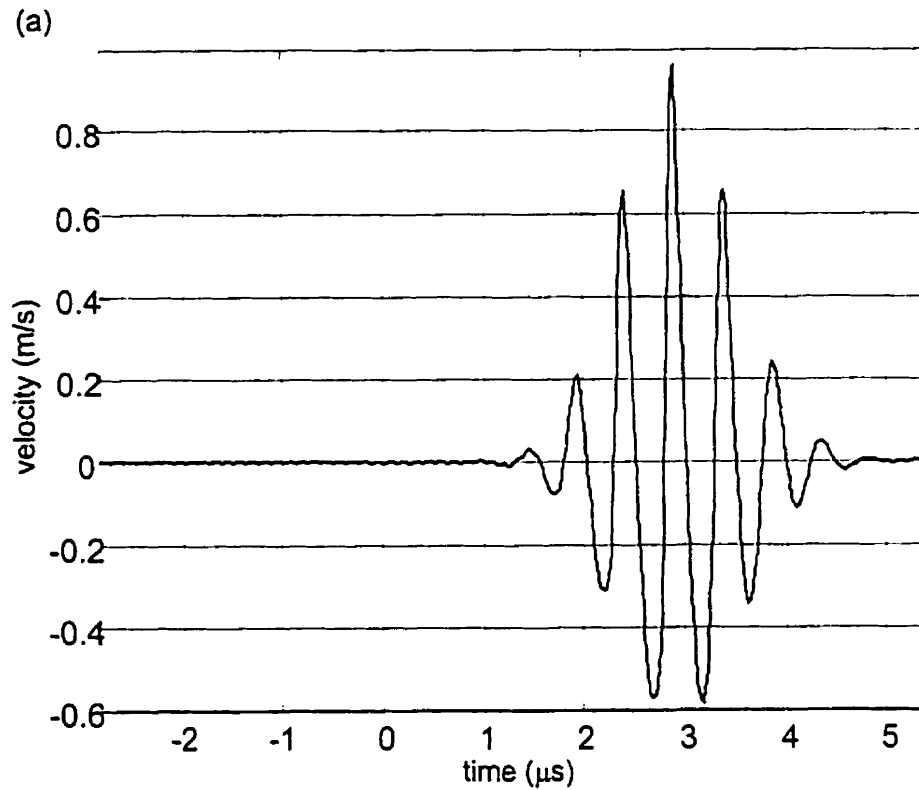
Figure 7 (a) Waveform at the focus of a Gaussian apodized, focused disk transducer after propagation through a tissue medium. The disk radius was 1.5 cm, the focal length was 6 cm, and the Gaussian amplitude shading of the source was such that the half-amplitude radial distance was 0.84 cm. The pulse used was a sinusoid modulated by the square root of a Gaussian function with 50% bandwidth, and amplitude 257 kPa. The tissue had parameters β=5, α_o=3 dB/cm at 1MHz and b=1.3.

7.7 Computational Resources and Memory Management

Simulation of transient excitation nonlinear propagation from non-axisymmetric sources can require tremendous computational resources. For any given propagation plane, several hundred megabytes – and even Gigabytes of data must be processed. Even with 512 Mbytes of RAM, and a 550 MHz Pentium III processor, extensive memory management was required. Several Gigabytes of free hard-disk space were used as a swap-space to temporarily store data. Fortunately, even with the time consuming processes used to manage the deluge of data, the code could be run within a few hours. Qualification should be given, however, to clarify that increasing the number of lateral samples in the propagation planes above 256 x 256 or 512 x 512 points may incur a huge computational load, and the code may take days to run.

Chapter 8: Conclusions

8.1 Summary

The primary contribution of this thesis has been the development of an efficient computer model for simulating nonlinear ultrasound propagation in tissue. This model shall enable accurate modeling of finite amplitude effects in modern clinical ultrasound scanners, and in particular, may be useful as a tool for optimising the design of tissue harmonic imaging systems.

Because current modeling techniques involve great computational burden, a primary focus of this work was to develop an algorithm which is as computationally efficient as possible. Towards this end, a second order operator splitting approach similar to that of Tavakkoli et. al. (1998) has been devised, so as to enable the computation of diffraction, attenuation and nonlinearity separately over small steps. The second order nature of this scheme allows the use of relatively large axial increments in a fractional step marching scheme. Our model has accurately reproduced published experimental and theoretical data with as few as 20 axial increments. This may be contrasted with other techniques which typically require hundreds or thousands of axial steps. Our computer model has been able to evaluate the nonlinear field response of continuous wave sources in as little as a few minutes, and wideband transient responses in a few hours. In comparison, numerical modeling of nonaxisymmetric pulsed sources using current methods has taken on the order of days.

Synthesizing an efficient diffraction algorithm was a primary thrust of our efforts. Of the effects of diffraction, attenuation, and nonlinearity, diffraction is by far the most computationally complex. Tavakkoli et. al. have estimated that the Rayleigh integral – based diffraction algorithm which they used in their nonlinear propagation model took 90% of the computation time, even for axisymmetric sources. We investigated several methods of computing diffraction, including the Rayleigh integral, impulse response methods, and the angular spectrum method. Because the impulse response method is not valid for non-separable field distributions, it was discounted as a candidate for a

diffraction algorithm appropriate for a plane-to-plane fractional step marching scheme. The angular spectrum approach was found to be the most computationally efficient of the diffraction algorithms when fast transform algorithms are used. Moreover, the angular spectrum method is valid for non-separable field distributions. Because of these reasons, we chose the angular spectrum method to calculate the effects of diffraction in our nonlinear propagation algorithm.

Christopher and Parker (1991) have used the angular spectrum approach for acoustic field propagations, however, the techniques they describe are for axisymmetric sources. Although Christopher has also simulated non-axisymmetric sources (e.g. Christopher, 1997), the step sizes he used were very small (often less than a wavelength), and thus his approach does not well describe the large step approach we wish to take. In this thesis, a new numerical scheme for implementing the angular spectrum technique, applicable for large axial steps, has been devised for sources which do not possess radial symmtery.

For continuous wave signals, attenuation and nonlinearity were combined together, and the nonlinear substep was computed using the frequency domain solution to Burgers equation. For CW sources propagating in tissue, only a few harmonic were non-negligible, and so evaluation of the nonlinear substep in the frequency domain was relatively efficient. It was also seen that the attenuation of tissue afforded additional stability to the FDSBE algorithm.

For wideband signals, a time domain algorithm was used to compute the nonlinear substep, as the frequency domain approach has an undesirable computational load for large numbers of frequency components. Attenuation was combined with the diffraction substep in this case. Pulsed simulations were a good deal more time consuming than the continuous wave scenario, and often required extensive memory management. Several gigabytes of free hard disk space were sometimes needed- even with 512 Mbytes of system RAM.

The continuous wave algorithm was verified with the linear algorithm in the case of vanishing nonlinear parameter β. Moreover, our model compared well with published results for nonlinear propagation in both water and tissue.

The algorithm for nonlinear pulsed propagtions was verified in the quasi-continuous wave case, and in the linear limit.

8.2 Recommendations and Future Work

The most obvious recommendation for extension of this research is the experimental verification of the pulsed nonlinear model. Once the model is verified experimentally, various investigations can be done using the model.

So far, only one way (transmit) propagation has been considered. A pulse echo imaging system may very well be simulated by adding code for scattering of objects, and for propagation of the echoes back to the transducer. Since tissue scattering is typically fairly weak, linear propagation is sufficient for simulation of the reception portion of the algorithm. The impulse response method of Ullate and San Emeterio (1988) would be a good candidate for simulating the received response.

Because Tissue Harmonic Imaging is a relatively new modality, there is still much to be understood about optimizing system parameters. Design of an imaging system based on nonlinearly generated harmonics should have some distinct differences as compared with design of a typical pulse-echo B-mode imaging system. To this end, our model may be used to simulate a tissue harmonic imaging system, and computationally investigate optimal design parameters. Some points to investigate are as follows:

- A high-pass or band-pass filter must be designed to filter the spectrum of the received echo and pass the second harmonic. The ability of the filter to reject the fundamental is critical since its presence will contribute to a loss of contrast resolution. A novel pulse inversion scheme has been proposed by Simpson et. al. (1999), for rejection of the fundamental band in contrast harmonic imaging. This scheme may also be applied to tissue harmonic imaging. The premise of pulse inversion is to send two pulses – the second being an inversion of the first. The echoes of these pulses may be added, thus

extracting the nonlinear portion of the signal, and rejecting the fundamental band. Use of our model to better understand pulse inversion and its role in harmonic imaging would be a valuable for tissue harmonic imaging system design.

● The dynamic range of the A-D converter in an imaging system must be large enough to not only detect the second harmonic, but to differentiate the second harmonic from the noise floor. The small signal amplitude is a significant concern in tissue harmonic imaging. This means that one typically will want to employ either large drive levels from the source, or use aggressive focusing. Aggressive focusing, however must be traded for depth of field. The investigation of drive levels, focusing and depth of field using our model would be very worthwhile.

● Given a certain available bandwidth for the transducer, it must be decided in what band the transmitted pulse may be sent at, and what band the second harmonic signal should be received at. We must also define what we mean by the second harmonic signal. We may use as our second harmonic signal the absolute magnitude of the pressure, or the second harmonic level relative to the fundamental. If we select the absolute definition of second harmonic signal, we wish to transmit in a band such that the fundamental p_1 is maximized AND the received signal p_2 is maximized. Suppose that the amplitude of the passband for the fundamental is L_1, and that the amplitude of the passband for the second harmonic is L_2. If we make a crude approximation that the amplitude of the fundamental signal is approximately the square of the second harmonic, we should then maximize $L_1^2 \times L_2$. Given a semicircular frequency response of the transducer, this results in transmitting at approximately 2/3 of the center frequency of the transducer, and receiving at approximately 4/3 of the center frequency (Fig. 1).
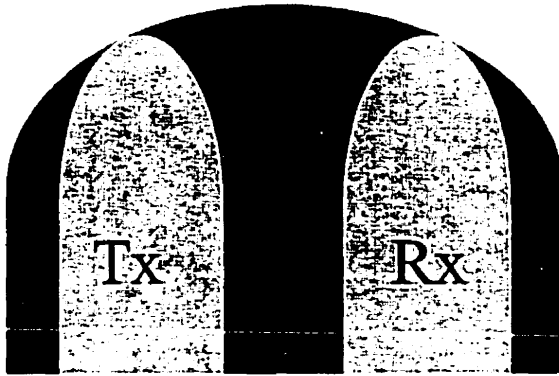
Fig. 1. One possible way of selecting
transmit (T_x) and receive (R_x) bands

•• Should we choose as our definition, however, the second harmonic level relative to
the fundamental, and we approximate this level as the fundamental squared, we want
to maximize L_1^2 x (L_2/L_1^2), or in other words, maximize L_2. This means receiving at
the center frequency f_c of the transducer and transmitting at $\frac{1}{2} f_c$ as shown in Fig. 2.
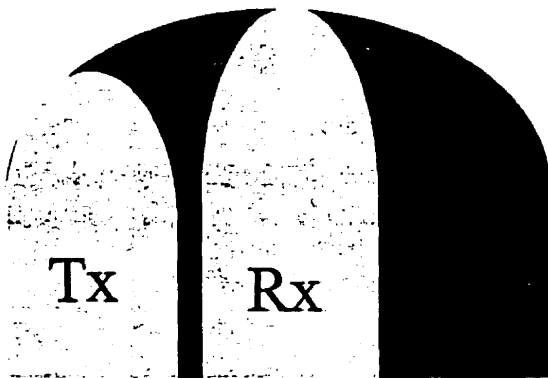

Figure 2 Another possible scheme for
choosing the transmit (T_x) and receive
(R_x) bands

If we do transmit at $\frac{1}{2} f_c$, the transmit band may be more band-limited than if we were
to transmit at $2/3 f_c$.

Using our model to investigate which of these schemes is optimal may enable a gain
of a few decibels of signal level, or some amount of improvement in system
performance.

♪ For harmonic imaging, one must use caution when trying to transmit very short pulses. Short pulses will have a wide spectral envelope, which, may interfere with the second harmonic signal in the receive band, complicating the filtering procedure, as is shown in Fig. 3. Thus, sometimes axial resolution must be sacrificed for contrast resolution. The pulse inversion scheme mentioned above may help in this regard, allowing wider bandwidth pulses to be sent without sacrificing contrast resolution. Simulation may play a valuable role in understanding how to choose the transmit waveform, and how pulse inversion may be used to overcome the problem of harmonic band interference.
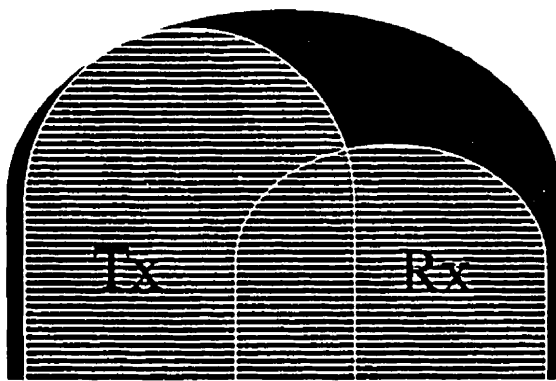
Fig. 3. Wideband signals may overlap
in their harmonic bands, complicating
the filtering procedure.

♪ The signal to noise ratio (SNR) is of critical importance in harmonic imaging. For linear B-mode imaging, several investigators (O'Donnell, 1993; Welsh, 1998; Misaridis, 2000) have explored the use of coded excitation and pulse compression to improve the SNR of the received tissue echo. The premise of coded excitation is to send a long coded waveform, and compress the received echo – often by a matched filtering technique. By using a long pulse, one may increase the received energy without increasing the signal level above standards. Compression of the signal thus enables the signal energy to be temporally localised, while the noise level is unaffected by the compression. Li (1999) has recently explored the use of coded excitation in tissue harmonic imaging. One of the problems of the technique of Li is the inability to completely reject the fundamental band using filtering. It may be possible to use pulse inversion to reject the fundamental signal. Our model could be

used to simulate nonlinear distortion of coded waveforms. The results of these simulations may well be used to investigate the feasibility of pulse inversion and pulse compression in tissue harmonic imaging.

8.3 Conclusion

We have developed a computer model of nonlinear ultrasound propagation in tissue, which can simulate the acoustic field from non-axisymmetric transducers. Our model appears to offer some amount of computational savings compared with existing techniques. The continuous wave response of disk transducers has been simulated and compared with published results for nonlinear propagation in both water and tissue. Transient excitation simulations have also been done, and have been verified in the quasi-CW limit, and in the limit where nonlinearity is negligible. The model we have developed appears to be a promising tool for simulation of nonlinear propagation from a medical phased array scanner. Such a tool may be extremely useful in optimizing the design of a tissue harmonic imaging system.

References

Aanosen, S.I., Barkve, T., Naze Tjotta, J., Tjotta, S., Distortion and harmonic generation in the nearfield of a finite amplitude sound beam, *J. Acoust. Soc. Am.*, **75**, 749-768, 1984.

Atkinson, K.E., *An introduction to numerical analysis*, Wiley, New York, 1978.

Averkiou, M.A., Lee, Y.S., Hamilton, M.F., Self-demodulation of amplitude- and frequency- modulated pulses in a thermoviscous fluid, *J. Acoust. Soc. Am.*, **94**, 2876-2883, 1993.

Averkiou, M.A., Hamilton, M.F., Measurements of harmonic generation in a focused finite-amplitude sound beam, *J. Acoust. Soc. Am.*, **98**, 3439-3442, 1995.

Averkiou, M.A., Roundhill, D.N., Powers, J.E., A new imaging technique based on the nonlinear properties of tissues, *IEEE Ultrasonics Symposium*, 1561-1566, 1997

Baker, A.C., Anastasiadis, K., Humphrey, V.F., The nonlinear pressure field of a plane circular piston: Theory and experiment, *J. Acoust. Soc. Am.*, **84**, 1483-1487, 1988.

Baker, A.C., Humphrey, V.F., 1992, Distortion and high frequency generation due to nonlinear propagation of short ultrasonic pulses from a plane circular piston, *J. Acoust. Soc. Am.*, **92**, 1699-1705, 1992.

Baker, A.C., Berg, A.M., Sahin, A., Naze Tjotta, J., The nonlinear pressure field of plane, rectangular aperatures: Experimental and theoretical results, *J. Acoust. Soc. Am.*, **97**, 3510-3517, 1992.

Baker, A.C., Nonlinear effects in ultrasound propagation. In *Ultrasound in Medicine*, Duck, F.A., Baker, A.C., and Starritt, H.C., eds., Institute of Physics Publishing, the Institute of Physics, London, 1998.

Bakhvalov, N.S., Zhileikin, Y.M., Zabolotskaya, E.A., Khokhlov, R.V., Nonlinear propagation of a sound beam in a nondissipative medium, *Sov. Phys. Acoust.*, **22**, 272-274, 1976.

Bakhvalov, N.S., Zhileikin, Y.M., Zabolotskaya, E.A., Khokhlov, R.V., Focused high amplitude sound beams, *Sov. Phys. Acoust.*, **24**, 10-15, 1978a.

Bakhvalov, N.S., Zhileikin, Y.M., Zabolotskaya, E.A., Khokhlov, R.V., Nonlinear propagation of finite-amplitude sound beam in a dissipative medium, *Sov. Phys. Acoust.*, **24**, 271-275, 1978b.

Bakhvalov, N.S., Zhileikin, Y.M., Zabolotskaya, E.A., Khokhlov, R.V., Harmonic generation in sound beams, *Sov. Phys. Acoust.*, **25**, 101-106, 1979a.

Bakhvalov, N.S., Zhileikin, Y.M., Zabolotskaya, E.A., Khokhlov, R.V., Parametric interaction of sound beams, *Sov. Phys. Acoust.*, **25**, 280-283, 1979b.

Bakhvalov, N.S., Zhileikin, Y.M., Zabolotskaya, E.A., Khokhlov, R.V., Nonlinear propagation of Gaussian beams, *Sov. Phys. Acoust.*, **25**, 458-460, 1979c.

Bakhvalov, N.S., Zhileikin, Y.M., Zabolotskaya, E.A., Khokhlov, R.V., Nonlinear propagation of a sound beams with a uniform amplitude distribution, *Sov. Phys. Acoust.*, **26**, 95-100, 1976.

Beyer, R.T., *Nonlinear Acoustics*, Navy Sea Systems Command, Washington, D.C., 1974 (reprinted, with a new appendix containing more recent references and published by: Acoustical Society of America, Woodbury, N.Y., 1997)

Beyer, R.T., *Nonlinear Acoustics in Fluids*, Van Norstrand Reinhold, New York, 1983.

Burns, P.N., Powers, J.E., Simpson, D.H., Uhlendorf, V., Fritzsh, T., Harmonic imaging: Principles and preliminary results, *Angiology*, S63-S74, 1996

Cahill, M.D., Baker, A.C., Increased off-axis energy deposition due to diffraction and nonlinear propagation from rectangular sources, *J. Acoust. Soc. Am.*, **102** , 199-203, 1997a.

Cahill, M.D., Baker, A.C., Numerical simulation of the acoustic field of a phased array medical ultrasound scanner, *J. Acoust. Soc. Am.*, **104** , 1274-1283, 1997b.

Cahill, M.D., Baker, A.C., Numerical simulation of the acoustic field of a phased-array medical ultrasound scanner, *J. Acoust. Soc. Am.*, **104**, Pt. 1, 1274-1284, 1998.

Christopher, P.T., Parker, K.J., New approaches to the linear propagation of acoustic fields, *J. Acoust. Soc. Am.*, **90**, 507-521, 1991.

Christopher, P.T., Parker, K.J. New approaches to nonlinear diffractive field propagation, *J. Acoust. Soc. Am.*, **90**, 488-499, 1991.

Christopher, P.T., A nonlinear plane-wave algorithm for diffractive propagation involving shock waves, *J. Comp. Acoustics*, **1**, 371-393, 1993.

Christopher, T., Modeling the Dornier HM3 lithotripter, *J. Acoust. Soc. Am.*, **95**, Pt.1, 3088-3095, 1994.

Christopher, T., Finite amplitude distortion-based inhomogeneous pulse echo ultrasonic imaging, *IEEE Trans. Ultrason. Ferroelect. Freq. Contr.*, **44**, 125-139, 1997.

Christopher, T., Experimental investigation of finite amplitude distortion-based, second harmonic pulse echo ultrasonic imaging, *IEEE Trans. Ultrason. Ferroelect. Freq. Contr.*, **45**, 158-162, 1998.

Cincotti, G., Cardone, G., Gori, P., Pappalardo, M., A new beamforming technique for ultrasonic imaging systems, *Ultrasonics* **38**, 156-160, 2000.

Cleveland, R.O., Hamilton, M.F., Blackstock, D.T., Time-domain modeling of finite-amplitude sound beams in relaxing fluids, *J. Acoust. Soc. Am.*, **99**, 3312-3318, 1996.

Crombie, P., Bascom, P.A.J., Cobbold, R.S.C., Calculating the pulsed response of linear arrays: accuracy versus computational efficiency, *IEEE Trans. Ultrason. Ferroelect. Freq. Contr.*, **44**, 997-1009,1997.

Fenlon, F.H., A recursive procedure for computing the nonlinear spectral interactions of progressive finite-amplitude waves in nondispersive fluids, *J. Acoust. Soc. Am.*, **50**, 1299-1312, 1971.

Froysa, K.E., Naze Tjotta, J., and Berntsen, J., Finite amplitude effects in sound beams. Pure tone and pulse excitation. In *Advances in Nonlinear Acoustics*, H. Hobaek, ed., World Scientific, Singapore, pp.233-238, 1993.

Fubini, E., Anomalie nella propagazione di ande acustiche de grande ampiezza. *Alta Frequenza*, **4**, 530-581, 1935.

Gaskill, J.D., *Linear Systems, Fourier Transforms, and Optics*, Wiley, New York, 1978.

Goodman, J.A., *Introduction to Fourier Optics*, McGraw-Hill, New York, 1968.

Godunov, S.K., Difference method for the numerical calculation of discontinuous solutions of hydrodynamical equations, *Mat. Sb.*, **47**, 271-306 (in Russian), 1959.

Hamilton, M.F., Naze Tjotta, J., Tjotta, S., Nonlinear effects in the farfield of a directive sound source, *J. Acoust. Soc. Am.*, **78**, 202-216, 1985.

Hamilton, M.F., and Blackstock, D.T. (Eds.), *Nonlinear Acoustics*, Academic Press, New York, 1998.

Hart, T.S., Hamilton, M.F., Nonlinear effects in focused sound beams, *J. Acoust. Soc. Am.*, **84**, 1488-1496, 1988.

Haran, M.E., Cook, B.D., Distortion of finite amplitude ultrasound in lossy media, *J. Acoust. Soc. Am.*, **73**, 774-779, 1983.

Hinkleman, L.M., Liu, D.L., Metlay, L.A., Waag, R.C., Measurements of ultrasonic pulse arrival time and energy level variations produced by propagation through breast wall, _J. Acoust. Soc. Am._, **95**, 530-541, 1994.

Humphrey, V.F., Nonlinear propagation in ultrasonic fields: measurements, modelling and harmonic imaging, _Ultrasonics_ **38**, 267-272, 2000.

Kamakura, T., Hamada, N., Aoki, K., Kumamoto, Y., Nonlinearly generated spectral components in the nearfield of a directive sound source, _J. Acoust. Soc. Am._, **85**, 2331-2337, 1989.

Kamakura, T., Tani, M., Kumamoto, Y., Ueda, K., 1992, Harmonic generation in finite amplitude sound beams from a rectangular aperature source, , _J. Acoust. Soc. Am._, **91**, 3144-3151, 1992.

Karaman, M., Atalar, A., Koymen, H., O'Donnell, M., A phase aberration correction method for ultrasound imaging, _IEEE Trans. Ultrason. Ferroelect. Freq. Contr._, **40**, 275-288, 1993.

Kino, G.S., _Acoustic Waves: Devices, Imaging, and Analog Signal Processing_, Englewood Cliffs, NJ: Prentice-Hall, 1987.

Korpel, A., Frequency approach to nonlinear dispersive waves, _J. Acoust. Soc. Am._, **67**, 1954-1958, 1980.

Kuznetsov, V.P., Equations of nonlinear acoustics, Sov. Phys. - Acoust., **16**, 467-470, 1971.

Lee, Y.S., Hamilton, M.F., Time domain modeling of pulsed finite-amplitude sound beams, _J. Acoust. Soc. Am._, **97**, 906-917, 1995.

Li, P.C., Pulse compression for finite amplitude distortion based harmonic imaging using coded waveforms, _Ultrasonic Imaging_, **21**, 1-16, 2000.

Li, Y., Zagzebski, J.A., Computer model for harmonic ultrasound imaging, _IEEE Trans. Ultrason. Ferroelect. Freq. Contr._, **47**, 1000-1013, 2000

Liu, D.L., Waag, R.C., Time shift compensation of ultrasonic pulse focus degradation using least mean-square estimates of arrival time, _J. Acoust. Soc. Am._, **95**, 542-555, 1994.

Liu, D.L., Waag, R.C., Correction of ultrasonic wavefront distortion using backpropagation and a reference waveform method for time-shift compensation, _J. Acoust. Soc. Am._, **96**, 649-660, 1994.

Lu, J.Y., Greenleaf, J.F., A study of two-dimensional array transducers for limited diffraction beams, _IEEE Trans. Ultrason. Ferroelect. Freq. Contr._ **41**, 724-739, 1994.

Macovski, A., *Medical Imaging Systems*, Englewood Cliffs, NJ: Prentice-Hall, 1983.

Mallart, R., Fink, M., Adaptive focusing in scattering media through sound speed inhomogeneities: The van Cittert Zernicke approach and focusing criterion, *J. Acoust. Soc. Am.*, **96**, 3721-3732, 1994

McKendree, F.S., A numerical solution to the second-order nonlinear acoustic wave equation in one and three dimensions, Ph.D., dissertation, Pennsylvania State University, 1981.

Misaridis, T.X., Gammelmark, K., Jorgensen, C.H., Lindberg, N., Thomsen, A.H., Pedersen, M.H., Jensen, J.A., Potential of coded excitation in medical ultrasound imaging, *Ultrasonics*, **38**, 183-189, 2000.

Muir, T.G., Nonlinear effects in acoustical imaging, *Acoustical Imaging*, (edited by Wang, K.Y.), volume 9, Proc. 9th Int. Symp. on Acoustical Imaging, Plenum Press, NY, Dec. 1979.

Naze Tjotta, J., Tjotta, S., Vefring, E.H., Propagation and interaction of two collimated finite amplitude sound beams, *J. Acoust. Soc. Am.*, **88**, 2859-2870, 1990.

Naze Tjotta, J., Tjotta, S., Vefring, E.H., Effects of focusing on the nonlinear interaction between two collinear finite amplitude sound beams, *J. Acoust. Soc. Am.*, **89**, 1017-1027, 1991.

Nock, L., Trahey, C.E., Phase aberration correction in medical ultrasound using speckle brightness as a quality factor, *J. Acoust. Soc. Am.*, **85** 1819-1833, 1989.

O'Donnell, M., Coded excitation system for improving the penetration of real-time phased array imaging systems, *IEEE Trans. Ultrason. Ferroelect. Freq. Contr.*, **39**, 341-351, 1992.

Pishchal'nikov, Y.A., Sapozhnikov, O.A., Khokhlova, V.A., A modification of the spectral description of nonlinear acoustic waves with discontinuities, *Acoustical Physics*, **42**, 362-367, 1996.

Ratcliffe, J.A., Some aspects of diffraction theory and their applications to the ionsphere, *Rep. Prog. Phys.*, **19**, 188-263, 1956.

Schafer, M.E., Transducer characterization in inhomogeneous media using the angular spectrum method, Ph.D. Thesis, Drexel University, 1988.

Simpson, D.H, Chien T.C., Burns, P.N., Pulse inversion doppler: a new method for detecting nonlinear echoes from microbubble contrast agents, *IEEE Trans. Ultrason. Ferroelect. Freq. Contr.*, **46**, 372-381, 1999.

Stephanishsen, P.R., Benjamin, K.C., Forward and backward projection of acoustic fields using FFT methods, *J. Acoust. Soc. Am.*, 71, 803-812, 1982.

T'Hoen, P.J. Aperature apodization to reduce off-axis intensity of the pulsed-mode directivity function of linear arrays, *Ultrasonics* 231-236, 1982

Tavakkoli, J., Cathignol, D., Souchon, R., Modeling of pulsed finite-amplitude focused sound beams in time-domain, *J. Acoust. Soc. Am.*, 104, 2061-2072, 1998.

Tranquart, F., Grenier, N., Eder, V., Pourcelot, L., Clinical use of ultrasound tissue harmonic imaging, *Ultrasound Med. Biol.*, 25, 889-894, 1999.

Trivett, D.H., Van Buren, A.L., Propagation of plane, cylindrical, and spherical finite amplitude waves, *J. Acoust. Soc. Am.*, 69, 943-949, 1991.

Ullate, L.G., San Emeterio, J.L., A new algorithm to calculate the transient near-field of ultrasonic phased arrays, *IEEE Trans. Ultrason. Ferroelect. Freq. Contr.*, 39, 745-753, 1992.

Waag, R.C., Campbell, J.A., Ridder, J., Mesdag, P.R., Cross-sectional measurements and extrapolations of ultrasonic fields, *IEEE Trans. Sonics Ultrason.*, SU-32, 26-35, 1985.

Ward, B., Baker, A.C., and Humphrey, V.F., Nonlinear propagation applied to the improvement of resolution in diagnostic medical imaging, *J. Acoust. Soc. Am.*, 101, 143-154, 1997.

Welsh, L.R., Fox, M.D., Practical Spread Spectrum Pulse Compression for Ultrasonic Tissue Imaging, *IEEE Trans. Ultrason. Ferroelect. Freq. Contr.*, 45, 349-355, 1998.

Williams, E.G., and Maynard, J.D., Holographic imaging without the wavelength resolution limit, *Phys. Rev. Lett.*, 45, 544-557, 1980.

Williams, E.G., and Maynard, J.D, Numerical evaluation of the Rayleigh integral for planar radiators using the FFT, *J. Acoust. Soc. Am.*, 72, 2020-2030, 1982.

Wu, P., Stepinski, T., Extention of the angular spectrum approach to curved radiators, *J. Acoust. Soc. Am.*, 105, 2618-2627, 1999.

Zhu, Q., Steinberg, B.D., Wavefront amplitude distortion and image sidelobe levels: Part I – Theory and computer simulations, *IEEE Trans. Ultrason. Ferroelect. Freq. Contr.*, 40, 747-753, 1993

Zhu, Q., Steinberg, B.D., Wavefront amplitude distortion and image sidelobe levels: Part II – *In vivo* experiments, *IEEE Trans. Ultrason. Ferroelect. Freq. Contr.*, 40, 747-753, 1993

Appendix A: Proof of Operator Splitting Methods

Theorem: Proof of a second order operator splitting

Our starting point for the proof of the second order operator splitting, presented in chapter 4 is the model equation:

(1) $$\frac{\partial v}{\partial z} = \hat{L}_D \cdot v + \hat{L}_A \cdot v + \hat{L}_N \cdot v$$

Where the operators $\hat{L}_D, \hat{L}_A$, and $\hat{L}_N$ represent diffraction, absorption, and attenuation, respectively. Operators Γ are defined such that $\Gamma_{D,\Delta z}v(x,y,z_o,t)$ is a solution to the sub-equation

(2) $$\frac{\partial v}{\partial z} = \hat{L}_D \cdot v$$

at plane $z = z_0 + \Delta z$, given the initial distribution $v(x,y,z_o,t)$ at plane $z=z_o$. Operators $\Gamma_{A,\Delta z}$, $\Gamma_{N,\Delta z}$, $\Gamma_{D+A,\Delta z}$, $\Gamma_{D+A+N,\Delta z}$ etc. can be defined in a similar way.

We want to show that

(3) $$\Gamma_{D+A,\Delta z/2}\Gamma_{N,\Delta z}\Gamma_{D+A,\Delta z/2}v(x,y,z_o,t) = \Gamma_{D+A+N,\Delta z}v(x,y,z_o,t) + O(\Delta z^3) .\cdot$$

To do this we first must show that the operators L commute with the differential $\partial / \partial z$. We will then be in a position to apply the Taylor theorem to show the relation (3).

Lemma 1:

The diffraction operator $\hat{L}_D$ commutes with $\partial / \partial z$.

Proof:

If v is a solution to (2), it will also be a solution to the homogeneous wave equation. Since $\partial v / \partial z$ is also a solution to the homogeneous wave equation, we may make the substitution $v \rightarrow \partial v / \partial z$ in equation 2, yeilding

(4) $$\frac{\partial}{\partial z} \hat{L}_D v(z) = \hat{L}_D \frac{\partial v(z)}{\partial z}$$

which proves that $\hat{L}_D$ commutes with $\partial / \partial z$. □

Lemma 2:

The attenuation operator $\hat{L}_A$ commutes with $\partial / \partial z$.

Proof:

A general form for an attenuation operator may be written as a convolution integral:

(5) $\qquad \dfrac{\partial v}{\partial z} = \int\limits_{-\infty}^{\tau} K(z, \tau - \tau') \cdot v(z, \tau') d\tau' \equiv \hat{L}_A \cdot v,$

where K is a kernel which represents the frequency dependence of the attenuation (Tavakkoli, 1998). From (5) it is clear that

$\dfrac{\partial}{\partial z} \hat{L}_A v = \dfrac{\partial}{\partial z} \int\limits_{-\infty}^{\tau} K(z, \tau - \tau') v(z, \tau') d\tau' = \int\limits_{-\infty}^{\tau} K(z, \tau - \tau') \dfrac{\partial}{\partial z} v(z, \tau') d\tau' = \hat{L}_A \dfrac{\partial v}{\partial z},$

proving the commutation relation.

Lemma 3:

Although the nonlinear operator does not commute with $\partial / \partial z$, we can define an operator

(6) $\qquad \hat{\Lambda}_N = \left(\dfrac{\beta}{2c_o^2}\right)\dfrac{\partial}{\partial \tau},$

(such that $\hat{L}_N v = \hat{\Lambda}_N v^2$), which commutes with $\partial / \partial z$. As this is sufficiently clear, no proof is provided here. $\square$

We are now in a position to prove relation (3).

Step 1:

A solution to the evolution equation for diffraction and attenuation,

(7) $\qquad \dfrac{\partial v_o}{\partial z} = \hat{L}_{D+A} v_o$

at plane $z + \Delta z / 2$, given the initial condition $v_o = v(x, y, z, t)$ over plane z may be written as

$v_1(z) \equiv \Gamma_{D+A, \Delta z / 2} v_o(z)$

$= v_o(z) + \dfrac{\Delta z}{2} \dfrac{\partial v_o}{\partial z} + \dfrac{\Delta z^2}{8} \dfrac{\partial^2 v_o(z)}{\partial z^2} + O(\Delta z^3)$

$= v_o(z) + \dfrac{\Delta z}{2} \hat{L}_{D+A} v_o + \dfrac{\Delta z^2}{8} \hat{L}_{D+A}^2 v_o + O(\Delta z^3)$

Step 2:

We may propagate the result from step 1, presuming this result is located at plane z using a nonlinear propagator. A solution to the evolution equation for nonlinearity

(8) $\dfrac{\partial v}{\partial z} = \hat{L}_N v = \hat{A}_N v^2$

an incremental distance Δz from the result of step 1 may be given as

$$v_2(z) \equiv \Gamma_{N,\Delta z}\{\Gamma_{D+A,\Delta z/2}v(z)\} = \Gamma_{N,\Delta z}v_1(z)$$

$$= v_1(z) + \Delta z \frac{\partial v_o}{\partial z} + \frac{\Delta z^2}{2}\frac{\partial^2 v_o}{\partial z^2} + O(\Delta z^3)$$

$$= v_1(z) + (\Delta z)\hat{A}_N v_1^2 + \frac{\Delta z^2}{2}2\hat{A}_N\left[v_1\frac{\partial v_1}{\partial z}\right] + O(\Delta z^3)$$

Now substituting for v_1 we get:

$$v_2(z) = \left\{v_o(z) + \frac{\Delta z}{2}\hat{L}_{D+A}v_o + \frac{\Delta z^2}{8}\hat{L}^2_{D+A}v_o + O(\Delta z^3)\right\}$$

$$+ \Delta z \cdot \hat{A}_N\left\{v_o^2(z) + v_o\frac{\Delta z}{2}\hat{L}_{D+A}v_o + \frac{\Delta z}{2}(\hat{L}_{D+A}v_o)v_o + O(\Delta z^2)\right\}$$

$$+ \frac{\Delta z^2}{2}2\hat{A}_N\left\{\begin{array}{l}v_o(z) + \frac{\Delta z}{2}\hat{L}_{D+A}v_o\\ + \frac{\Delta z^2}{8}\hat{L}^2_{D+A}v_o + O(\Delta z^3)\end{array}\right\}\cdot\hat{A}_N\left\{\begin{array}{l}v_o^2(z) + v_o\frac{\Delta z}{2}\hat{L}_{D+A}v_o\\ + \frac{\Delta z}{2}(\hat{L}_{D+A}v_o)v_o + O(\Delta z^2)\end{array}\right\}$$

$$+ O(\Delta z^3)$$

Now collecting terms with common factors Δz, Δz^2, etc, we obtain

$$v_2(z) = v_o(z) + \Delta z\left\{\frac{\hat{L}_{D+A}v_o}{2} + \hat{A}_N v_o^2\right\} + \Delta z^2\left\{\frac{\hat{L}^2_{D+A}v_o}{8} + \hat{A}_N v_o\hat{L}_{D+A}v_o + \hat{A}_N v_o\hat{A}_N v_o^2\right\} + O(\Delta z^3)$$

Step 3:

We may propagate the effects of diffraction and attenuation from the result from step 2, presuming this result is located at plane $z + \Delta z/2$. A solution to the evolution equation (7) for diffraction and absorption given the initial condition defined in step 2 may be written as

$$v_3(z) \equiv \Gamma_{D+A,\Delta z/2}(\Gamma_{N,\Delta z}\Gamma_{D+A,\Delta z/2}v_o) = \Gamma_{D+A,\Delta z/2}v_2$$

$$= v_o(z) + \frac{\Delta z}{2}\frac{\partial v_o}{\partial z} + \frac{\Delta z^2}{8}\frac{\partial^2 v_o(z)}{\partial z^2} + O(\Delta z^3)$$

$$v_3(z) = v_2(z) + \frac{\Delta z}{2}\hat{L}_{D+A}v_2 + \frac{\Delta z^2}{8}\hat{L}^2_{D+A}v_2 + O(\Delta z^3)$$

Substituting for v_2 and collecting terms with common factors of Δz, Δz^2, etc. we obtain:

$$v_3(z) = v_o + \Delta z\{\hat{L}_{D+A}v_o + \hat{A}_N v_o^2\}$$

$$+ \Delta z^2 \left\{ \frac{\hat{L}_{D+A}^2 v_0}{2} + \hat{A}_N v_o \hat{L}_{D+A} v_o + \hat{A}_N v_o \hat{A}_N v_o^2 + \frac{\hat{L}_{D+A}}{2}\hat{A}_N v_o^2 \right\} + O(\Delta z^3)$$

We are now in a position to compare the result from step 3 with the field profile obtained from the combined effects of diffraction, nonlinearity, and attenuation. Thus we wish to compare v_3 with a solution to the evolution equation

(9) $\dfrac{\partial v_o}{\partial z} = \hat{L}_{D+A}v_o + \hat{A}_N v_o^2$

a distance Δz away from plane z, given the initial profile $v(x,y,z,t)$ accross plane z. We have:

$$\Gamma_{D+A+N,\Delta z}v_o = v_o + \Delta z \frac{\partial v_o}{\partial z} + \frac{\Delta z^2}{2}\frac{\partial^2 v_o}{\partial z^2} + O(\Delta z^3)$$

$$= v_o + \Delta z\{\hat{L}_{D+A}v_o + \hat{A}_N v^2\} + \frac{\Delta z^2}{2}\{\hat{L}_{D+A}[\hat{L}_{D+A}v_o + \hat{A}_N v^2] + 2\hat{A}_N v_o[\hat{L}_{D+A}v_o + \hat{A}_N v^2]\} + O(\Delta z^3)$$

$$= v_o + \Delta z\{\hat{L}_{D+A}v_o + \hat{A}_N v^2\} + \frac{\Delta z^2}{2}\{\hat{L}_{D+A}^2 v_o + \hat{L}_{D+A}\hat{A}_N v_o^2 + 2\hat{A}_N v_o \hat{L}_{D+A}v_o + 2\hat{A}_N v_o \hat{A}_N v_o^2\}$$

Comparing this expression with the expression for v_3, we find that

$$\Gamma_{D+A,\Delta z/2}\Gamma_{N,\Delta z}\Gamma_{D+A,\Delta z/2}v(x,y,z_o,t) = \Gamma_{D+A+N,\Delta z}v(x,y,z_o,t) + O(\Delta z^3)$$

Thus we have shown that this operator splitting scheme is second order.

End of proof. $\square$

Corollary 1: A second order operator splitting for the KZK equation

The retarded time integral of the KZK equation may be expressed as an evolution equation (described in equation 3-14 through 3-17) which satisfies the second order operator splitting theorem proved above.

Proof:

The attenuation operator defined by (3-16), and the diffraction operator (3-14) clearly commute with the operator $\partial / \partial z$. The form of nonlinear operator may be redefined as

the operator $\hat{\Lambda}_N$ described above, proving its commutivity with $\partial/\partial z$. Any operators which satisfy an evolution equation (1) and commute with $\partial/\partial z$ are subject to the second order operator splitting theorems of Tavakkoli et. al. (1998) and the scheme provided above. Thus these second order operator splitting techniques may be extended to the KZK equation. $\square$

Corollary 2: The approach of Christopher and Parker (1991) is equivalent to a first order operator splitting

$$\Gamma_{N,\Delta z}\Gamma_{D+A,\Delta z}v(x,y,z_o,t) = \Gamma_{D+A+N,\Delta z}v(x,y,z_o,t) + O(\Delta z^2)$$

of the evolution equation (9).

Proof:

Step 1:

A solution to the evolution equation (7) for diffraction and attenuation, at plane $z+\Delta z$, given the initial condition $v_o=v(x,y,z,t)$ over plane z may be written as

$$v_1(z) \equiv \Gamma_{D+A,\Delta z}v_o(z)$$

$$= v_o(z) + \Delta z\frac{\partial v_o}{\partial z} + \frac{\Delta z^2}{2}\frac{\partial^2 v_o(z)}{\partial z^2} + O(\Delta z^3)$$

$$= v_o(z) + \Delta z\hat{L}_{D+A}v_o + \frac{\Delta z^2}{2}\hat{L}^2_{D+A}v_o + O(\Delta z^3)$$

Step 2: We may propagate the result from step 1, presuming this result is located at plane z using a nonlinear propagator. A solution to the nonlinear evolution equation (8) an incremental distance Δz from the result of step 1 may be given as

$$v_2(z) \equiv \Gamma_{N,\Delta z}\{\Gamma_{D+A,\Delta z/2}v(z)\} = \Gamma_{N,\Delta z}v_1(z)$$

$$= v_1(z) + \Delta z\frac{\partial v_o}{\partial z} + \frac{\Delta z^2}{2}\frac{\partial^2 v_o}{\partial z^2} + O(\Delta z^3)$$

$$= v_1(z) + (\Delta z)\hat{\Lambda}_N v_1^2 + \frac{\Delta z^2}{2}2\hat{\Lambda}_N\left[v_1\frac{\partial v_1}{\partial z}\right] + O(\Delta z^3)$$

Now substituting for v_1 we get:

$$v_2(z) = \left\{ v_o(z) + \Delta z \hat{L}_{D+A} v_o + \frac{\Delta z^2}{2} \hat{L}_{D+A}^2 v_o + O(\Delta z^3) \right\}$$

$$+ \Delta z \cdot \hat{\Lambda}_N \left\{ v_o^2(z) + v_o \Delta z \hat{L}_{D+A} v_o + \Delta z (\hat{L}_{D+A} v_o) v_o + O(\Delta z^2) \right\}$$

$$+ \frac{\Delta z^2}{2} 2 \hat{\Lambda}_N \left\{ v_o(z) + O(\Delta z^1) \right\} \cdot \hat{\Lambda}_N \left\{ v_o^2(z) + O(\Delta z^1) \right\}$$

$$+ O(\Delta z^3)$$

which may be written as

$$v_2(z) = v_o(z) + \Delta z \left(L_{D+A,\Delta z} v_o + \Lambda_N v_o^2 \right)$$

$$+ \Delta z^2 \left(\frac{1}{2} \hat{L}_{D+A}^2 v_o + \Lambda_N v_o L_{D+A} v_o + \Lambda_N (L_{D+A} v_o) v_o + \Lambda_N v_o \Lambda_N v_o^2 \right) + O(\Delta z^3)$$

We are now in a position to compare with the field profile obtained from the combined effects of diffraction, nonlinearity, and attenuation. Thus we wish to compare v_2 with a solution to the evolution equation (9) a distance Δz away from plane z, given the initial profile $v(x,y,z,t)$ accross plane z. We have:

$$\Gamma_{D+A+N,\Delta z} v_o = v_o + \Delta z \frac{\partial v_o}{\partial z} + \frac{\Delta z^2}{2} \frac{\partial^2 v_o}{\partial z^2} + O(\Delta z^3)$$

$$= v_o + \Delta z \left\{ \hat{L}_{D+A} v_o + \hat{\Lambda}_N v^2 \right\} + \frac{\Delta z^2}{2} \left\{ \hat{L}_{D+A} [\hat{L}_{D+A} v_o + \hat{\Lambda}_N v^2] + 2 \hat{\Lambda}_N v_o [\hat{L}_{D+A} v_o + \hat{\Lambda}_N v^2] \right\} + O(\Delta z^3)$$

$$= v_o + \Delta z \left\{ \hat{L}_{D+A} v_o + \hat{\Lambda}_N v^2 \right\} + \frac{\Delta z^2}{2} \left\{ \hat{L}_{D+A}^2 v_o + \hat{L}_{D+A} \hat{\Lambda}_N v_o^2 + 2 \hat{\Lambda}_N v_o \hat{L}_{D+A} v_o + 2 \hat{\Lambda}_N v_o \hat{\Lambda}_N v_o^2 \right\}$$

Comparing this with the expression for v_2, we see that the two expressions are valid to first order, but not to second order. $\square$

Appendix B: The Angular Spectrum Approach for Radially Symmetric Sources

B.1 Introduction to Approach of Christopher and Parker

Christopher and Parker (1991) have investigated plane to plane diffractive propagation using the Angular Spectrum approach. Their paper treats the field propagation of planar, baffled, radially symmetric acoustic sources. Because the sources considered had radial symmetry, Christopher and Parker showed that a Discrete Hankel Transform (DHT) could be used to numerically implement the convolution of the source with the propagator function, h, described in 4.6. The Hankel transform is equivalent to a 2D-Fourier transform, when there is radial symmetry. The double integral of the Fourier transform relation reduces to a single integral with a radial coordinate transformation. As the name suggests, the discrete Hankel transform is a discrete implementation of the analytic Hankel transform.

Two approaches have been taken to sampling the propagator functions for numerical implementation of diffractive propagation. One method is to sample the propagator function h (the point spread function) in the spatial domain. The other is to sample the transfer function H in the spatial frequency domain. These two approaches may have very different consequences, which will be discussed after introducing some notation.

B.2 Notation

Consider a disk transducer of radius a, transmitting at a single frequency f. Let us denote the source field, and point spread functions as $s(r)$ and $h(r)$, respectively, where r is the radial coordinate. Their analytic transforms will be denoted by $S(k_r)$ and $H(k_r)$ respectively, where k_r is the radial spatial frequency.

The discrete implementation of the angular spectrum method uses sampled versions of s and h, which may be defined as $s_d[m]=s(r_m)$, and $h_d[m]=h(r_m)$, where $r_m = m\Delta r$ is the mth radial point, and Δr is the sampling interval. The distance between samples, Δr, can be chosen to be less than ($\lambda/2$), which is the Nyquist rate of the fundamental frequency. The

124

extent T of the radial spatial domain, should be chosen such that T is greater than $r_o + a$, where r_o is the extent to which correct results are desired. This choice of T prevents aliasing in the region of interest $0 < r < r_o$.

We shall denote the discrete Hankel transform (DHT) of s_d as S_d, and that of h_d as H_d. A hat '^' and a subscript 'd' will be used to denote sampling done in the spatial frequency domain. Frequency domain sampling of H, thus gives a sequence

$$\hat{H}_d[i] = H(k_i).$$

The inverse discrete Hankel transform of the frequency-sampled transfer function is denoted by:

$$\hat{h}_d = IDHT\{\hat{H}_d\}.$$

Note that all these discrete sequences defined above can be thought of as implicitly periodic.

B.3 The Spatially Sampled Convolution (SSC) Algorithm

One approach to numerical implementation of the angular spectrum method, called the spatially sampled convolution (SSC) algorithm, directly convolves the sequences s_d and h_d. We desire the discrete convolution of sequences s_d and h_d to approximate the analytic convolution of the functions s and h. The field profile represented by the analytic convolution of s and h will of necessity be of infinite extent. Beyond a few source radii in the lateral direction, the field may very well be nearly zero, however, it will not be exactly zero. Thus, in using a discrete implementation of the angular spectrum method, only a finite extent of the field in the observation plane may be calculated. Suppose that across an observation plane a distance Δz away from the disk transducer, we wish to compute the field profile out to a lateral extent r_o. The normal velocity field profile of the source will have a finite extent of radius a. The analytic point spread function h, however, will have an infinite extent, but must be truncated at some point. By ensuring that h is sampled out to a lateral extent of $T \geq r_o + a$, the linear discrete convolution $s_d * h_d$ will accurately represent the desired field profile out to r_o. In the region between r_o and T, the result of the linear convolution may not accurately reflect the true values for the field profile due to truncation of the infinite-extent point spread function h.

It is well known that the **circular** convolution can be used to implement the linear convolution of two sequences. The point spread function h may be sampled out to extent r_o, then zero padding may be used to pad s_d and h_d out to extent $T \geq r_o + a$. The DHT of s_d and h_d are computed, then their transforms are multiplied together. The inverse DHT of this product is the circular convolution of s_d and h_d. The circular convolution is equivalent to the discrete linear convolution of s_d and h_d through the whole extent of the result (out to T), and represents the analytic convolution (the true field profile) in the region of lateral extent out to r_o. The use of zero padding prevents wraparound errors.

Alternatively, h may be sampled out to $T \geq r_o + a$ without zero padding (although s_d should be zero padded), and DHT-based circular convolution may be performed on the resulting sequences. The result of the circular convolution will be equivalent to that of linear discrete convolution out to r_o, while the region $r_o < r < T$ will contain a region with wraparound error. Thus, in either scheme the correct field profile is represented out to r_o, as long as both the source and the point spread functions are adequately sampled.

B.4 The Frequency Sampled Convolution (FSC)

In contrast to the SSC approach, the frequency sampled convolution (FSC) algorithm samples the transfer function H directly in the spatial frequency domain, and thus implements the convolution as follows

(1) $\quad s \underset{FSC}{*} h = IDHT\left\{DHT[s_d] \times \hat{H}_d\right\}$,

which is equivalent to circular convolution of the aperature s_d with

(2) $\quad \hat{h}_d = IDHT\ \{\hat{H}_d\}$.

The FSC Algorithm zero pads s_d out to some spatial extent $T \geq r_o + a$, while sampling the transfer function H across the entire frequency domain. Although the region $r_o < r < T$ will contain "wraparound errors", the resulting field given by (1) represents the correct field profile out to r_o, as long as both the source and the transfer functions are adequately

sampled. The criterion of adequate sampling is, however, a nontrivial issue as will be discussed in the following sections.

B.5 Sampling of a spatially limited source

If the source has an abrupt edge, very dense sampling must be used. The farther the observation plane from the source, the more accurate the computed field profile (based on the given gridding scheme) will be. Reasonably accurate results may be obtained for observation planes which are in the farfield of each sampling element, assuming that an ideal propagator function is used.

B.6 Sampling the Transfer Function H

Sampling of the propagator function H can also be troublesome. Figs. 1(a)-(d) show the real part of H as a function of radial spatial frequency k_r for different propagation distances and frequencies. Notice that for large propagation distances, H has an abrupt change at $k_r = k$, where $k=2\pi f/c$ is the magnitude of the wave vector. Notice also the chirp-like behavior of H. The apparent frequency modulation looks like a nonlinear sweep over a band of frequencies, with the chirp ending in a cusp at k. Beyond k, H appears to drop off exponentially fast. This evanescent tail is most significant for sub-wavelength propagation distances, and virtually negligible for larger propagation distances.
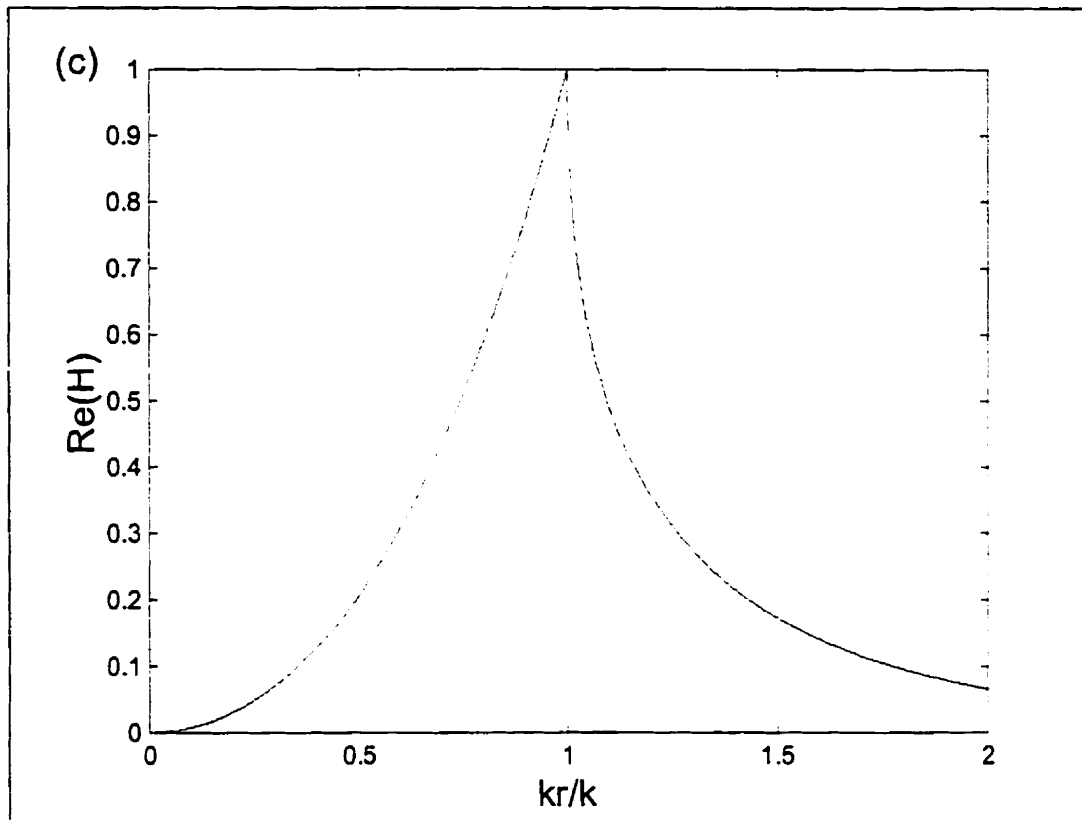
(a)

Re(H)

kr/k

(b)

Re(H)

kr/k
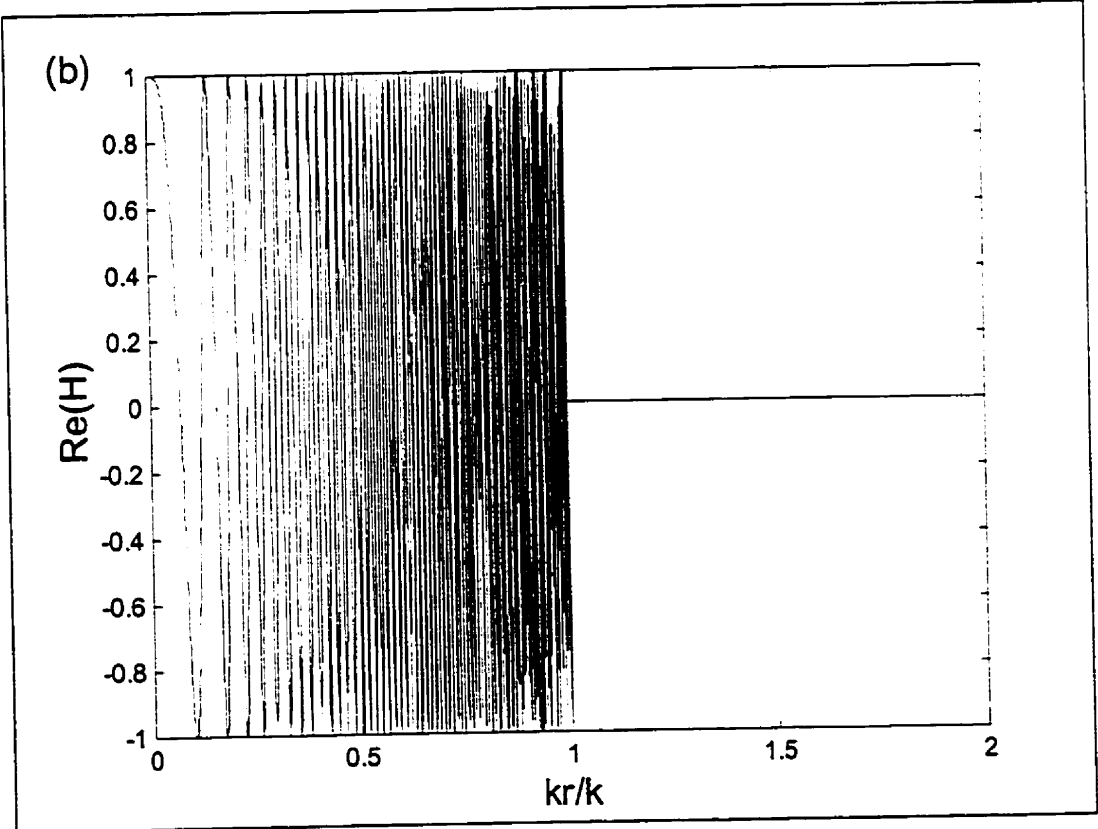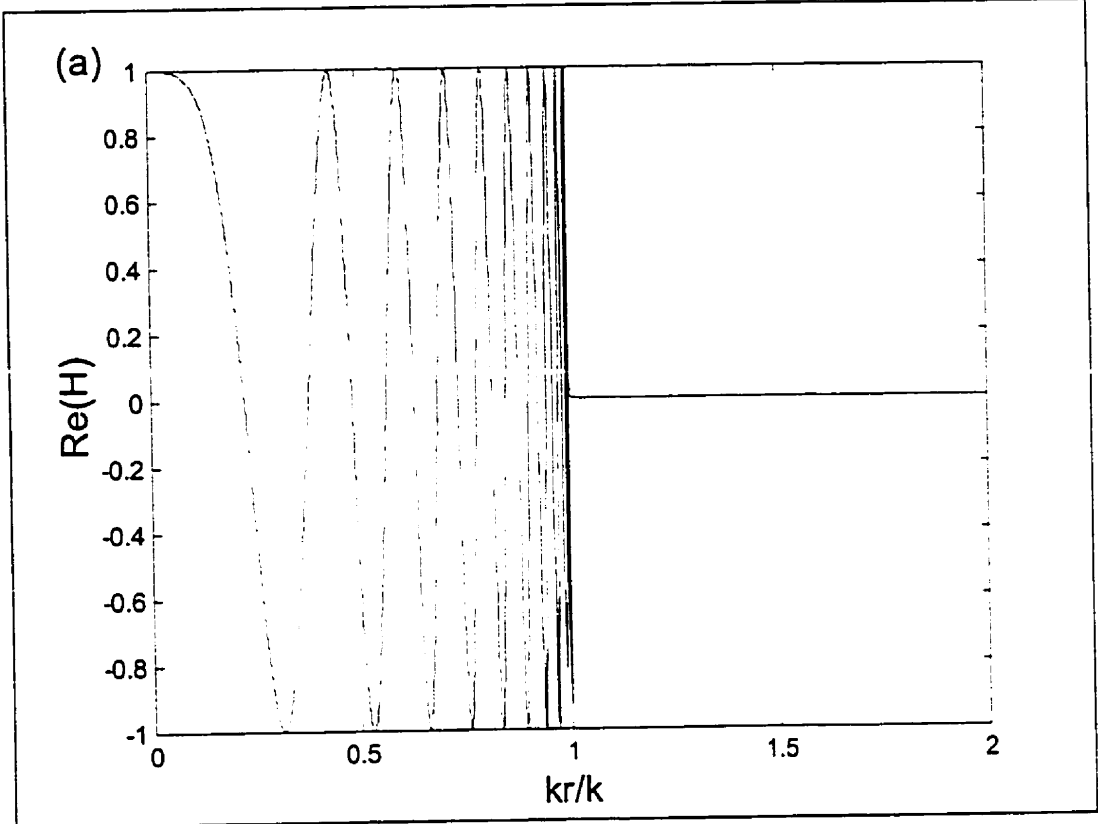
Figure 1: The real part of the transfer function H for $f=$ 1MHz and (a) z=10λ (b) z = 100λ , and (c) z = λ/4.

When using the FSC algorithm for large propagation distances, adequate sampling of H may be difficult to obtain. Reasonable sampling may be obtained for sub-wavelength propagation distances, since the cusp at $k_r=k$ is less narrow, and the evanescent tail tapers off more slowly, providing a less abrupt change. Otherwise, sampling of the transfer function H may be a precarious matter.

Although the FSC algorithm affords the computational shortcut of not having to transform the point spread function into the spatial frequency domain, it involves perils associated with aliasing problems.

It was noted earlier that the FSC approach is equivalent to discrete convolution of the aperature s_d with $\hat{h}_d = IDHT\ \{\hat{H}_d\}$. As Christopher points out, the $\hat{h}_d$ correspond to samples of an aliased version of the infinite function h. This wraparound phenomenon

could be physically approximated by propagating the field of point source down a cylindrical reflecting tube of radius T.

Wraparound errors associated with $\hat{h}_d$ degrade the accuracy of the FSC - based convolution. Such aliasing problems are more severe for larger propagation distances and higher frequencies, as illustrated in Figs. 2(b) and (d).
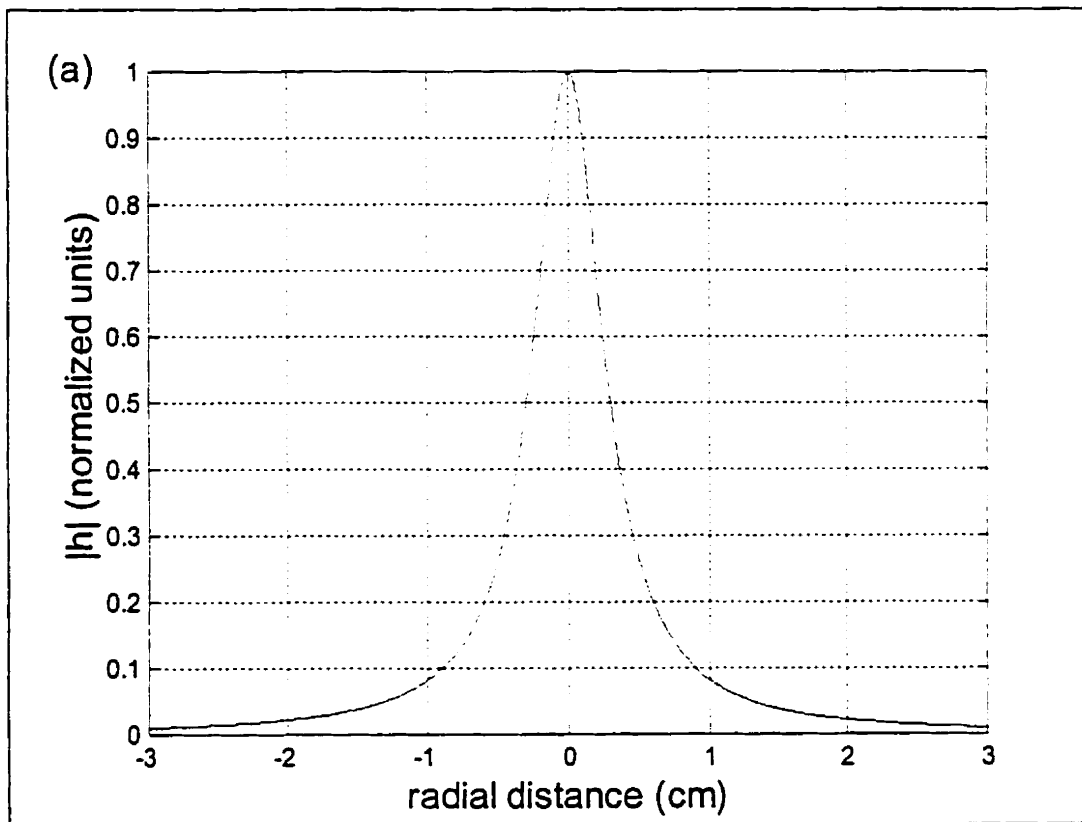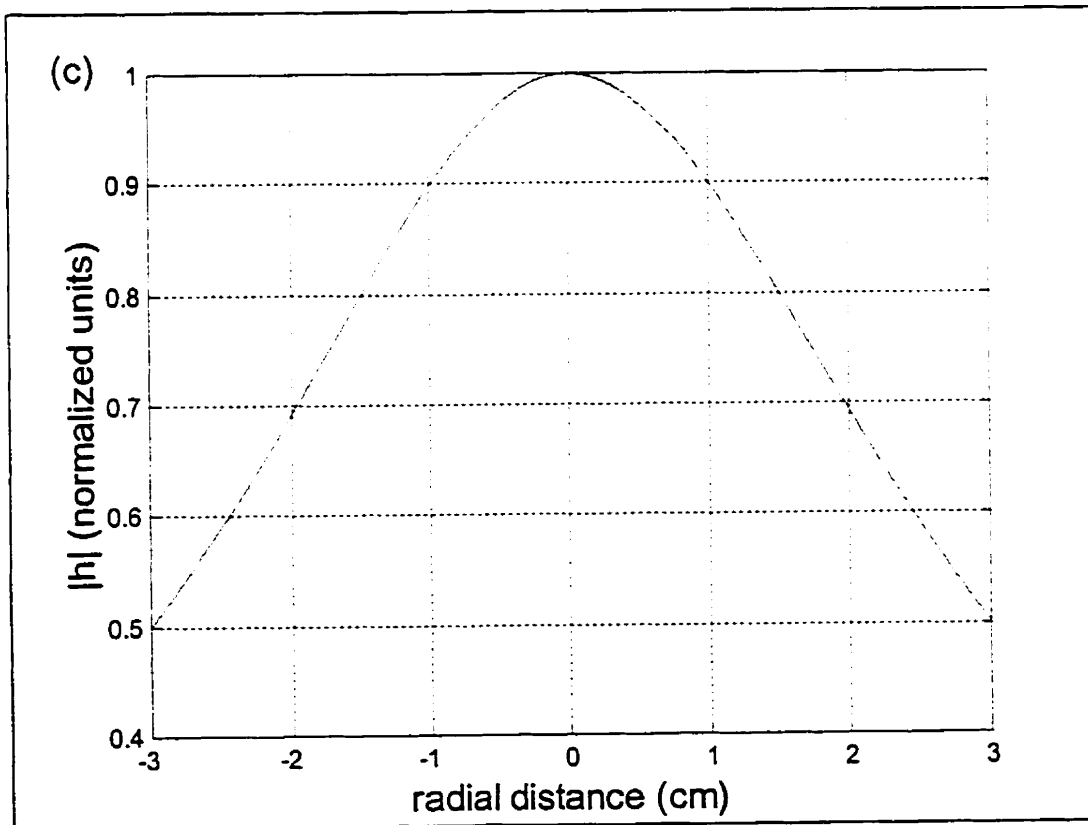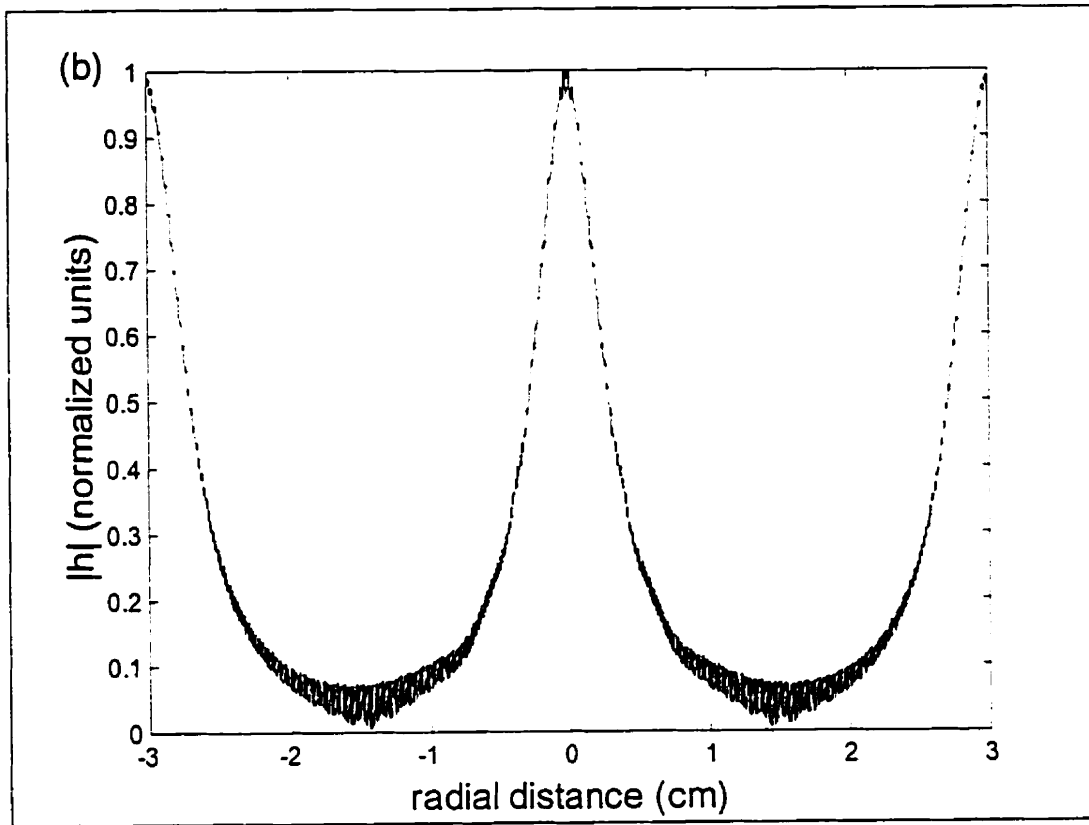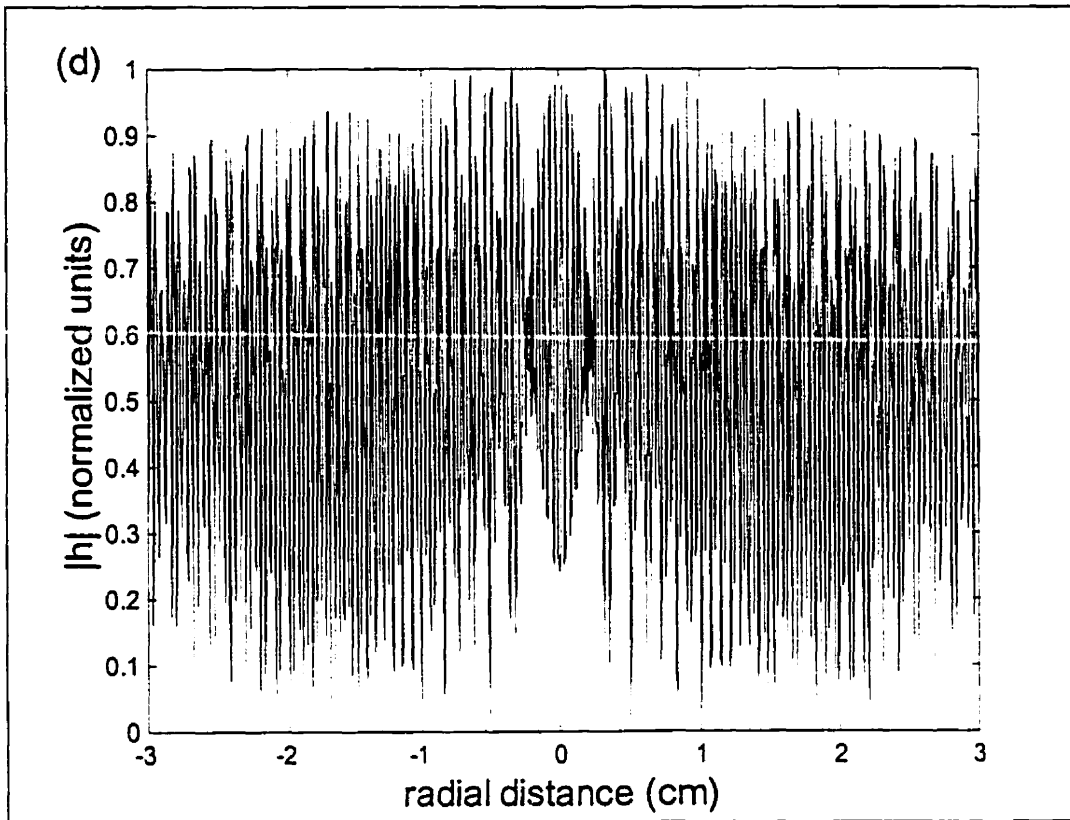
Figure 2 (a) shows the normalized magnitude of the point spread function h for $f =$ 5MHz, z=10λ. (b) illustrates the aliasing and wraparound errors evident in $\hat{h}_d$ for $T =$ 1.5cm, when the transfer function H is sampled in the spatial frequency domain. The distribution should reproduce (a), but does so with significant error. (c) shows the normalized magnitude of the point spread function for $f =$ 5MHz and z=100λ. (d) shows that the errors introduced in $\hat{h}_d$ from frequency domain sampling are very severe.

B.7 The SSC Algorithm

In contrast to the FSC algorithm, the SSC algorithm introduces negligible errors due to aliasing. Finite extent sampling of the relatively smooth point spread function h (see Figs. 2(a) and (c)), can be done at moderate sampling rates, while the transform H_d has virtually no wraparound error. H_d corresponds to the infinite extent H wrapping around itself to produce a finite sequence H_d. If sampling is done at greater than the Nyquist rate of $2f/c$, the evanescent tail of H_d will be well represented, and because the evanescent tail exponentially falls off to zero, there will be very little wraparound error in H_d.

B.8 A Ray Theory Truncation for the FSC Algorithm

Waag et. al. (1985) first presented a ray theory truncation which Christopher and Parker used to modify their FSC algorithm. It is based on the premise that at distances greater than λ, the field of a point source can be well described by a ray theory (which neglects any evanescent waves). Consider, as depicted in Fig. 3, a plane a distance z away from a point source.
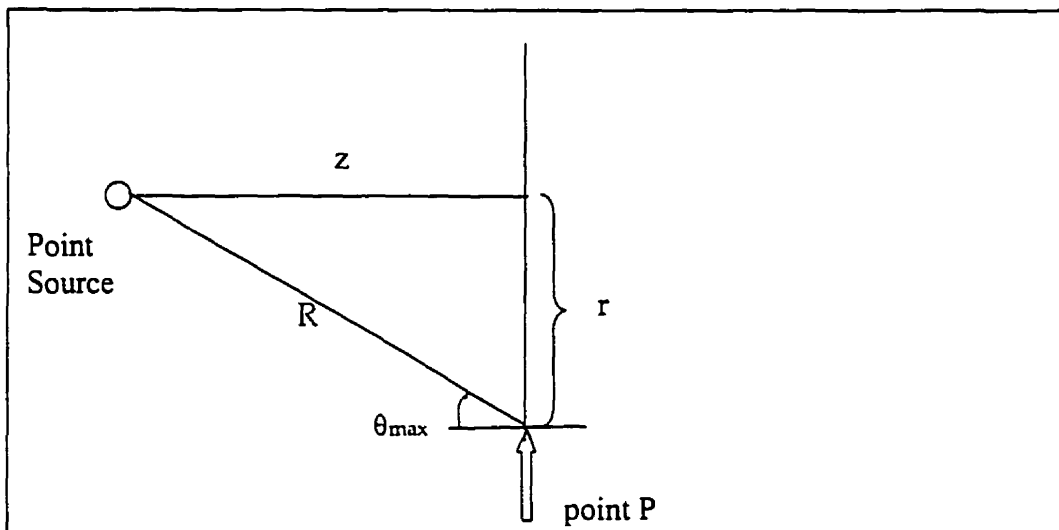

Figure 3: Illustration of the coordinate system used in a ray theory described in this section

According to a ray theory interpretation, the radial spatial frequency, k_r, at point P in the observation plane, is given, by

(3) $k_r = (2\pi f / c)\sin(\theta_r)$,

where θ_r is the angle between the observation point and the point source, as depicted in Fig. 3.

We can use this ray theory relation with Huygens principle, by applying it to a collection of point sources representing a finite source. For a finite extent source of radial extent a, the angle subtended by the edge of the transducer and the point P may be labeled θ_{max}, as depicted in Fig. 4, and given by

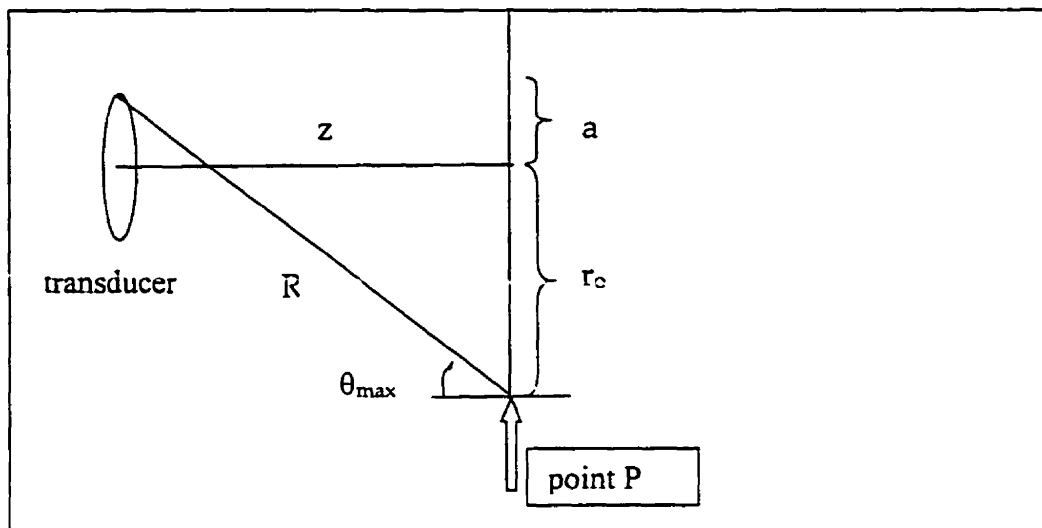(4) $\tan(\theta_{max}) = \dfrac{a + r_o}{z}$.

Figure 4: Coordinates and parameters for a ray theory truncation described in this section

Ignoring evanescent components, we may say that $k_{max} = k\, sin(\theta_{max})$ is the maximum spatial frequency in the angular spectrum of the field across plane P. We can modify $H(z,k_r)$ in the spatial frequency domain by doing a truncation, so that H is represented only out to $k_{max} = k\, sin(\theta_{max})$. This would not only exclude the evanescent tail of H, but also the cusp at $k_r = 2\pi f/c$, and the dense oscillations in the neighbourhood of this cusp. Simultaneously, sampling requirements for both the FSC and SSC algorithms would be reduced.
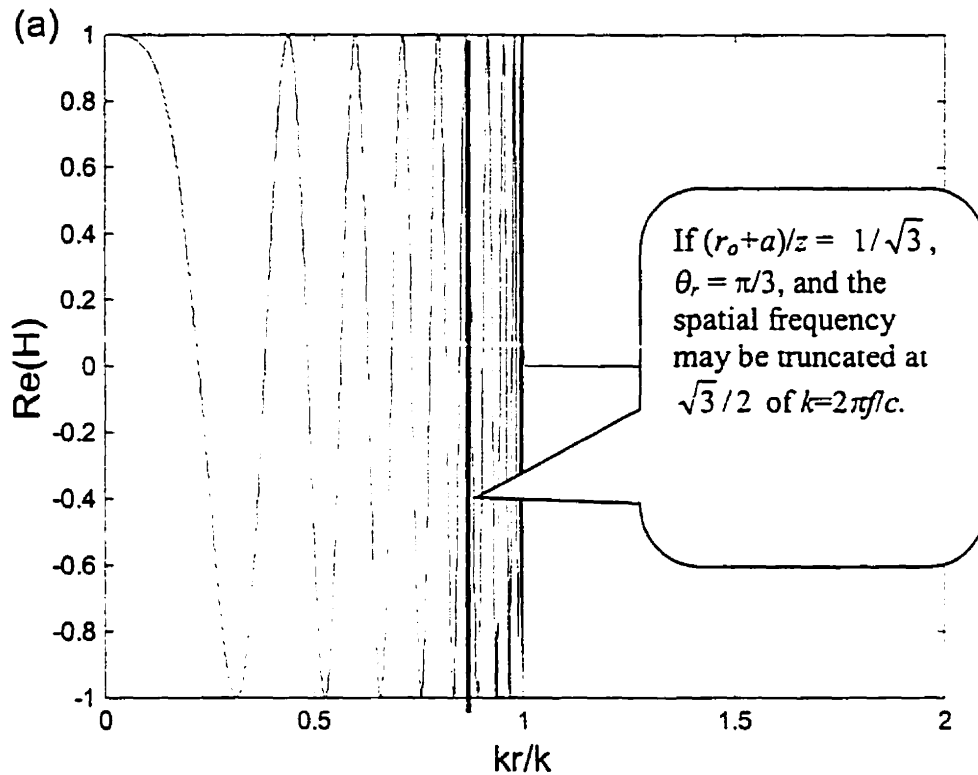
(a)

Figure 5: By using a ray theory, H may be truncated at a point where sampling of the oscillations of H is manageable.

B.9 Sampling of H with and without the Ray Theory Truncation

The Nyquist theorem requires that we sample a function at a rate of twice its highest spectral component. The transfer function H, however, has no finite Nyquist frequency limit, and thus infinitely dense sampling would be required to accurately represent H. Fortunately, the Ray Theory introduced in the previous section allows an elegant and practical way of implementing the FSC algorithm without requiring an infinitesimally small sampling grid. The truncation of H at a spatial frequency $k_{max} < 2\pi f/c$ bypasses the need to sample the dense oscillations, and cusp surrounding the radiation circle. This means we can define a finite Nyquist rate for the truncated propagator function H.

To further show how the ray theory truncation surpresses aliasing problems associated with the FSC algorithm, we prove here a theorem, which we will use as a basis for sampling in more complicated scenarios in subsequent sections and chapters. Assuming

that we have no prior knowledge of the Ray Theory Truncation, suppose that we wish to truncate H at a particular spatial frequency, which we shall call k_{max}. We will show by means of a Taylor series expansion that the optimal choice for k_{max} so as to suppress aliasing errors, is the k_{max} given by the Ray Theory Truncation.

B.10 Sampling Theorem

We want to approximate $H(k_x, k_y; z_1 \mid z_o) = e^{-j\Delta z \sqrt{k^2 - (k_x^2 + k_y^2)}}$ in the neighbourhood of k_{rmax} by a sinusoid of frequency β. We do this by expanding the argument of H in a Taylor series about k_{rmax}. Let $g(kr) = \Delta z \sqrt{k^2 - k_r^2}$ so that from the Taylor series expansion

$$g(x) = g(a) + g'(a)(x - a) + \frac{g''(a)}{2!}(x - a)^2 + \dots + \frac{g^{(n)}(a)}{n!}(x - a)^n + R_{n+1}$$

we have

$$g(kr) \cong \Delta z \sqrt{k^2 - k_{rmax}^2} - \frac{k_{rmax} \Delta z}{\sqrt{k^2 - k_{rmax}^2}}(k_r - k_{rmax}) + R_2.$$

Thus around k_{rmax},

$$e^{j\Delta z \sqrt{k^2 - k_r^2}} \approx e^{j(\alpha - \beta k_r)}$$

where

$$\alpha = \Delta z \sqrt{k^2 - k_{rmax}^2} + \frac{k_{rmax}^2 \Delta z}{\sqrt{k^2 - k_{rmax}^2}} + R_2, \quad \text{and} \quad \beta = \frac{k_{rmax} \Delta z}{\sqrt{k^2 - k_{rmax}^2}}$$

is the desired spectral frequency. Thus in the neighbourhood of k_{rmax}, H can be approximated by a sinusoid with 'frequency' β. Since this is the highest spectral component of H, by the Nyquist theorem, we need to sample H at a rate of 2β:

$$\Delta k_r \le \frac{\pi}{2\beta} = \frac{\pi \sqrt{k^2 - k_{max}^2}}{2 k_{max} \Delta z}.$$

The number of samples across H is therefore

$$N \ge \frac{k_{rmax}}{\Delta k_r},$$

which determines the extent of the zero padding required.

Since $k_{rmax} = ksin\theta$, we may note that

$$\beta = \Delta z \tan\theta = r_o + a$$

This is just another way of saying that if we require correct results (without wraparound errors) out to r_o, we can use the ray theory truncation with the FSC approach.

B.11 Conclusions Regarding the Radially Symmetric FSC and SSC Algorithms

Christopher and Parker concluded that for plane-to-plane diffractive propagation, the SSC algorithm was to be preferred over the FSC algorithm when no ray theory truncation was used. They also concluded that modifying the FSC to include a Ray theory truncation (section B.7) can greatly improve the accuracy of the FSC method, while simultaneously reducing the computational burden.